R-13-30

# Hydrogeochemical modelling and evolution of the groundwater types and processes in geosphere of SFR, SR-PSU

Gabriela Román-Ross, Paolo Trinchero,
Flávia Maia, Jorge Molinero

Amphos 21

December 2014

**Svensk Kärnbränslehantering AB**
Swedish Nuclear Fuel
and Waste Management Co

Box 250, SE-101 24 Stockholm
Phone +46 8 459 84 00

ISSN 1402-3091
**SKB R-13-30**
ID 1471559
December 2014

# Hydrogeochemical modelling and evolution of the groundwater types and processes in geosphere of SFR, SR-PSU

Gabriela Román-Ross, Paolo Trinchero,
Flávia Maia, Jorge Molinero

Amphos 21

# Summary

Modeling the geochemical evolution of the geosphere in the frame of a nuclear performance assessment of a waste is important to properly understand the hydrochemical conditions prevailing at repository depth. In fact, these hydrochemical conditions and their evolution in time might have impact for the long-term performance of the engineered barriers.

In this study we present a detailed account of a number of numerical models focused on the assessment of the evolution of the hydrogeochemical conditions at SFR (i.e. the repository for low- and intermediate level waste of Sweden). The models provide predictions of the geochemical conditions in a rock volume that surrounds the existing facility (SFR1) and also the future extension (SFR3).

The conceptual model on which the study is based, assumes that the hydrochemical evolution of the groundwater at repository depth is the result of infiltration and geochemical processes from the surface of the domain to the repository. The infiltration occurs in an extended and complex network of deformation zones and fractures in which the infiltrating waters (i.e. boundary waters), in turn, undergo geochemical reactions with the rock and minerals. These rock-water interaction processes are relevant for determining the buffering capacity of the hydrogeological/geochemical system. Mass exchange between the transmissive zones and the low permeable matrix is simulated using a dual porosity approach. Matrix is assumed to be chemically inert meaning that all the geochemical reactions mimic the interaction between the water that moves along the fractures and the fracture filling minerals.

With the aim of reproducing the mutual interplay between the hydrodynamic and geochemical processes, the reactive transport calculations summarized in this document integrate the results of complex hydrogeological models (i.e. Darcy Tools models) with a number of geochemical reactions whose parameterization is based on the data available for the site. In all the reactive transport calculations denoted as “Base Case” hematite is assumed to be the main iron mineral in the fracture filling under local equilibrium constraints. An alternative geochemical case, denoted as “Variant Case”, has been defined where $FeS_{(am)}$ , instead of hematite, is assumed to be present in the fracture filling. Given the importance of climatic cycles in the space-time domain of interest, two different climatic periods (i.e. temperate and periglacial) have been considered.

During the temperate period the infiltration of altered meteoric water generates a front which progressively reaches repository depth. As a consequence of the hydrogeological evolution of the site, salinities decrease within the candidate repository volume in a period time of 600 years from 2500 AD. This evolution depends on the infiltration of meteoric waters from recharge locations, which in turn is controlled by landscape evolution, and the buffer capacity of the rock-matrix.

Despite the strong compositional contrast between infiltrating meteoric water and fracture water, changes in the redox conditions at repository depth is not expected, as the infiltrating water will interact, first with the soils and then with fracture minerals. These abiotic reactions along with aerobic microbial consumption (not accounted for in the models) will deplete the dissolved oxygen. It turns out that redox conditions are strongly controlled by the available fracture minerals.

The signature of meteoric water is evident in the whole domain, being a direct consequence of infiltration processes. During the temperate period the salinity at SFR varies between 6 g/L, at the beginning of the simulation, and $1 \cdot 10^{-2}$ g/L at the end of the simulation. The evolution of the computed concentrations of major cations shows the same trend of chloride, as a result of dilution processes triggered by the infiltration of meteoric waters. The cations with the highest charge concentrations are Na and Ca, and to a much lower extent, Mg and K.

Due to high uncertainties on hydraulic conditions and mineralogical composition of the fracture filling minerals and their distribution along the fractures, a number of sensitivity cases were defined based on the available information for the area. These uncertainties were handled by performing Monte Carlo simulations and analysis of geochemical processes along a single streamline. Three main sources of uncertainties were identified and analysed: travel time of groundwaters, kinetic dissolution of silicates and cation exchange reactions. The results of the sensitivity analyses show that high residence times for groundwaters would impact on the chemical composition of the water due

to kinetically controlled reactions that will increase pH and release Si and Al to the waters. On the other hand, the assessment of the role of clays as exchanger in the fractures has allowed predicting a limited extent of these processes in the SFR system.

Simulations performed for the periglacial periods are affected by important sources of uncertainty, specially related to the underlying hydrogeological model. The modelling approach of this set of simulations is analogous to that used for the temperate simulations, regarding how the reactive transport calculation is applied. From a conceptual point of view, we assumed the same geochemical model defined for the temperate period, with a Base Case under equilibrium conditions with calcite/hematite and a Variant Case where the presence of $FeS_{(am)}$ instead of hematite is considered in the fracture fillings. Specifically in this case, two simulation cases representative of two opposite situations, have been defined and simulated. The first approach takes into account the infiltration of a lake water and in the second one a glacial water infiltrates through the transmisive zone.

The recharge flow paths are taken from a DarcyTools model representative of permafrost hydrogeological conditions (see Section 2.3).

Under periglacial conditions the hydrogeological conditions will change and the groundwater residence time will be longer compared to that defined for the temperate period. Only slight changes are foreseen in the chemical composition of groundwaters at repository level during this period as boundary waters from the taliks and lakes will not be substantially different from those considered during the temperate period.

In contrast, the results of the simulations performed with the glacial water show an important decrease in the salinity values at repository depth. During infiltration, a progressive increase in pH is induced by calcite dissolution in the interface fracture fillings-waters. In term of redox characteristics, reducing conditions prevail during the whole simulated period (10 ky) with Eh values at repository depth ranging from –271 mV to –352 mV.

# Contents

# 1 Introduction

## 1.1 Background and motivation

The Swedish Nuclear Fuel and Waste Management Company (SKB) have a plan for a future extension of the final repository for low and medium level radioactive operational waste, SFR, located about 150 km north of Stockholm. A number of investigations studies have been carried out in order to study the plausible bedrock volume suitable for an extension (Figure 1-1) (SKB 2013).

According to present plans, all Swedish nuclear power plants will, need to be decommissioned in a foreseeable future. Thus, the objective of the site investigations was to ensure a sound technological and scientific basis for the preparation for the application of the extension of SFR (SKB 2013).

The present study focus on giving underlying information for the analysis on the long-term safety of the current repository (SFR1), the future extension (SFR3) and its surroundings.

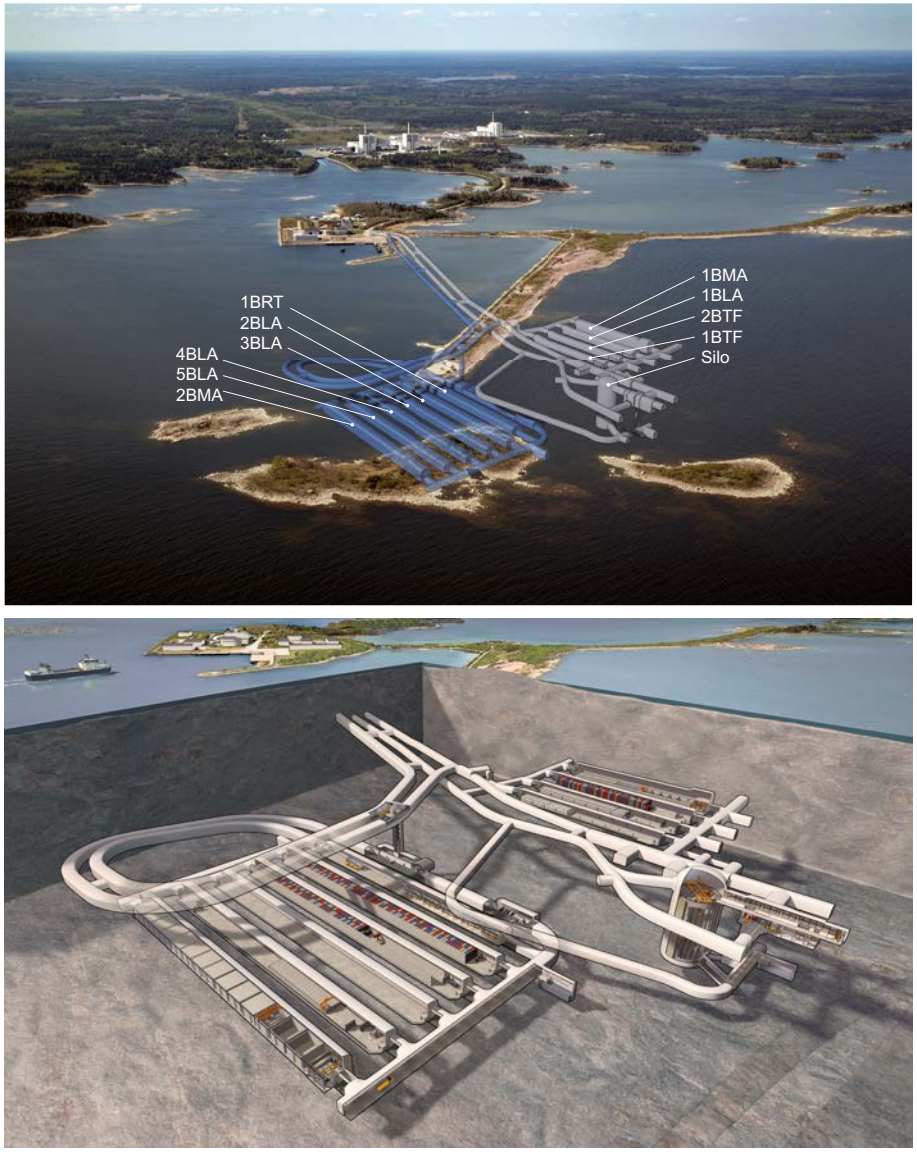


***Figure 1-1.*** *Location of SFR1 and the future extension, SFR3. SFR1 (light grey colour) is located at 60 m depth whereas the future extension (blue colour) will be constructed at about 120 m depth.*

Disposal of radioactive waste in engineered facilities located underground is the system selected in Sweden as well as in other countries. To this end, the host rock should provide a "favourable" environment in terms of chemical, mechanical, hydraulic and thermal conditions. For this reason, the geological host formations are selected taking into account their long term-stability, their availability to accommodate wastes, their ability to attenuate potential release of radionuclides and their buffering capacity related to internal or external perturbation. Erosion and climatic change have been reported in previous studies as the main relevant natural events regarding the long-term perturbation of exogenic origin (SKB 2014a and references therein). Endogenic perturbations mainly include seismicity. Other key issues to be also considered are the efficiency of transport processes over geological times and the geochemical buffering of the geosphere (SKB 2014b). In this framework, it is of great concern to evaluate the resilience of the geosphere to natural perturbations taking into account chemical reactions and transport properties. Therefore, the chemical reliance of the system needs to be analyzed in a coupled fashion with the hydrological conditions.

Reliable predictive geochemical models need to incorporate all the relevant data available for the site. In this sense, in SKB (2013, 2014a) the SFR site is thoroughly described including the current hydrochemical conditions in the geosphere and the ongoing natural processes that can influence the long-term evolution of the repository. In addition, Auqué et al. (2013) provided a set of reference water for the different climatic domains based on previous studies in the area. All this information has been carefully analyzed and used to parameterize the reactive transport models.

It is worthwhile noting that the adopted modelling approach integrates hydrogeological models (i.e. recharge particle trajectories) with the relevant site-specific reactive transport processes. This integration aims at capturing the mutual interdependence of flow and relative transport patterns. On the other hand, the high underlying uncertainty is addressed using Monte Carlo simulation.

## 1.2 Objective and scope

The main objective of the study is to provide a description of the hydrogeochemical evolution in the groundwaters surrounding the SFR1 and SFR3 repositories over the climatic-related periods relevant for the repository evolution. The hydrogeological environment has been reproduced by implementing a set of reactive transport simulations. In order to shed light on uncertainties associated to input data, a number of Monte Carlo simulations are performed to identify the most sensitive processes and provide a range of variation for the computed results. These stochastic simulations allow getting insights into key properties of the geological medium such as its buffering capacity against "external" perturbation events.

## 1.3 Report layout

This report consists of 6 chapters. The introduction is detailed in Chapter 1. Chapter 2 provides a detailed description of the conceptual and numerical model. This includes a summary of previous site studies, the methodological approach adopted and the model parameterization with a description of all the sensitivity cases performed. The geochemical evolution of groundwaters during the temperate period is addressed in Chapter 3 and, in Chapter 4, an analogous analysis is performed for the periglacial period. The main uncertainties associated to the model approach are discussed in Chapter 5 and the conclusions are presented in Chapter 6.

# 2 Conceptual model and numerical implementation

## 2.1 Conceptual understanding of the site

### 2.1.1 Geological setting

The SFR facility is located in northern Uppland close to the Forsmark nuclear power plant within about 120 km north of Stockholm. The area forms part of a crustal segment in the Fennoscandian Shield. The strongly deformed rocks in the SFR area consist of a heterogeneous package of mainly felsic to intermediate metavolcanic rocks intercalated with biotite-bearing metagranodiorite (to granite) types (Bodén and Lundin 2007). The bedrock around the SFR nuclear repository is composed of three main rock:

(i) Felsic to intermediate metavolcanic rocks formed early during the Svecofennian orogeny.

(ii) Granitoids of Svecofennian age, more or less foliated. The granitoids dominate in the northern half of the repository area and also constitute the dominant rock type in adjacent land areas.

(iii) Pegmatites (coarse-grained rocks) of at least two generations. The older pegmatite is partially granitic and constitutes the dominant rock type from about 600 metres into the access tunnels up to the southern part of the repository area. The rocks in the younger igneous suite occur typically as subordinate bodies and dykes. However, at the scale of the SFR underground facility, they constitute a substantial volume of the rock mass (Figure 2-1).

Geology at local scale has been reinterpreted in terms of four rock domains, mainly on the basis of rock composition and degree of heterogeneity (SKB 2013) (Figure 2-2):

i) Domain RFR01 is dominated by pegmatites.

(i) Domain RFR02 consists of fine-to medium-grained metagranite-granodiorite and felsic to intermediate metavolcanic rocks.

(ii) Domain RFR03 is not well described in the SFR site due to the peripheral location of this domain. It is composed, in general terms, by pegmatites and rocks affected by deformation.

(iii) The composition of Domain RFR04 is uncertain, a composition similar to that for Domain FRF02 is assumed.

The SFR area is situated within a high-strain belt that forms the north-easterly margin to the so-called Forsmark tectonic lens (SKB 2008). The north-western part of this tectonic lens hosts the target area for siting SFR. The rock types, their grouping and temporal relationship in this rock volume are virtually identical to that of the rocks in the adjacent Forsmark tectonic lens.

In general terms, two types of fractures have been observed in this area: regional (larger than 10 km) and local (smaller than 10 km). Detailed studies of fracture mineralogy and wall rock alteration were carried out during the site investigations for the deep repository of spent nuclear fuel in Forsmark (PLU) between 2002 and 2007 (Sandström and Tullborg 2009, Sandström et al. 2006, 2008, 2009, 2010). During these studies, a sequence of four major events of fracture mineralisation was observed based on e.g. crosscutting relations, stable isotopes and 40Ar/39Ar dating:

**Generation 1:** Precipitation of epidote, chlorite and quartz under hydrothermal conditions at temperatures between ca. 200° and 300°C in preferably sub-horizontal to gently-dipping fractures and fracture zones but also in steep WNW-ENE to NW-SE fractures. The wall rock was hydrothermally altered and red-stained by hematite dissemination during this event. The minerals precipitated during the Proterozoic between 1.8 and 1.1 Ga.

**Generation 2:** Hydrothermal precipitation of a sequence of fracture minerals at temperatures between 150° and 250°C. The fracture mineral generation is dominated by hematite-stained adularia and albite, prehnite, hematite-stained laumontite, calcite and chlorite which precipitated along preferably steep ENE-WSW to NNE-SSW and NNW-SSE fractures. The wall rock was hydrothermally altered, causing redstaining by hematite dissemination. After precipitation of these fracture minerals, a period with some dissolution of fracture minerals occurred, the age and cause of this dissolution is uncertain.

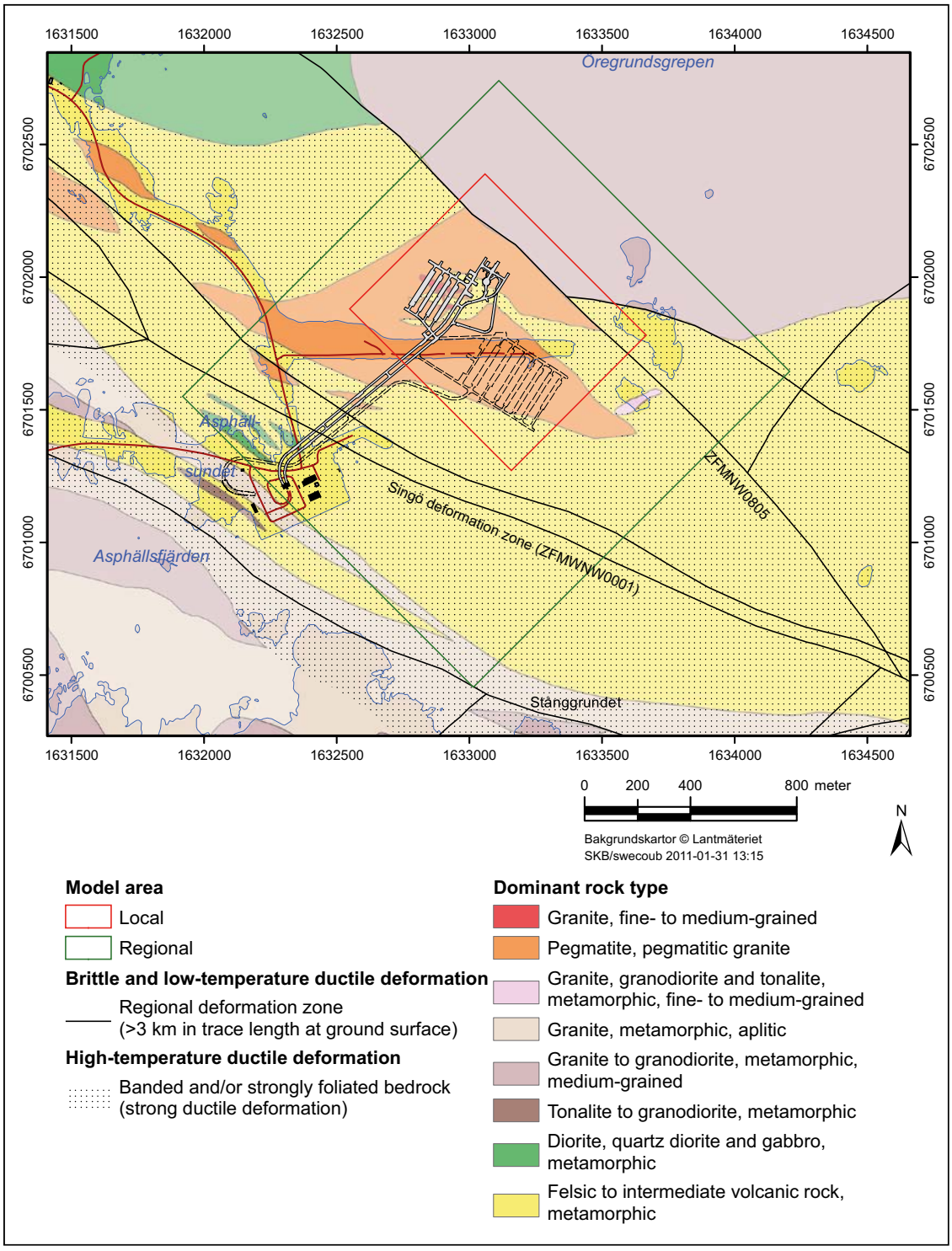


***Figure 2-1.*** *Bedrock geological map of the area around SFR based on the bedrock geological map, Forsmark stage 2.3 (Stephens et al. 2007). Figure taken from Curtis et al. (2011).*

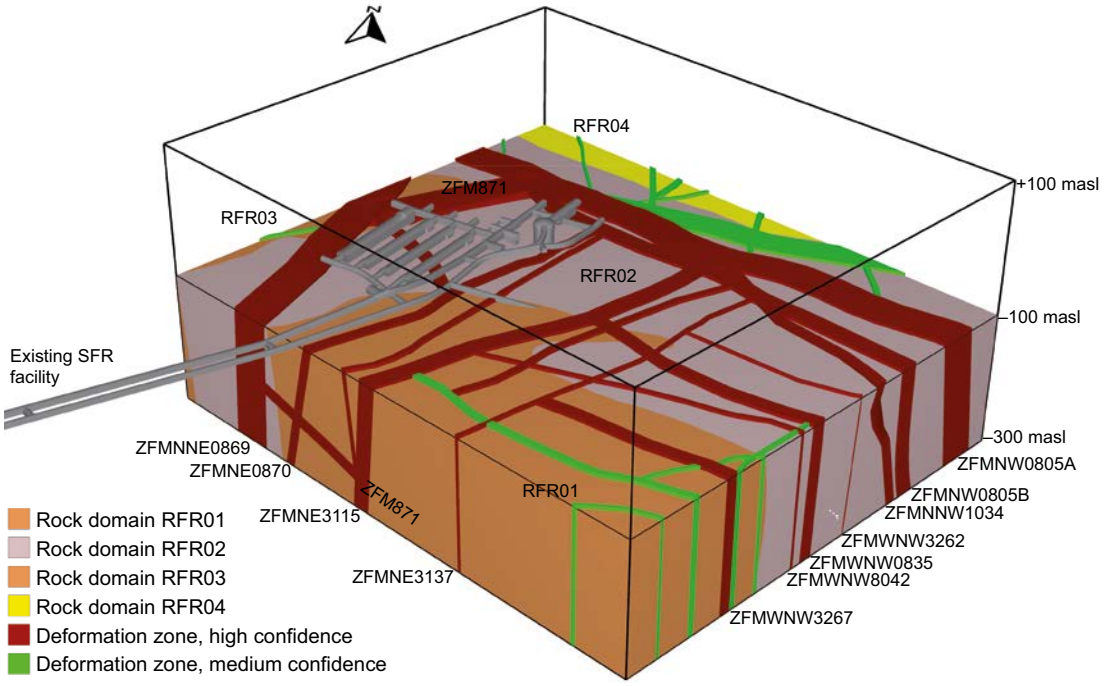


***Figure 2-2.*** *Rock domains and deformation zones in the SFR local model (SKB 2013).*

**Generation 3:** Fracture minerals were precipitated at temperatures between 60° and 190°C during several episodes in the Palaeozoic. Generation 3 is dominated by quartz, calcite and pyrite with minor occurrences of e.g. asphaltite, analcime, corrensite, galena, adularia and fluorite.

**Generation 4:** Predominantly clay minerals and thin precipitates of calcite. Minor occurrences of pyrite and goethite are also found. Precipitation has probably occurred at low temperatures (< 50°C) during a prolonged period, possibly since the late Palaeozoic until present by groundwater circulation.

Due to the proximity between the area investigated during the Forsmark site investigations and SFR, the areas have experienced similar geological evolution. However, some differences may exist between the two areas, possibly due to that SFR is situated outside the "tectonic lens" that borders the Forsmark site investigation (Stephens et al. 2007, Curtis et al. 2011).

### 2.1.2 Climatic conditions

Climate change is mentioned as the main source of exogenic perturbation vis-à-vis the long-term assessment of the SFR repository (SKB 2014a). Thus, here we have included a description of the different climatic cases considered in the SR-PSU safety assessment (Table 2-1) (SKB 2014c).

**Table 2-1. Climate cases considered in the SR-PSU safety assessment.**

| Case number | Climate Case | Description |
|---|---|---|
| 1 | *Global warming* | Temperate conditions until 50 ka AP followed by natural variability and cooling of climate until 100 ka |
| 2 | *Early periglacial* | As case 1 except for a 3 ka period of periglacial conditions centered at 17 ka AP |
| 3 | *Extended global warming* | Temperate conditions until 100 ka AP |
| 4 | *Weichselian glacial cycle* | Repetition of reconstructed last glacial cycle conditions |

According to the description provided in SKB (2014d), the first three climatic cases are related to future scenarios with different human carbon emissions. The early periglacial climate case considers low human carbon emissions and a relatively fast decrease in atmospheric $CO_2$ concentrations. The global warming climate case is associated to an intermediate level of human carbon emissions and the extended global warming climate case represents high human carbon emissions. The last climate case is the Weisschselian glacial cycle climate which represents a repetition of the last glacial cycle. Figure 2-3 provides a schematic representation of the temporal evolution of the aforementioned climate cases. The cases are based on the processes that have been identified as relevant for long-term repository safety and on the present scientific knowledge and uncertainties of future climate evolution (SKB 2014c).

The Weichselian glacial cycle climate case describes a climate evolution fully dominated by natural climate variability (i.e. without anthropogenic influence). The present scientific knowledge indicates that the Earth´s climate evolution will differ significantly from that observed in the past. Based on the other three climatic cases, the following general conclusions have been summarized in SKB (2014a):

- During the first 1,000 years after closure the climate is predicted to remain temperate. Most of the activity will decay and the engineered barriers are expected to retain their properties.
- During the period from 3000 AD to 20,000 AD, the climate continues to be temperate, possibly with some sporadic shallow permafrost and the shoreline may be considerably displaced.
- From 20,000 AD until around 100,000 AD different and relatively long frozen periods can occurs.

Based on the SR-PSU reference evolution, two variants of the main climatic scenario are defined: i) the global warming climate case and ii) the early periglacial climate case (Figure 2-3).

The temperate domain is characterized by the absence of permafrost and a temperate climate in a broad sense, with cold winters and either warm or cold summers. Precipitation occurs throughout the year, as either rain or snow.

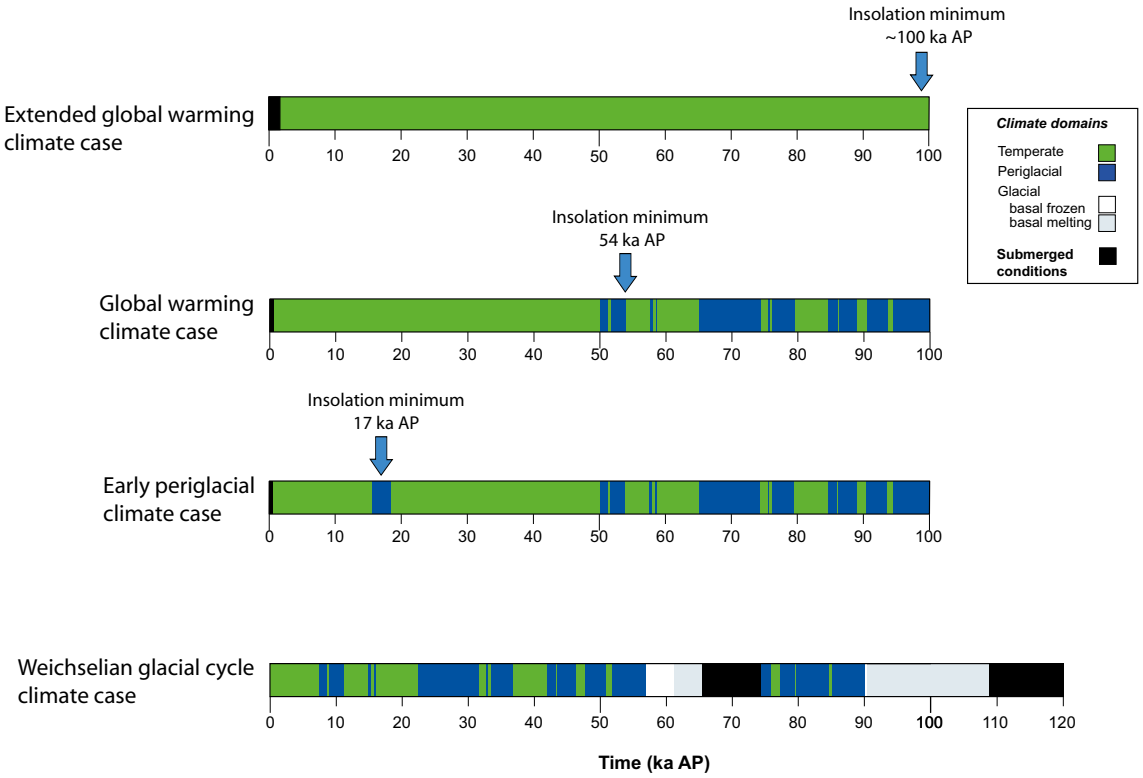


***Figure 2-3.*** *Summary of future climate cases analysed in the SR-PSU safety assessment. The cases go from warmer/wetter climates at the top to colder/dryer climate at the bottom. Taken from SKB (2014d).*

The term periglacial is used for a range of cold but non-glacial processes with permafrost as a central but not defining element (French 2007). In this climate domain the atmospheric temperature remains at or below 0°C for at least two years in a row and permafrost can grow depending of different factors such as the heat balance at the ground surface, the thermal properties of the rock, the nature of the ground surface and the geothermal gradient. However, it is important to mention that regions included in the periglacial climate domain are not necessarily the same as regions with a climate that supports permafrost growth. The periglacial domain has a cold climate, colder than the temperate domain, but warmer than periods with a glacial domain.

Nevertheless, as it can thus not be ruled out that a glaciation will occur in the area during the 100,000 year considered for the safety assessment (SKB 2014c), a glacial conditions scenario shoud be taken into account as a less probable scenario (SKB 2014a). The *glacial climate domain* is defined as regions that are covered by glaciers or ice sheets. This climatic domain has the coldest temperatures of the three climate domains and abundant precipitations in the form of snow.

Specifically for SFR and due to the relatively short half-life of the stored radioactive waste, SKB and the regulatory authorities highlighted the first thousand years as the most important period that require the most detailed analysis (SKB 2013, 2014a). In agreement with this recommendation, two different climatic domains have been considered in order to simulate the hydrochemical evolution of groundwaters at repository level: the temperate and the periglacial periods.

### 2.1.3 Hydrogeological conditions

The reactive transport calculations presented in this report are heavily dependent on the groundwater-flow models used in the framework of the SR-PSU project, from which they inherit all the hydrogeological inputs (i.e. recharge paths and related travel times). These flow models (i.e. Odén et al. 2014, Öhman et al. 2014, Vidstrand et al. 2014), in turns, are built based on the conceptual information gathered during the SFR site investigation (SKB 2013) and summarized in the site-descriptive model, SDM-PSU.

In the aforementioned groundwater flow models, the hydraulic properties of the geological medium are described based on three types of hydrogeological units:

- The Hydraulic Conductor Domain (HCD): represents well known deformation zones, which are deterministically represented.
- The Hydraulic Rock mass Domain (HRD): represents the (less) fractured bedrock in between deformation zones. It is generated using stochastic Discrete Fracture Networks (DFNs).
- The Hydraulic Soil Domain (HSD): represents the regolith; i.e. the soil and loose material that covers the bedrock (e.g. Quaternary deposits, filling material, atc.)

All the hydrogeological units are upscaled over an Equivalent Continuous Porous Medium (ECP) and groundwater flow is solved using the code DarcyTools (Svensson 2010). Our reactive transport models implicitly neglect the HSD, as all the calculations are carried out along recharge paths that start at the interface between the HRD and the HSD.

Concerning the hydrogeological models for the temperate conditions (Öhman et al. 2014), these focus on assessing how the progressive shoreline retreat will alter the current groundwater flow conditions. One of the key results of these models is that, due to the ongoing shoreline displacement, the Forsmark-SFR site will change from a discharge area to a recharge area at approximately 3000 AD (Odén et al. 2014). For this reason, recharge travel times decrease dramatically if compared to the ones computed using current groundwater conditions (see Section 2-3-1). Once the shoreline has reached the SFR1 location, the local groundwater system will evolve towards a steady-state situation that will be mainly controlled by the local topography.

The groundwater flow models for periglacial climatic conditions were developed by Vidstrand et al. (2014). The authors assessed different variant cases with different bedrock properties (i.e. “low-flow”, “base case” and “high flow” bedrock properties) and with variable permafrost depth (shallow and deep). The general conclusions of the authors are that during periglacial climate conditions the flow through the rock vaults is significantly decreased and that the resulting path lengths are significantly increased.

### 2.1.4 Geochemical conditions

Future geochemical conditions will be influenced by the evolution of climate and climatic-related conditions (i.e. shoreline displacement, permafrost development). In consequence, water flow and chemistry will change. In the surroundings rock volume of the SFR nuclear repository, the water-rock interactions processes in the geosphere can be described by advective and diffusive reactions with the fracture system and the rock matrix, respectively. Thus, the mineralogy of the facture fillings and chemical composition of infiltration water will be determinant factors for the future evolution of the groundwater at repository depth and therefore, for the global evolution of the system.

SFR is covered today by the Baltic Sea, and infiltrating water can be characterized as a brackish water. However, due to the ongoing shoreline displacement (see Section 2.1.3), the boundary conditions (i.e. infiltrating waters) will evolve in time and the influence of altered meteoric water is expect to become more important.

In terms of chemical processes, the most relevant chemical reactions that could affect the water composition are mineral dissolution/precipitation, ion exchange reactions and sorption. The most reactive minerals will dissolve/precipitate to attain equilibrium conditions and the less reactive ones will kinetically react under kinetic control. In addition, minerals with large specific surface area (i.e. clay minerals) could potentially behave like active solid exchangers for mono- and divalent cations. Ion exchange processes can be described by reversible chemical reactions that take place between ions held near a mineral surface and ions in groundwaters in contact with the mineral. Exchange reactions are particularly important due to their ability to control uptake/release processes in aquifers exposed to intrusion of meteoric, marine or glacial waters. Generally, ion exchange processes result in the retardation of solute transport.

Complexation is other process that could influence the sorptivity of solutes. However, this process is highly dependent on the redox conditions, pH and concentration of complexing agents. Due to the lack of information about complexing agents in the groundwaters, this process have not been included in our simulations. A more detailed description of the geochemical model constraints (conceptualization and parameterisation) is presented in Section 2.4.

## 2.2 Methodological approach of the reactive transport simulations

The reactive transport simulations have been carried out using the FASTREACT approach. FASTREACT (Trinchero et al. 2014a) is based on the theory of Stochastic-Convective (SC) models (Shapiro and Cvetkovic 1988). In most cases, these models rely on the assumption that local-scale dispersion can be neglected and flow is steady. Under these conditions, a geometrically complex transport problem can be reduced to a set of streamlines that in turn can be treated independently. Specifically, when transverse local dispersion is neglected, no mass exchange occurs between adjacent streamlines, which then can be handled separately in the transport model (see Figure 2-4).

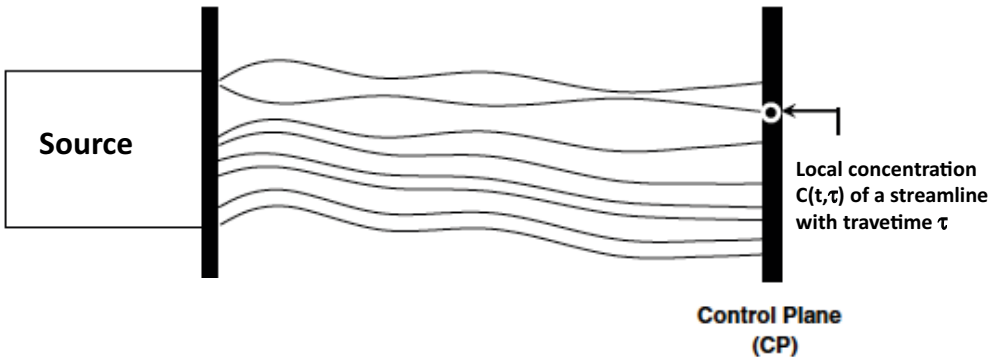


***Figure 2-4.*** *Schematic representation of a transport problem decomposed into a set of independent streamlines (modified from Malmström et al. 2008).*

The methodology consists of the following steps:

- Step 1. Collection of information on advective transport, i.e. solute travel times, associated with one or multiple sets of streamlines in the transport domain of interest.
- Step 2. Parameterisation and calculation of one or several one-dimensional reference reactive transport simulations.
- Step 3. Modelling of reactive transport by coupling the reactive reference simulation(s) and travel times along the considered set(s) of streamlines.

One of the key point of FASTREACT is that the concentration of the whole set of streamlines is typically provided by one single reference simulation. This simulation is carried out over a one-dimensional domain that is discretized into N nodes each of them having a related residence time expressed as:

$$\tau_j^{RS} = \frac{v}{d_j} \qquad \text{(Equation 2-1)}$$

where $v$ is the advective groundwater velocity in the reference simulation and $d_j$ is the distance of the $j$-th node from the inlet boundary. It turns out that the travel time of the $i$-th streamline is approximated as:

$$\tau_i = \tau_k^{RS} \qquad \text{(Equation 2-2)}$$

being $k$ the cell of the reference simulation with the closest residence time. This approximation implies that there is an explicit relationship between the parameterization of the reference simulation (Step 2) and the accuracy of how the underlying distribution of travel times is reproduced. In fact, if we consider a 1D reference simulation that is discretized into equally-spaced grid cells of size $\Delta x$, we get a discrete distribution of travel times that has a time-bin width $\Delta\tau=\Delta x/v$ . It turns out that, when the reference simulation has a "fine" spatial discretization (i.e. small $\Delta x$ / short $\Delta\tau$) the approximation to the underlying distribution of travel times (i.e. the travel times of the ensemble of considered streamlines) is good and vice versa (Figure 2-5). In the same expression, the link between the considered particle travel time and the related node of the reference simulation is given by:

$$k = \mathrm{int}\left(\frac{\tau_i \cdot v}{\Delta x}\right) + 1 \qquad \text{(Equation 2-3)}$$

where k is the node number.

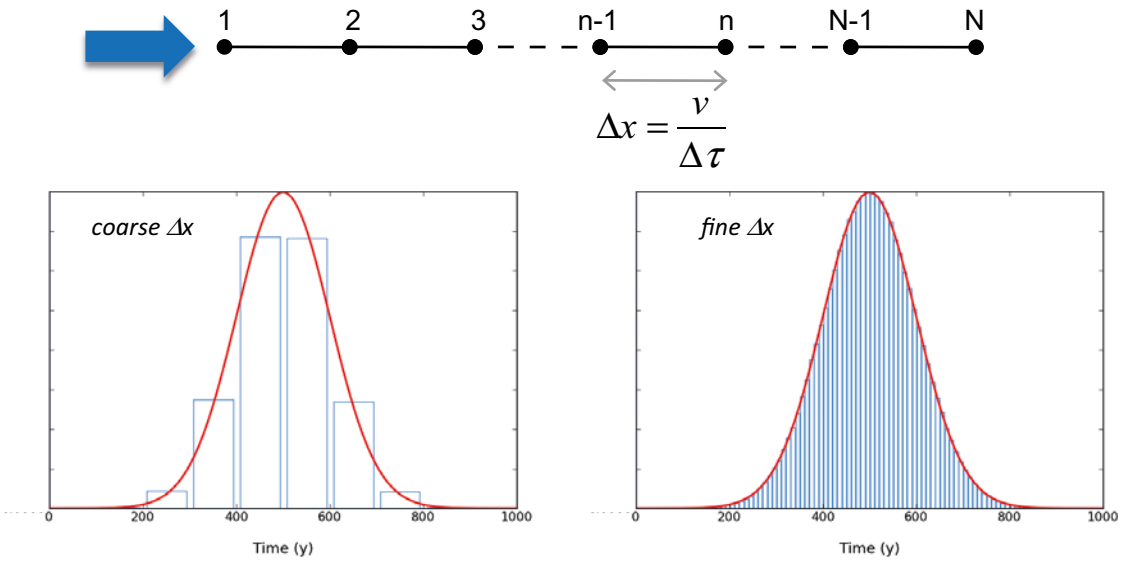


***Figure 2-5.*** *A reference 1D simulation, with constant velocity, v, and constant grid size, Δx, is defined and used in FASTREACT. Depending on its discretization, the travel time PDF of the considered set of streamlines (red line – bottom) is poorly approximated (bars – bottom left) or well represented (bars – bottom right).*

When the ensemble of streamlines shows a very heterogeneous behaviour (i.e. when the travel time histogram spans many order of magnitudes), it is convenient to subdivide them in different sub-groups according to their travel times (e.g. extremely slow, slow, fast and extremely fast streamlines).

An illustrative sketch of the functioning of the FASTREACT methodology is shown in Trinchero et al. (2014a), (Figure 2-6).

## 2.3 Analysis of travel times

As specified in Section 2.2, in FASTREACT travel times are explicitly assimilated from sets of particle trajectories computed by external hydrogeological simulators. These travel times are then used to provide time-variable maps of concentration at the interface between the different tunnel vaults and the surrounding rock.

Thus, the first step of this modelling exercise required to analyse the travel time of a number of representative recharge paths (i.e recharge trajectories from the surface to repository depth). This was done using the results of particle tracking calculations carried out for the temperate (Öhman et al. 2014) and the periglacial period (Vidstrand et al. 2014). Each of these calculations, which are referenced in Appendix 1 and have not been performed by the authors of this report, consists of 1 million particles, which were backtracked from both SFR1 and SFR3 to the surface. Particles were released at repository depth proportionally to fluxes and this is why their distribution is uneven (Figure 2-7).

A visual analysis of the location of the recharge points was also performed. This analysis determines the type of boundary water that is used for each set of streamline-based reactive transport calculations (e.g. altered meteoric water is used for the calculations along recharge trajectories starting from the inland; whereas marine water is used for those pathways, if any, which originates from the sea).

For the temperate period, the FASTREACT calculations are performed using the hydrogeological base case "TD11 BASE_CASE1_DFN_R85". The repository layout is the same described in Task Description TD11 (Öhman et al. 2014). The following periods are simulated: 2000 AD, 2500 AD, 3000 AD, 3500 AD, 5000 AD and 9000 AD.

For the periglacial conditions, one single FASTREACT calculation is carried out from SFR1 and SFR3. This calculation is representative of the shallow permafrost and the bedrock base case (Vidstrand et al. 2014).

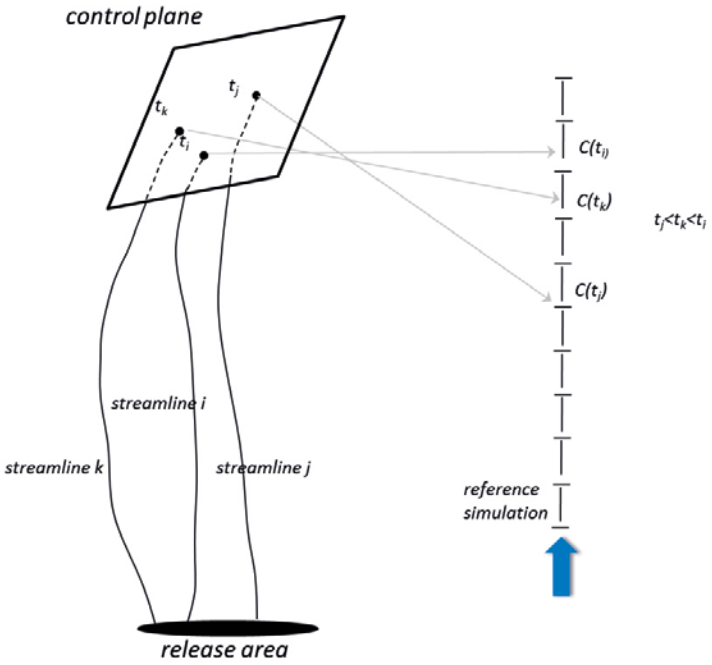


***Figure 2-6.*** *Illustrative sketch showing the use of FASTREACT to provide maps of concentrations at the intersection between the ensemble of streamlines and a given control plane.*

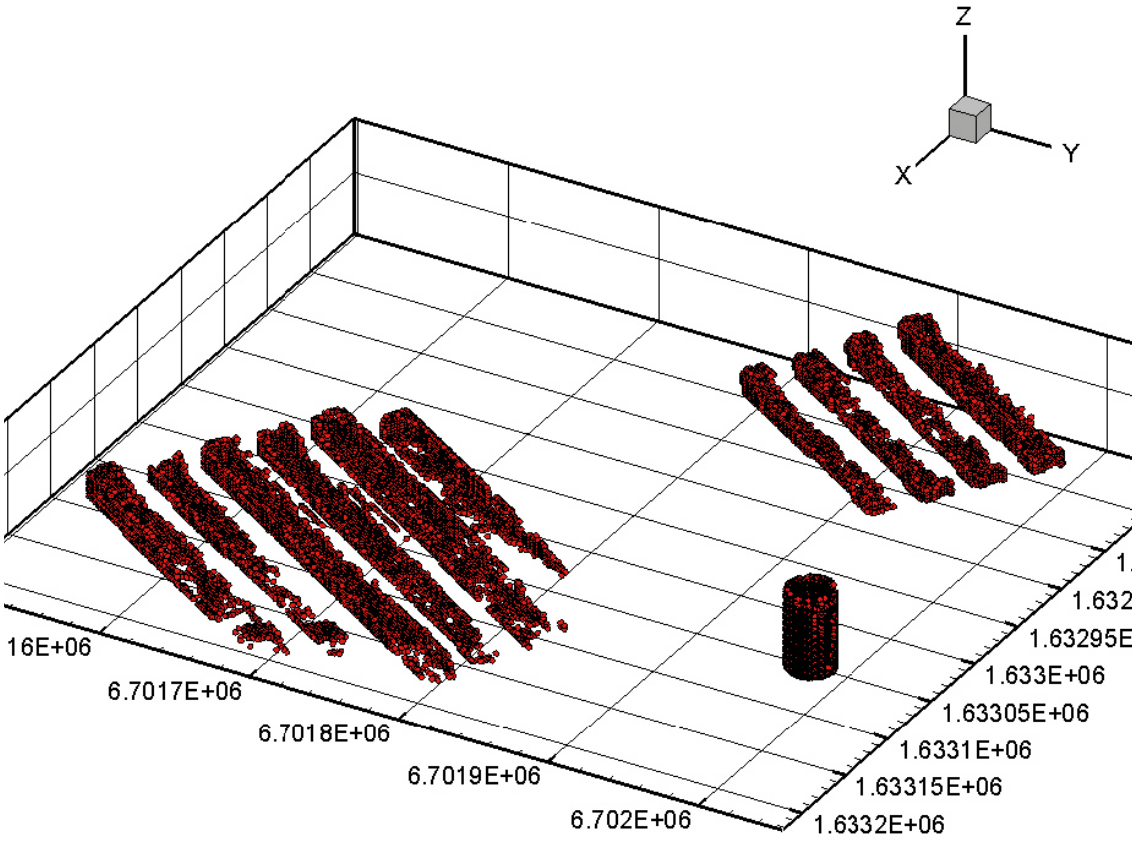


***Figure 2-7.*** *View of the release location for the 1 million particles injected at SFR1 and SFR3 for the temperate calculations. Each particle is represented as a small circle having a black edge and filled with red color.*

As explained in Section 2.1.3, in order to parameterize the reference(s) simulation(s) of FASTREACT, an exhaustive analysis of the recharge paths is needed. This analysis must focus on:

- Recharge locations. They determine the boundary water to be used in the reactive transport simulations (e.g. sea-water or altered meteoric water).
- Travel time distributions. They determine the length and discretization of the underlying reference simulation (see Figure 2-5 and Section 2.2).

### 2.3.1 Temperate period calculations

For the temperate simulation, the travel time histograms of the ensemble of recharge paths of SFR1 and SFR3 are shown in Figure 2-8 and Figure 2-9 respectively.

The recharge locations at the different times are shown in Figure 2-10 to Figure 2-15. In this set of figures, red dots indicate recharge locations for SFR1 whereas blue dots show recharge locations for SFR3. Blue and red dots are not always clearly distinguishable as in many cases recharge locations coincide. In these figures, the position of the shoreline is also shown.

Full reference to the afore-mentioned data sets, which were computed by Öhman et al. (2014), is provided in Appendix 1.

Concerning the travel times, one can notice that flow conditions are quite heterogeneous and slow during the first 500 years (i.e. 2000 AD). If one looks at the percentiles (Table 2-2 for SFR1 and Table 2-3 for SFR3), it is evident that from 2500 onward, travel times become very short (e.g. for SFR1, 90% of the particles have travel times shorter than 40 y at 2500 AD and 6 y at 3000 AD). From 3000 AD the system reaches quasi steady-state conditions and no major changes occur.

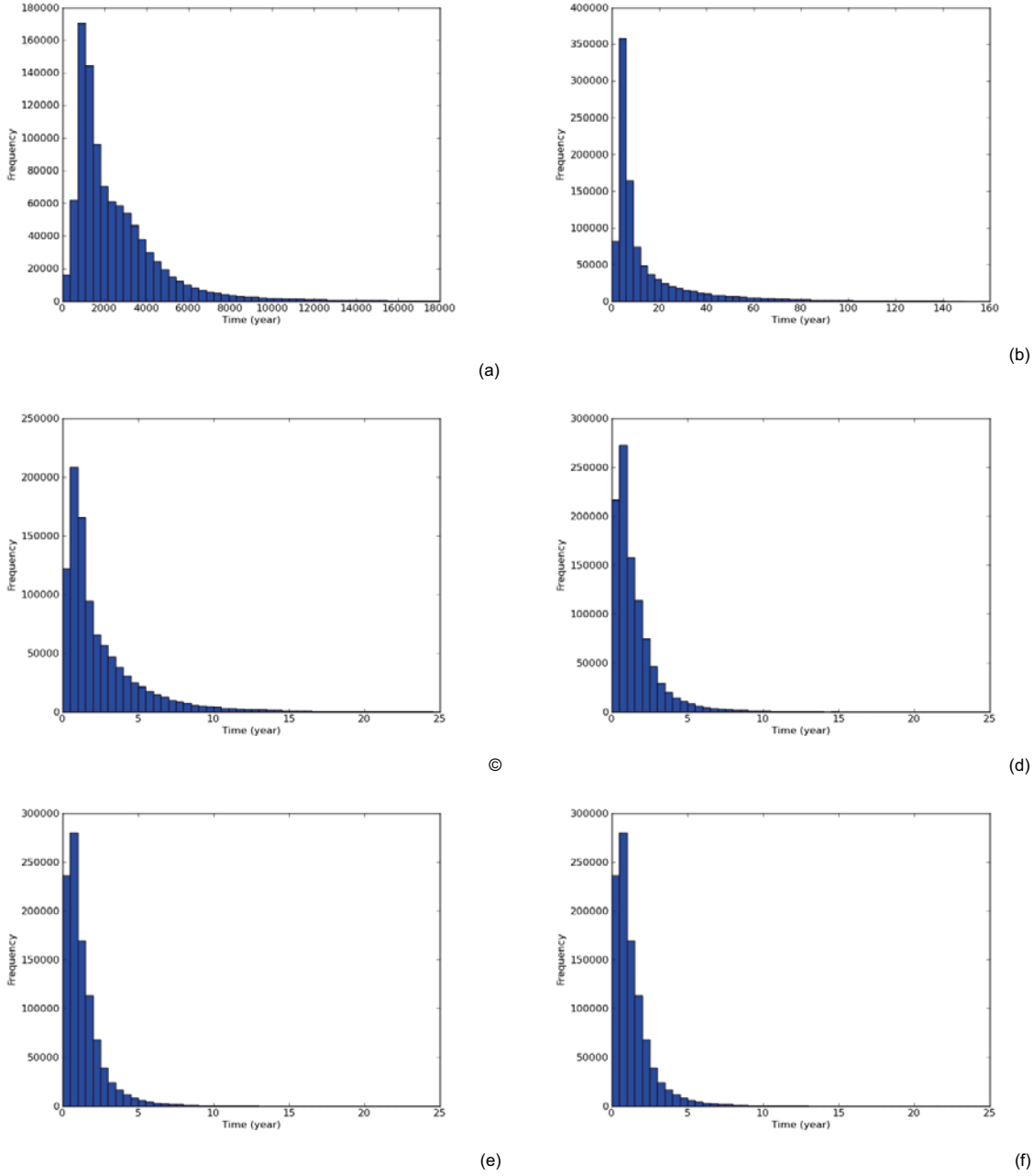


***Figure 2-8.*** *Travel time histograms for the ensemble of recharge paths ($1{\cdot}10^6$) of SFR1 at (a) 2000 AD, (b) 2500 AD, (c) 3000 AD, (d) 3500 AD (e) 5000 AD and (f) 9000 AD.*

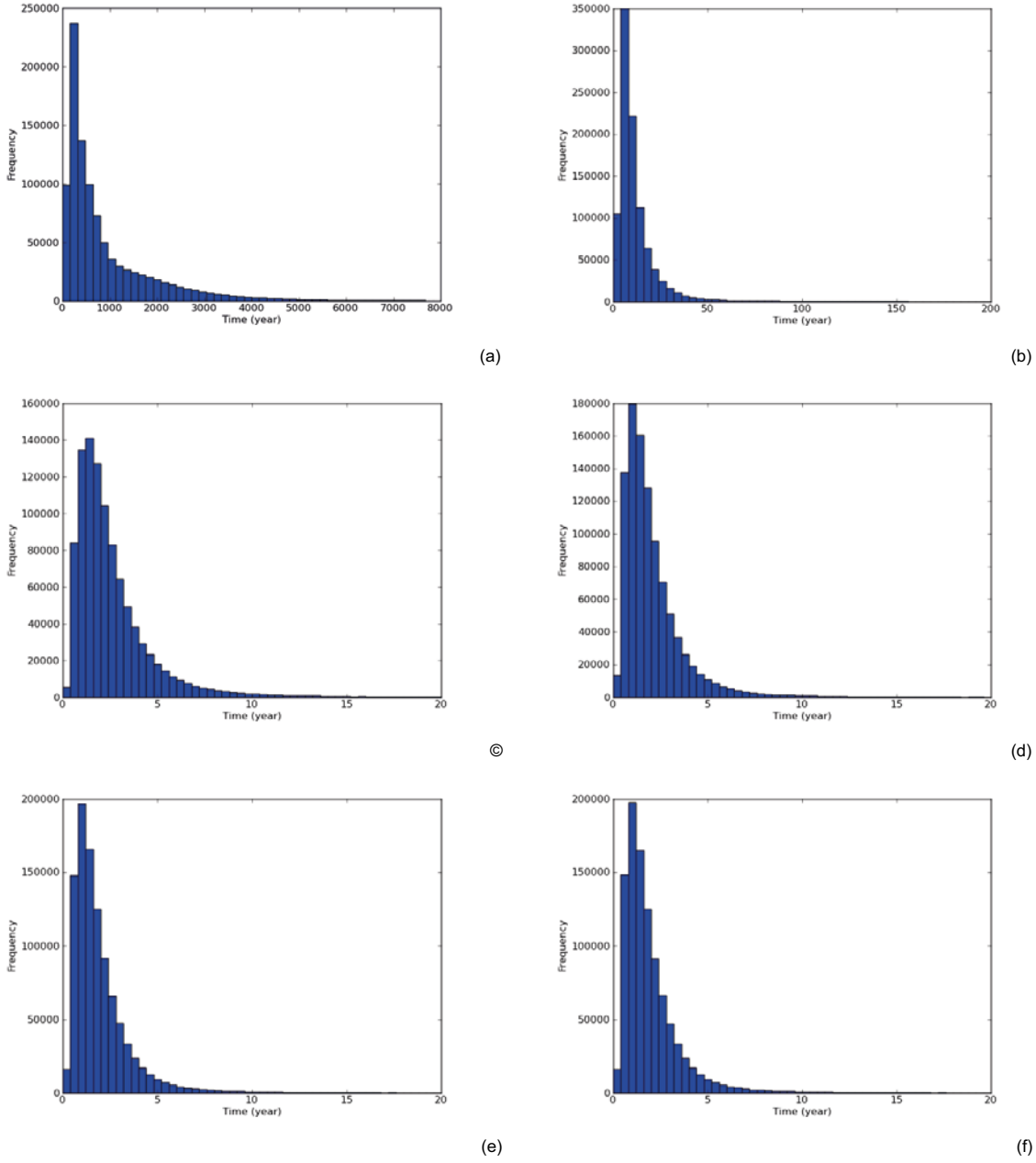


***Figure 2-9.*** *Travel time histograms for the ensemble of recharge paths ($1 \cdot 10^6$) of SFR3 at (a) 2000 AD, (b) 2500 AD, (c) 3000 AD, (d) 3500 AD (e) 5000 AD and (f) 9000 AD.*

Looking at the recharge locations one can infer similar conclusions. At 2000 AD ( Figure 2-10 and Figure 2-11) particles infiltrate predominantly through the topographic high while at 2500 AD some of the particles infiltrate directly from the pier located above the repository while another group of particles infiltrates from the topographic high (Figure 2-12 and Figure 2-13). At 5000 AD almost all the particles infiltrate from above the repository (this explains the very short residence times observed) (Figure 2-14 and Figure 2-15). No major differences are observed in the infiltration patterns of SFR1 and SFR3.

As specified in the methodological section, one of the underlying assumptions of the FASTREACT methodology is that flow is at steady state. For these specific simulations (i.e. temperate period) and the related time frame of analysis (i.e. 10,000 y) this assumption seems to be particularly restrictive as the land uplift results in an intrinsically transient regime. Yet, the analysis of the travel time histograms (Figure 2-8 and Figure 2-9) shows that big changes in flow occur in the first 1,000 years. More specifically, in the first 500 years (i.e. from 2000 AD to 2500 AD) groundwater flow velocities are quite slow

while from 2500 AD onward, flow conditions become very fast. From 3000 AD onward the system reaches a quasi-state-state regime (this is further confirmed by the analysis of the percentiles Table 2-2 and Table 2-3). Furthermore, the histograms of travel times at 2500 AD and 3000 AD are qualitatively similar and resemble a log-normal distribution, with the same variance but different mean values. This is mathematically equivalent to scaling the travel time at 2500 AD by a scaling factor, C:

$$t_{3000\ AD} \approx C \cdot t_{2500\ AD} \qquad \text{(Equation 2-4)}$$

This empirical value has been inferred by visually fitting the travel time histograms for the ensemble of recharge paths ($1 \cdot 10^6$) of SFR3 at 2500 AD and 3000 AD with two parametric log-normal PDFs, having the same standard deviation but different mean value (see Figure 2-16). The resulting value is C=0.28.

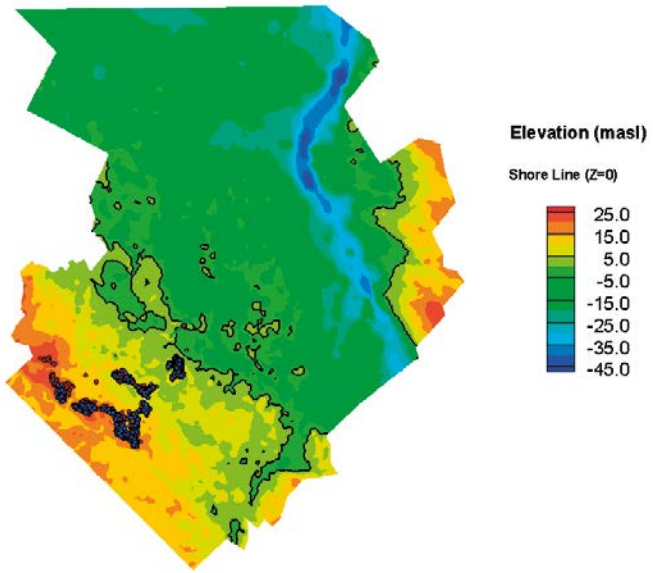


***Figure 2-10.*** *Recharge locations for SFR1 (red dots) and SFR3 (blue dots) at 2000 AD. The black line indicates the shoreline position.*

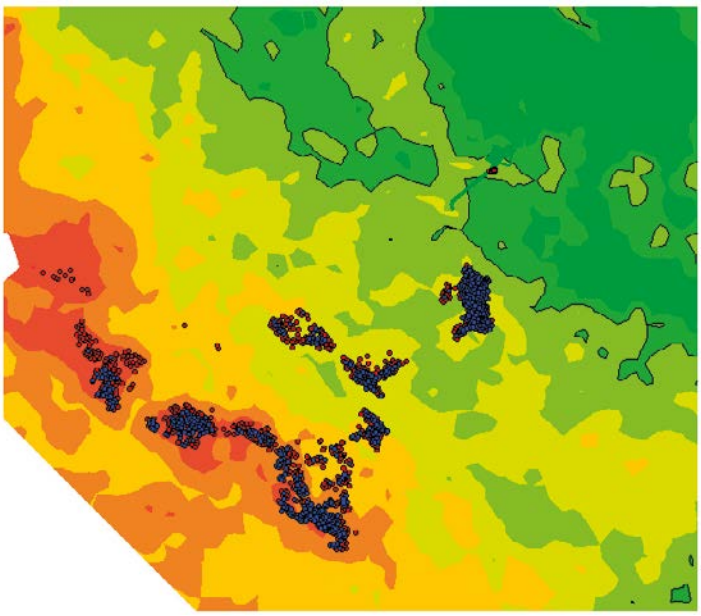

***Figure 2-11.*** *Zoom of the recharge locations for SFR1 (red dots) and SFR3 (blue dots) at 2000 AD. The black line indicates the shoreline position.*

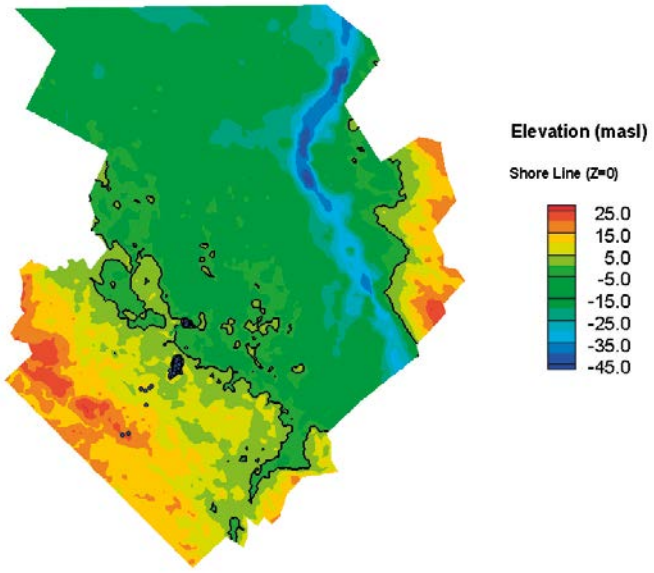


***Figure 2-12.*** *Recharge locations for SFR1 (red dots) and SFR3 (blue dots) at 2500 AD. The black line indicates the shoreline position.*

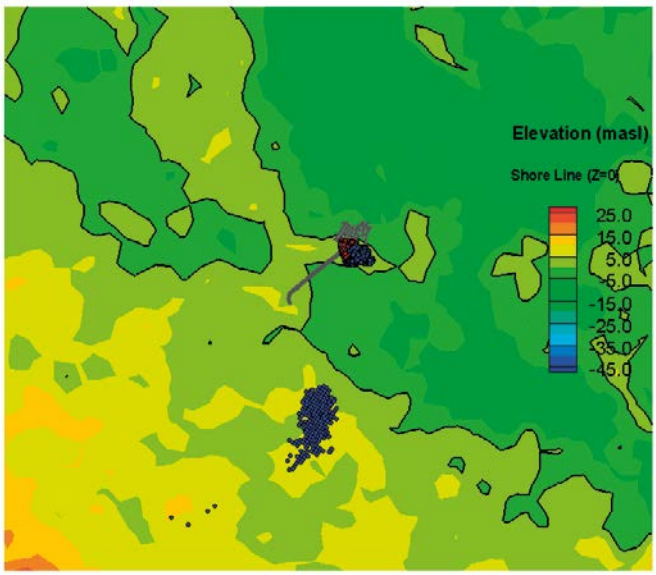


***Figure 2-13.*** *Zoom of the recharge locations for SFR1 (red dots) and SFR3 (blue dots) at 2500 AD. The black line indicates the shoreline position.*

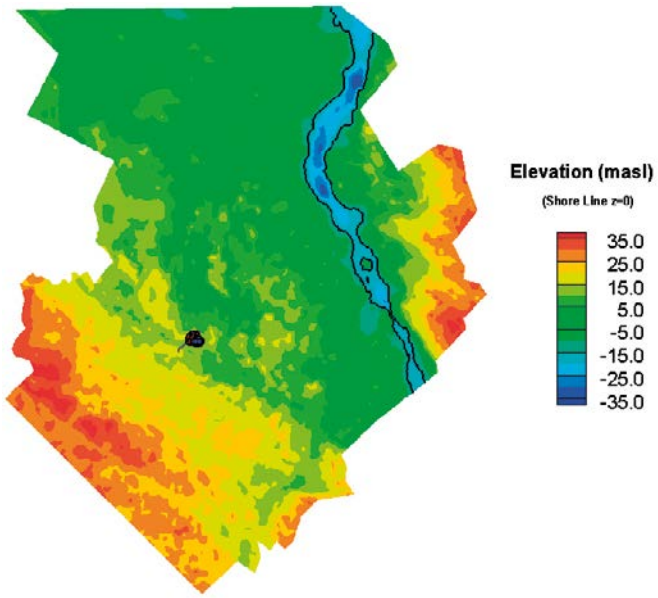


***Figure 2-14.*** *Recharge locations for SFR1 (red dots) and SFR3 (blue dots) at 5000 AD. The black line indicates the shoreline position.*

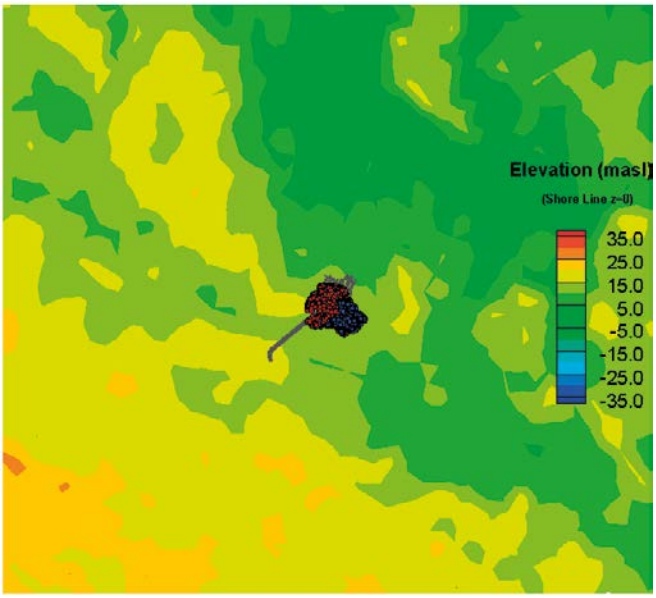


***Figure 2-15.*** *Zoom of the recharge locations for SFR1 (red dots) and SFR3 (blue dots) at 5000 AD. The black line indicates the shoreline position.*

**Table 2-2. Percentiles of travel times(y) for the $1 \cdot 10^6$ particles injected at SFR1 at the different simulation periods.**

| Percentile | 2000 AD | 2500 AD | 3000 AD | 3500 AD | 5000 AD | 9000 AD |
|---|---|---|---|---|---|---|
| 1 | $2.73 \cdot 10^2$ | 2.08 | $2.36 \cdot 10^{-1}$ | $1.64 \cdot 10^{-1}$ | $1.54 \cdot 10^{-1}$ | $1.54 \cdot 10^{-1}$ |
| 10 | $7.75 \cdot 10^2$ | 3.16 | $4.45 \cdot 10^{-1}$ | $3.12 \cdot 10^{-1}$ | $2.93 \cdot 10^{-1}$ | $2.93 \cdot 10^{-1}$ |
| 25 | $1.08 \cdot 10^3$ | 4.28 | $8.10 \cdot 10^{-1}$ | $5.51 \cdot 10^{-1}$ | $5.21 \cdot 10^{-1}$ | $5.21 \cdot 10^{-1}$ |
| 50 | $1.85 \cdot 10^3$ | 6.82 | 1.52 | 1.03 | $9.63 \cdot 10^{-1}$ | $9.63 \cdot 10^{-1}$ |
| 75 | $3.36 \cdot 10^3$ | $1.69 \cdot 10^1$ | 3.39 | 1.95 | 1.76 | 1.76 |
| 90 | $5.24 \cdot 10^3$ | $4.09 \cdot 10^1$ | 6.28 | 3.30 | 2.90 | 2.90 |
| 99 | $1.62 \cdot 10^4$ | $1.36 \cdot 10^2$ | $2.01 \cdot 10^1$ | $1.06 \cdot 10^1$ | 8.90 | 8.90 |

**Table 2-3. Percentiles of travel times (y) for the $1 \cdot 10^6$ particles injected at SFR3 at the different simulation periods.**

| Percentile | 2000 AD | 2500 AD | 3000 AD | 3500 AD | 5000 AD | 9000 AD |
|---|---|---|---|---|---|---|
| 1 | $6.90 \cdot 10^1$ | 2.25 | $4.47 \cdot 10^{-1}$ | $3.77 \cdot 10^{-1}$ | $3.61 \cdot 10^{-1}$ | $3.60 \cdot 10^{-1}$ |
| 10 | $1.61 \cdot 10^2$ | 3.94 | $8.34 \cdot 10^{-1}$ | $6.81 \cdot 10^{-1}$ | $6.63 \cdot 10^{-1}$ | $6.62 \cdot 10^{-1}$ |
| 25 | $2.53 \cdot 10^2$ | 5.62 | 1.27 | 1.02 | $9.71 \cdot 10^{-1}$ | $9.70 \cdot 10^{-1}$ |
| 50 | $5.19 \cdot 10^2$ | 8.63 | 2.03 | 1.62 | 1.53 | 1.53 |
| 75 | $1.21 \cdot 10^3$ | $1.43 \cdot 10^1$ | 3.24 | 2.58 | 2.43 | 2.43 |
| 90 | $2.36 \cdot 10^3$ | $2.51 \cdot 10^1$ | 5.15 | 4.00 | 3.74 | 3.74 |
| 99 | $5.99 \cdot 10^3$ | $1.59 \cdot 10^2$ | $1.69 \cdot 10^1$ | $1.26 \cdot 10^1$ | $1.16 \cdot 10^1$ | $1.16 \cdot 10^1$ |

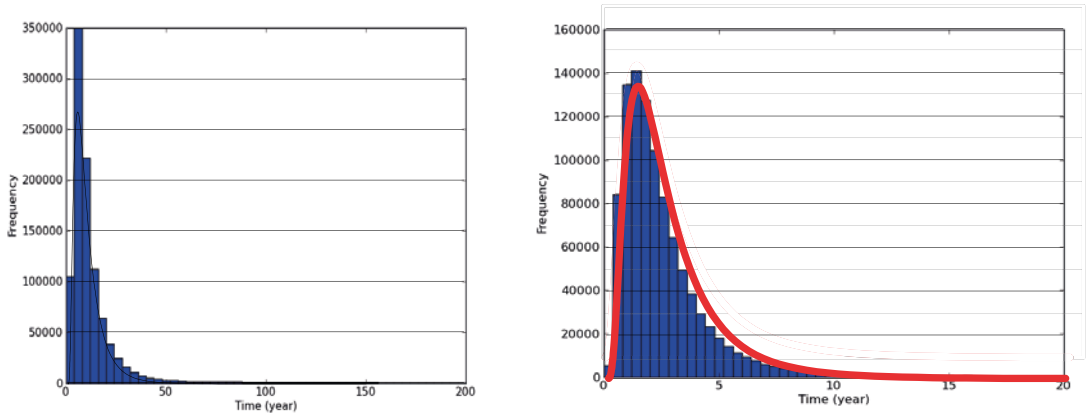


***Figure 2-16.*** *Fit between the travel time histograms for the ensemble of recharge paths ($1 \cdot 10^6$) of SFR3 at (a) 2500 AD and (b) 3000 AD and two parametric log-normal PDFs, having the same standard deviation but different mean value (i.e. 5.0 y and 1.4 y for 2500 AD and 3000 AD respectively).*

The reactive transport simulations have been started at t=2500 AD. In order to account for the afore-mentioned change in flow conditions, the underlying travel time distribution was updated after 500 years of simulation (i.e. at 3000 AD) using the afore-mentioned scaling procedure. A sketch of the simulation time frame is shown in Figure 2-17.


***Figure 2-17.*** *Sketch of the time discretization of the reactive transport simulations for the temperate period.*

### 2.3.2 Periglacial domain

The recharge trajectories used for the periglacial and glacial calculations have been taken from the results of periglacial groundwater simulations (Vidstrand et al. 2014), namely the simulation representative of the shallow permafrost and the bedrock base case (BASE_CASE1_DFN_R85). In this set of calculations, the underlying set of travel times is kept fixed during the whole simulation time frame (in the temperate calculations, travel time distributions were updated and scaled after 500 years from the beginning of the calculation).

Figure 2-18 and Figure 2-19 show the travel time histograms of the ensemble of recharge paths of SFR1 and SFR3. The two histograms, which are based on one million particle travel times, are similar and present an evident tail, which indicates that few recharge paths have very large travel times. This tailed distribution is indeed attributable to the high heterogeneity of the fractured bedrock.

The similarity between the two distributions is confirmed by the analysis of the different percentiles (Table 2-4 ). At SFR1, 90% of the recharge paths have travel time shorter than 100 years. At SFR3, the same percentile is observed for travel times shorter than 90 years. At both locations almost all the recharge paths have travel times shorter than 400 years. If one compares these distributions with the ones obtained for the temperate conditions (Table 2-3) and in particular for 2500 AD (i.e. the starting point of the temperate calculation) it is evident that travel times for periglacial domain are much slower. For instance, the ratio between percentile 50 for SFR1 computed for the periglacial and the temperate (2500 AD) conditions is 5.5.

Both distributions have been reproduced using a single reference calculation (see Section 2.2) with 400 cells having time bin width of 1.0 years. Thus, those few recharge paths having a travel time larger than 400 years have been implicitly neglected.

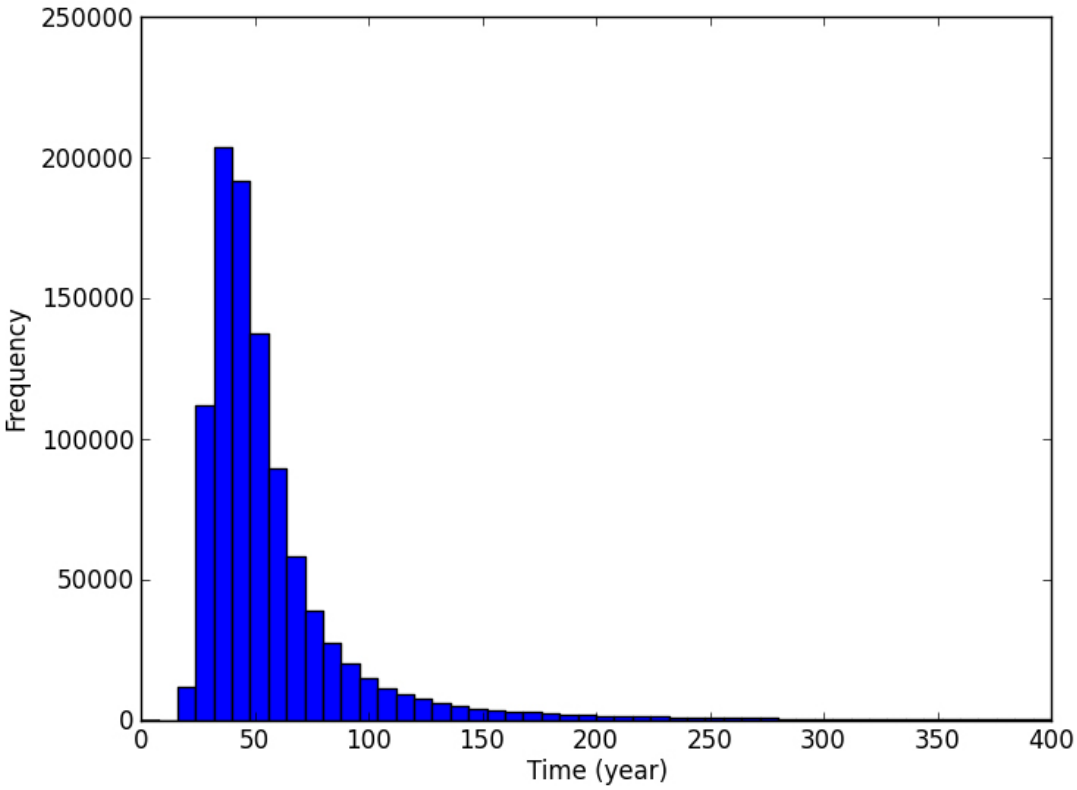


***Figure 2-18.*** *Periglacial domain – travel time histogram for the ensemble of recharge paths ($1 \cdot 10^6$) of SFR1.*

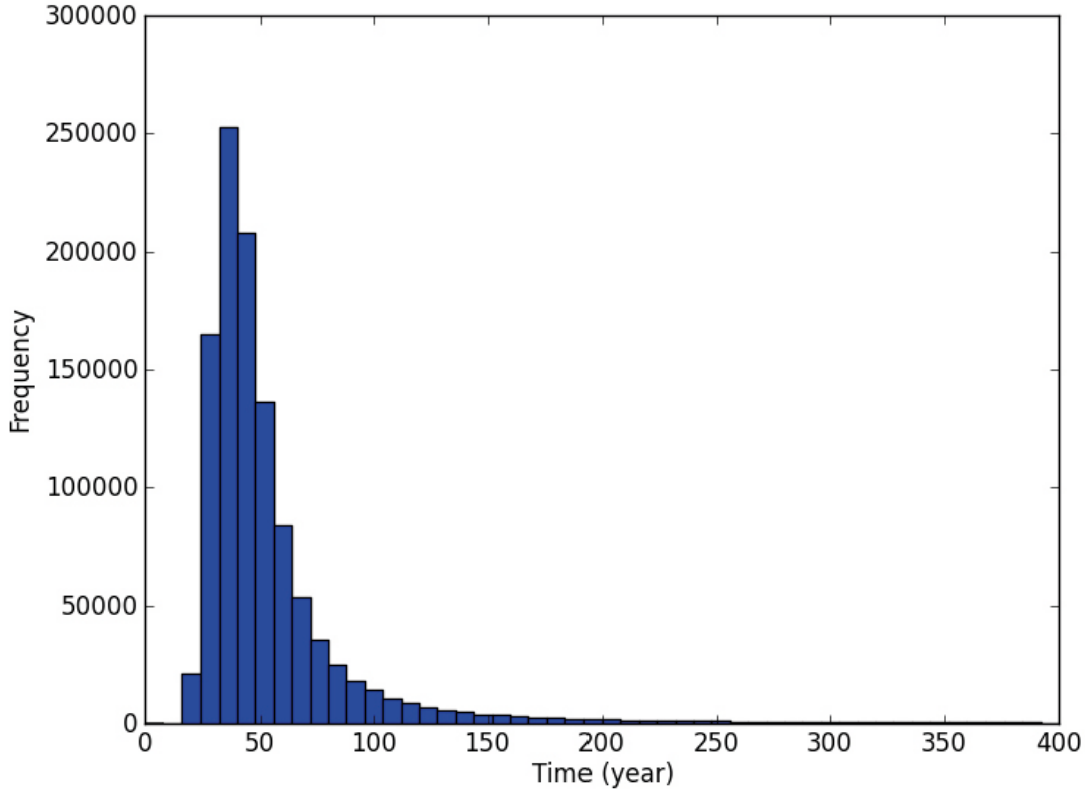


***Figure 2-19.*** *Periglacial domain – travel time histogram for the ensemble of recharge paths ($1{\cdot}10^6$) of SFR3.*

**Table 2-4. Periglacial domain – Percentiles of travel times for the $1{\cdot}10^6$ particles injected at SFR1 and SFR3.**

| Percentile | SFR1 | SFR3 |
|---|---|---|
| 1 | 23.6 | 22.7 |
| 10 | 30.9 | 29.2 |
| 25 | 37.1 | 34.9 |
| 50 | 47.1 | 43.9 |
| 75 | 64.0 | 59.5 |
| 90 | 100.0 | 91.4 |
| 99 | 448.1 | 394.5 |

### 2.3.2 Dual porosity parameters

To mimic the interplay between the "mobile" domain (i.e. deformation zones and fractures with relatively high hydraulic conductivity) and the low-conductive matrix, a dual-porosity approach has been adopted. The DP representation of the fractured medium consists of two continua (i.e. matrix and fractures), which are described by a parallel fracture model (Figure 2-20).

The values used for model parameterization are summarized in Table 2-5. The exchange at mass between the fracture and the matrix is simulated using a first-order approximation (van Genuchten 1985). The fracture aperture is assumed constant for all the considered flow paths.

It is worthwhile noting that the matrix is assumed to be inert from a chemical point of view (all the geochemical reactions take place in the fracture). The implications of this first order approximation are discussed in Appendix 2.

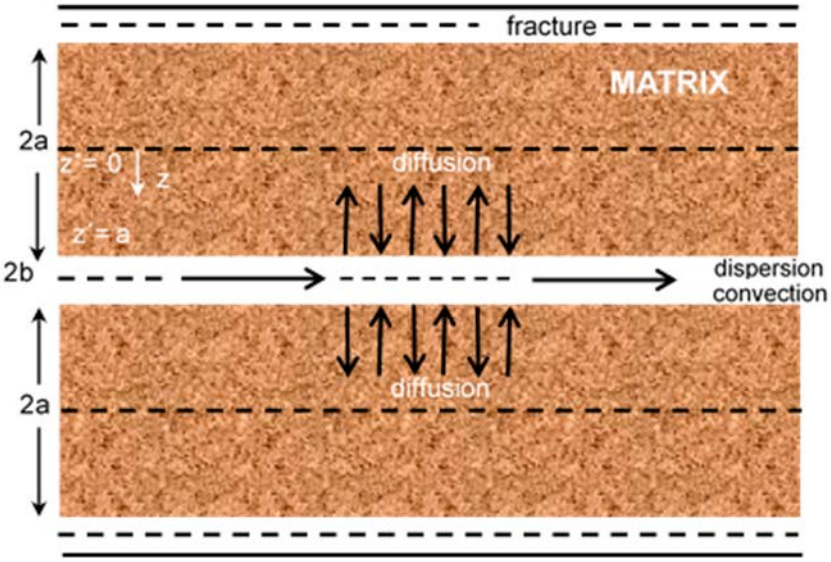


***Figure 2-20.*** *Parallel fracture model used to describe the fractured system (modified from Löfman et al. 2010).*

**Table 2-5. Parameters and values used for the DP model parameterization. The values are consistent with those used by Ecolego in the radionuclide transport calculation of the SR-PSU project.**

| Symbol | Parameter | Value |
|---|---|---|
| a | Half matrix thickness | 0.7 m |
| b | Half fracture aperture | $1.6 \cdot 10^{-4}$ m |
| $D_0$ | Effective diffusivity | $4.0 \cdot 10^{-14}$ $m^2/s$ |
| $\phi_{im}$ | Matrix porosity | $1.8 \cdot 10^{-3}$ (–) |

## 2.4 Geochemical conceptual model

### 2.4.1 Numerical Tool

The reference reactive transport simulations, on which FASTREACT is based, have been carried out with PHREEQC-2 (Parkhurst and Appelo 1999) and the database TDB_SKB-2009 (SKBdoc 1261302 ver 1.0). This database was developed by Hummel et al. (2002) and some modifications related to thermodynamic data of radionucleides and some iron and sulphur species were implemented by Duro et al. (2006) and Grivé et al. (2010). Some specific mineral phases, not included in this database, have been added in the Phreeqc inputs (Table 2-6).

**Table 2-6. List of mineral reactions included in the reactive transport models for the Base and Variant Cases.**

| Mineral | Reaction | log K |
|---|---|---|
| Calcite | $CaCO_3 + H^+ = Ca^{2+} + HCO_3^-$ | 1.85 |
| $Fe(OH)_3$ | $Fe(OH)_3 + 3H^+ = Fe^{3+} + 3H_2O$ | –1.10 |
| FeS | $FeS + H^+ = Fe^{2+} + HS^-$ | –3.00 |
| Kaolinite | $Al_2Si2O_5(OH)_4 + 7H_2O = 2Al(OH)_4^- + 2H^+ + 2Si(OH)_4$ | –37.3 |
| Siderite | $FeCO_3 + 1H^+ = Fe^{2+} + HCO_3^-$ | –0.56 |
| $SiO_{2(am)}$ | $SiO_2 + 2H_2O = Si(OH)_4$ | –2.71 |
| Gypsum | $CaSO_4 \cdot 2H_2O = Ca^{2+} + 1SO_4^{2-} + 2H_2O$ | –4.58 |

### 2.4.2 Boundary and Reference waters

The chemical composition of the boundary (meteoric and periglacial waters) and fracture waters used in calculations for the different climate domains are compiled in Table 2-7. Depending on the simulated climatic periods, different boundary and fracture water have been selected. For the temperate period, infiltrating water corresponds to a real sample of meteoric water (HBHO2, 1931 (Salas et al. 2010, p 165). Due to the lack of reported concentrations of Al and Fe, both elemental contents have been taken from the "Altered Meteoric Water" defined by Salas et al. (2010, p 37). Fracture water (*i.e.* initial water present in the fracture) is assumed to have the chemical composition defined by Auqué et al. (2013, Table 5-2) (i.e. penetrating brackish water). Aluminium concentration is assumed to be in equilibrium with kaolinite.

The selection of the boundary water for the periglacial period was based on the hydrological characteristics defined by Vidstrand et al. (2014). The landscape evolution for this period is highly uncertain, and in turn, will be influenced by the future evolution of the climate-related conditions. In this framework, shallow ponds as taliks could act as remaining permafrost patches during the melting of permafrost (Vidstrand et al. 2014) and infiltrate in the system. In order to use a representative infiltrating water for this period, we have selected a lake water sample from the water composition database of Forsmark (Tröjbom and Söderbäck 2006, Appendix 2) (Table 2-7).

A variant case, representing an extreme scenario, have been simulated by using as infiltration water a diluted water denoted as "glacial water" by Auqué et al. (2013, Table 5-3). An "evolved" water, computed at the end of the temperate simulations of this work, have been initially linked to each hydrochemical zone and defined as fracture waters at the initial state (Table 2-7).

**Table 2-7. Chemical composition of waters used in the numerical simulations. * corresponds to Al concentration in equilibrium with kaolinite. # (Salas et al. 2010). The term "altered" refers to a meteoric water which composition has been modified by equilibration with calcite, quartz, kaolinite and hematite. * (Auqué et al. 2013). ♦ (Tröjbom and Söderbäck 2006).**

| | TEMPERATE DOMAIN | | | | PERIGLACIAL DOMAIN | | |
|---|---|---|---|---|---|---|---|
| | Meteoric water | Altered meteoric water(#) | Fracture water (*) | Altered fracture water | Periglacial water (♦) | Fracture groundwater | Glacial water (*) |
| T °C | 15 | 15 | | | | | |
| pH | 7 | 7.3 | 7.3 | 7.3 | 8 | 8 | 9.3 |
| pe | | 0.55 | –3.81 | –3.81 | 0.55 | –4.47 | |
| | | | | mol/L | | | |
| Alkalinity | $1.03\cdot10^{-3}$ | $7.23\cdot10^{-3}$ | $1.48\cdot10^{-3}$ | $1.48\cdot10^{-3}$ | | | $3.72\cdot10^{-4}$ |
| Cl | $1.41\cdot10^{-4}$ | $5.11\cdot10^{-3}$ | $9.87\cdot10^{-2}$ | $9.87\cdot10^{-2}$ | $5.35\cdot10^{-4}$ | $1.41\cdot10^{-4}$ | $1.41\cdot10^{-5}$ |
| $SO_4^{2-}$ | $1.38\cdot10^{-4}$ | $8.86\cdot10^{-4}$ | $3.65\cdot10^{-3}$ | $3.65\cdot10^{-3}$ | $5.35\cdot10^{-5}$ | $1.38\cdot10^{-4}$ | $5.21\cdot10^{-6}$ |
| Ca | $3.85\cdot10^{-4}$ | $4.70\cdot10^{-4}$ | $1.50\cdot10^{-2}$ | $1.50\cdot10^{-2}$ | $1.47\cdot10^{-3}$ | $7.61\cdot10^{-4}$ | $1.70\cdot10^{-4}$ |
| Mg | $7.82\cdot10^{-5}$ | $3.09\cdot10^{-4}$ | $6.17\cdot10^{-3}$ | $6.17\cdot10^{-3}$ | $1.28\cdot10^{-4}$ | $7.82\cdot10^{-5}$ | $4.11\cdot10^{-6}$ |
| Na | $5.00\cdot10^{-4}$ | $1.19\cdot10^{-2}$ | $6.52\cdot10^{-2}$ | $6.52\cdot10^{-2}$ | $4.96\cdot10^{-3}$ | $5.00\cdot10^{-4}$ | $7.39\cdot10^{-6}$ |
| K | $5.88\cdot10^{-5}$ | $1.43\cdot10^{-4}$ | $5.13\cdot10^{-4}$ | $5.13\cdot10^{-4}$ | $5.65\cdot10^{-5}$ | $5.88\cdot10^{-5}$ | $1.02\cdot10^{-5}$ |
| Si | $1.21\cdot10^{-4}$ | $1.34\cdot10^{-4}$ | $1.83\cdot10^{-4}$ | $1.83\cdot10^{-4}$ | $8.00\cdot10^{-5}$ | $1.21\cdot10^{-4}$ | $2.13\cdot10^{-4}$ |
| Al | | $7.72\cdot10^{-8}$ | $1.00\cdot10^{-9}$ | $6.38\cdot10^{-8}$* | | | |
| Fe | | $1.79\cdot10^{-6}$ | $1.11\cdot10^{-8}$ | $1.11\cdot10^{-8}$ | | $8.43\cdot10^{-8}$ | |

### 2.4.3 Fracture Minerals

Rock and fracture mineralogy at SFR is not as widely studied as for Forsmark or Laxemar-Simpevarp areas. Within the SFR extension investigation programme, detailed fracture mineralogical studies has only been carried out on a limited set of samples which corresponds to the borehole sections sampled for groundwater chemistry and Eh (Sandström and Tullborg 2011). However, given the proximity and based on the current knowledge of the Forsmark area, some important evidences can be extended to the SFR site (Nilsson et al. 2011, Gimeno et al. 2011).

Fracture minerals constitute the primary reaction surface in the contact between groundwater and bedrock. These mineral coatings are often fine-grained (e.g. clay minerals), have large specific reactive surface and many of them (such as carbonates and sulphides precipitated on the fracture walls) are more reactive than the crystalline rock matrix minerals. Therefore, even though their quantity compared to the rock forming minerals is small, their contribution to the buffer capacity of the bedrock is important.

The available mineralogical information for the fracture fillings present in the SFR bedrock indicates that chlorite and calcite are the most abundant fracture filling minerals and they are widely distributed until 520 m depth (Sandström and Tullborg 2011) without significant variations with depth. Clay minerals, mainly mixed layer smectite-illite and illite, also appear in relatively large amounts in opened, conductive fractures. Quartz, adularia and albite are also present and other minerals, identified in lower amounts in the borehole sections, include laumontite, pyrite, barite, hematite, Fe-oxyhydroxide, muscovite, REE-carbonate, allanite, biotite, asphaltite, galena, sphalerite, arsenopyrite, uranium phosphate, uranium silicate, Y-Ca silicate, monazite, xenotime, harmotome and fluorite (Sandström and Tullborg 2011).

The fracture filling mineralogy described for SFR is similar to that found in Forsmark and Laxemar-Simpevarp sites. However, minor differences, some of which may be of significant importance for the understanding of past and present groundwater-mineral interaction, have been identified (Sandström and Tullborg 2011, Nilsson et al. 2011). For example, the amounts of clay minerals in the open, water conducting fractures are greater in the SFR drillcores compared with Forsmark and the relative abundance of different clay minerals also changes: mixed layer smectite-illite (poorly ordered) and illite are much more abundant at the SFR whereas corrensite (a mixed layer clay consisting of smectite-chlorite) is dominant at Forsmark. The important presence of clay minerals in the open water conducting fractures indicates that cation exchange reactions might play a relevant role for the groundwater evolution, contributing to the control of aqueous concentrations of calcium and other cations (Gimeno et al. 2011).

The main buffering mechanism against the infiltration of acid water is provided by calcite. This mineral is only present as trace amounts in the rock matrix but is one of the most abundant fracture filling mineral and it is widely distributed at all depths. Moreover, although the mineralogical data from the uppermost 10 m of the bedrock beneath the Baltic Sea is limited, no evidence exists of calcite dissolution (Nilsson et al. 2011).

There is no quantitative data about the amount of calcite available in the SFR fracture system. However, quantitative mapping were carried out during the Forsmark site investigation (calcite was estimated in 32% of the mapped fractures) and the data suggested for modelling purposes in the SR-Site safety analysis at Forsmark by Löfgren and Sidborn (2010) may be also considered for the SFR site (Nilsson et al. 2011).

The study of redox sensitive iron and/or sulphur minerals, such as pyrite and specially Fe-oxides and Fe-oxyhydroxides, can be used to trace the depths reached by past or present oxygenated waters (Sandström et al. 2014). At the SFR, no significant depth trends can be seen when selected redox-sensitive minerals in the sampled borehole sections are plotted against depth (Sandström et al. 2014). Fe-oxyhydroxides are present in hydraulically conductive fractures and fracture zones, suggesting that oxidised conditions have prevailed in some period of time in parts of the fracture system. Fe-oxyhydroxides are occasionally found down to an elevation of –650 m.a.s.l. as indicated by the drillcore mapping at SFR, but its presence is predominant up to to –200 m.a.s.l approximately (Sandström et al. 2014). However, the age of these oxidizing events is difficult to known and some of these minerals (e.g. hematite) are difficult to distinguish by visual inspection.

Sulphide phases occur as pyrite (arsenopyrite, chalcopyrite and galena have been sporadically described) (Sandström and Tullborg 2011) which appears irregularly distributed in the open fracture fillings in common with the Forsmark or the Laxemar-Simpevarp areas (Gimeno et al. 2011) and references therein). No occurrences of sulphides have been recorded in hydraulically conductive fractures in the upper 30 m of the bedrock at SFR, probably having been dissolved during events of intrusion of oxigenated fluids. However, no significant oxidation and/or dissolution of sulphide due to inflow of oxidised waters have been identified in the drill cores below 30 m (Nilsson et al. 2011) and the presence of pyrite at most depths would indicate prevailing reducing conditions.

### 2.4.4 Base Case and Variant Cases

When studying the hydrochemical evolution of a complex natural environment such as the bedrock of SFR, expert judgment is usually the only means to define a set of representative parameters that define the so-called Base Case. The high uncertainty related of these parameters is then addressed by means of a number of simulations denoted as Variant Cases where the values of these parameters are changed within a range provided by some underlying uncertainty distribution.

From a geochemical point of view, two different simulation cases have been defined, depending on the minerals present in the fracture filling material (Table 2-8). Dissolution/precipitation of calcite is assumed to take place under equilibrium conditions, thereby buffering the pH of the infiltrating groundwaters. The redox evolution of the system is assumed to be controlled by $Fe(OH)_{3(am)}$ for the Base Case. As the redox buffering capacity will depend on the available Fe-bearing mineral in the fracture fillings, a variant case is defined by the presence of Fe(II) sulphides reacting under equilibrium conditions. Both minerals have been reported to be present in the fracture fillings and could have a central role in the redox evolution of the system.

In this study, the "Base Case" defined in Table 2-8 will be used as the starting point for the uncertainty analysis.

**Table 2-8. Base Case and Variant Case defined for the numerical simulations.**

| Mineral | Assumption | Effects |
|---|---|---|
| **Base Case** | | |
| Calcite | Equilibrium Conditions | pH control |
| Hematite | Equilibrium Conditions | Eh control |
| **Variant Case** | | |
| Calcite | Equilibrium Conditions | pH control |
| $FeS_{(am)}$ | Equilibrium Conditions | Eh control |

As explained in Section 2.1.2, the reactive transport simulations consider two climatic periods: the temperate and periglacial domains. Nevertheless, due to the high uncertainty related to the long-term climatic prediction, the reactive transport models do not aim at reproducing a detailed continuous simulation of the whole glacial cycle but are rather focused on analyzing the impact of the different climatic domains in separate time windows.

As already discussed in Section 2.3.1, given the relatively high travel times observed at 2000 AD (i.e. mean travel times of 1,850 y for SFR1 and 519 y for SFR3), we have decided to start the reactive transport calculations at 2500 AD. In other words, based on the hydrogeological results, we assume that no major geochemical changes occur in the first 500 years (i.e. from 2000 AD to 2500 AD) and, thus, we start the calculations at 2500 AD. A sketch of the simulation time frame of the temperate period is shown in Figure 2-17. During the whole simulation, a meteoric water infiltrates (see Table 2-7) and progressively penetrates along the recharge paths.

As initial conditions of the periglacial period are uncertain, two geochemical cases, representative of two opposite situations have been defined and simulated. In the first approach a lake water infiltrate through the transmisive zone. The second approach assumes the infiltration of glacial water. The groundwater composition computed after 9,000 y for the temperate period has been used as initial conditions of the periglacial and glacial simulations (although, as explained before, the different climatic domains are conceptually treated as separate time windows). The simulation time of the periglacial domain is 10,000 years, during which the boundary waters listed in Table 2-7 (lake or glacial depending on the simulated geochemical case) progressively penetrates along the recharge paths.

In summary, 12 different reactive transport simulations have been carried out:

- SFR1 – Base Case and Temperate Domain.
- SFR1 – Variant Case and Temperate Domain.
- SFR1 – Base Case and Periglacial Domain (lake boundary water).
- SFR1 – Variant Case and Periglacial Domain (lake boundary water).
- SFR1 – Base Case and Periglacial Domain (glacial boundary water).
- SFR1 – Variant Case and Periglacial Domain (glacial boundary water).
- SFR3 – Base Case and Temperate Domain.
- SFR3 – Variant Case and Temperate Domain.
- SFR3 – Base Case and Periglacial Domain (lake boundary water).
- SFR3 – Variant Case and Periglacial Domain (lake boundary water).
- SFR3 – Base Case and Periglacial Domain (glacial boundary water).
- SFR3 – Variant Case and Periglacial Domain (glacial boundary water).

### 2.4.5 Methodological approach for the analysis of uncertainties

Uncertainty affects every modelling effort to model geochemical processes in complex natural environments. Thus, a robust uncertainty analysis is required to provide plausibility ranges to the modelled results.

One of the most important sources of uncertainty in the context of a nuclear repository settled in crystalline rocks is the chemical composition of the fracture filling and its distribution in the fractures. Most of geochemical models assume a homogeneous mineral distribution in contact with groundwaters. In this regards, the presence/absence of minerals must be assessed by means of sensitivity analysis of uncertainties varying, for instance, the minerals involved in the reactions, their amounts and surface areas, etc. To that end, a Monte Carlo-Phreeqc method was applied to provide a sensitivity study of two different processes: kinetic dissolution of silicates and cation exchange reactions, according to the geochemical constraints specified in Table 2-9.

The Monte Carlo-PHREEQC is a stochastic methodology that can be applied in order to perform a large number of sensitivity analysis but the provided results do not have spatial resolution. In the next section a description of the MC-Phreeqc approach is included. Calculations were implemented by using as reference the Base Case defined in Section 2.4.4. for the temperate domain. Reactive transport calculations were run with an associated random variable (travel time or CEC, depending on the case). The results were computed at repository level at a final time of 9000 AD. A more detailed description of the parameterization used in these simulations is provided in Section 3.3.1.

The aqueous solutions have been assumed to be affected by kinetic dissolution of silicates such as chlorite, albite, illite and K-feldspar. Silicate mineral kinetic dissolution is a slow process with great implications in pH buffering mechanisms in groundwaters. In general terms, the effect of these reactions on the water chemistry is the addition of cations and silica resulting from chemical reactions that consume protons and increase the pH according to the reactions presented in Table 2-6. The consumption of silicate minerals is controlled by the groundwater chemistry, dissolution rates and kinetics reactions. The random parameters implemented in the Monte Carlo simulation were the travel time and the reactive surface areas. The role of clay minerals as cation exchanger is computed assuming an illite-like phase to be the main solid exchanger and the model of Bradbury and Baeyens (2000) has been used to describe the reactions involved in the interface mineral/groundwater. Such model assumes cation exchange in illite based on 3 types of sites. The most abundant sites (around 80% of total cation exchange sites) are the so-called “planar sites”, which can adsorb either divalente or monovalent cations. The second and third types of sites called Type II and Frayed edge sites, whose density is much lower (20% and 0.25% of the total sites, respectively), have not been included in our model. The cation exchange reactions and related Gaines-Thomas selectivity coefficients are listed in Table 2-9. Ion exchange processes are described by reversible chemical reactions that take place between ions held near a mineral surface and ions in groundwaters in contact with the mineral. The key role of the exchange reactions is related to their ability to control uptake/release processes in aquifers exposed to intrusion of meteoric, marine or glacial waters. In this case, CEC was the random variable associated to Monte Carlo simulations.

**Table 2-9. Geochemical processes and uncertainty analysis.**

| Mineral | Geochemical Reaction | Characteristics | References |
|---|---|---|---|
| **Chlorite** | Kinetic dissolution | Source of Si, Al and Fe(II)<br>Increase of pH values | Lowson et al. (2005) |
| **K-feldspar** | Kinetic dissolution | Increase of pH values<br>Source of Al, Si and K | Sverdrup (1990) |
| **Albite** | Kinetic dissolution | Increase of pH values<br>Source of Al, Si and Na | Sverdrup (1990) |
| **Illite** | Kinetic dissolution | Increase of pH values<br>Source of Al, K and Mg | Sverdrup (1990) |
| **Clay minerals**<br>**Illite** | Cation exchange reactions | Changes on Na, K, Ca and Mg<br>Increase of pH values<br>Source of Al and Si | (Bradbury and Baeyens 2000) |
| | **Cation exchange reactions** | | |
| | Reaction | | Log K |
| Illite | $X^- + Na^+ = NaX$ | | 0.0 |
| Illite | $X^- + K^+ = KX$ | | 1.1 |
| Illite | $2X^- + Ca^{2+} = CaX_2$ | | 1.13 |
| Illite | $2X^- + Mg^{2+} = MgX_2$ | | 1.13 |

### *Monte Carlo-PHREEQC*

Due to the high heterogeneity of subsurface environments, accurate and verifiable predictions of the hydrochemical evolution of a considered site are difficult and the modelling results are always highly uncertain. This epistemic uncertainty is typically addressed by means of a limited number of sensitivity analyses, where the value of a few parameters is "manually changed" based on some expert decision. It is worthwhile stressing that sensitivity analyses are suitable to evaluate the uncertainty arising from the incomplete knowledge about a phenomenon or related parameters but are not intended to assess the implications of wrong modelling assumptions.

More rigorous uncertainty analyses involve the use of stochastic methods such as Monte Carlo simulations, moment equations, probability density function (pdf) methods, stochastic collocation methods and stochastic finite elements. In all the afore-mentioned methodologies, when parameters are mutually dependent, their dependency must be expressed using cross covariance functions.

In this modelling work, the uncertainty related to a number of hydrogeological and geochemical factors is addressed using Monte Carlo simulations. The probability density functions used to describe the parametric uncertainty of the selected variables are defined based on expert judgment (see Section 3.3.1).

The numerical simulations have been carried out using the software MCPhreeqc (de Vries et al. 2012). This software uses as input a Phreeqc input file, a PDF for each of the uncertain parameters and the settings for the Monte Carlo simulation. It comes with a graphical user interface to enter the configuration of the simulations that need to be run. In addition it can automatically generate histograms and scatter plots from the results. Simulations can be run in parallel to benefit from all the processor cores in the machine. It is written in the programming language Python and is released under an open source license (LGPL).

# 3 Geochemical evolution of groundwaters for the temperate period

## 3.1 Evolution of groundwaters at repository depth during the temperate period

During the temperate period the displacement of the Baltic shore line will influence the hydrology of the site and, as a consequence, the chemical composition of the groundwater at repository depth. The numerical calculations have been started at t=2500 AD (given the high residence times at 2000 AD, we have assumed that, no major changes occur during the first 500 years). A restart of the simulation has been done at t=3000 AD when the travel times have been scaled as explained in Section 2.3.1.

A detailed analysis of calculation results is provided for the most relevant parameters such as salinity, pH and redox conditions. In addition, other parameters including major cations, sulphide, Fe, Si and Al concentrations that could affect the stability of the engineered barriers and the migration of radioisotopes will be also discussed.

The results for the Base and the Variant Cases (see Section 3.2) are provided in terms of maps of concentrations at repository depth, box-and-whisker plots and statistics tables (Appendix 3).

## 3.2 Results

Water salinity at repository depth is related to chloride concentration. As chloride does not undergo chemical reactions, the evolution of groundwater salinity closely follows the hydrological patterns of the site. During the Temperate Period, most of the changes in chloride concentration are observed in the first 300 years of calculation (i.e. from 2500 AD to 2800 AD). More diluted water reaches progressively the repository and the variability of chloride concentrations is a direct consequence of preferential flow patterns along the transmissive zones. After 600 years, chloride contents at repository depth reach a new steady state and remain homogeneously distributed until the end of the temperate period for SFR1 (Figure 3-1 and Figure 3-2). Similar results have been obtained for SFR3 (Figure 3-2, Tables A3-1, A3-2, A3-3 and A3-4, Appendix 3).

It should be noted that the geochemical evolution of groundwaters has been calculated for a period of time of 6,500 y. However, the different climatic domains described in Section 2.1.2 assumes that the temperate period could last for 50 to 100 ky. Nevertheless, as the results highlight that a new steady-state is reached after less than 1,000 y, it has not been considered necessary to extend the simulation over such a long time-frame.

For the sake of comparison with other studies that use salinity expressed in g/L (TDS), chloride concentrations were converted into salinity values (TDS (g/L)) by using the approach defined by Salas et al. (2010), according to the following relation:

$$TDS(g/L) = Cl(g/L)/1.646 \qquad \text{(Equation 3-1)}$$

The coefficient 1.646 has been estimated from the correlation obtained of the analytical data for selected groundwaters from Laxemar, Simpevarp, Aspo and Forsmark (Salas et al. 2010). Calculated TDS values at repository depth for SFR1 and SFR3 are included in the Tables A3-1, A3-2, A3-3 and A3-4, Appendix 3.

The effects of infiltration processes on the individual chemical constituents will depend on their reactivity. Some groundwater components will behave as conservative (i.e. they do not participate significantly in chemical reactions) while others will be controlled by reactions with the fractures filling minerals.

The computed pH values range between 7 and 8 for both SFR1 and SFR3 (Figure 3-3, Figure 3-5 and Figure 3-6). The pH evolution shows a progressive and slight increase of the values as a consequence of calcite dissolution induced by diluted infiltrating waters. The evolution of alkalinity values clearly reflects this process (Tables A3-1, A3-2, A3-3 and A3-4, Appendix 3).

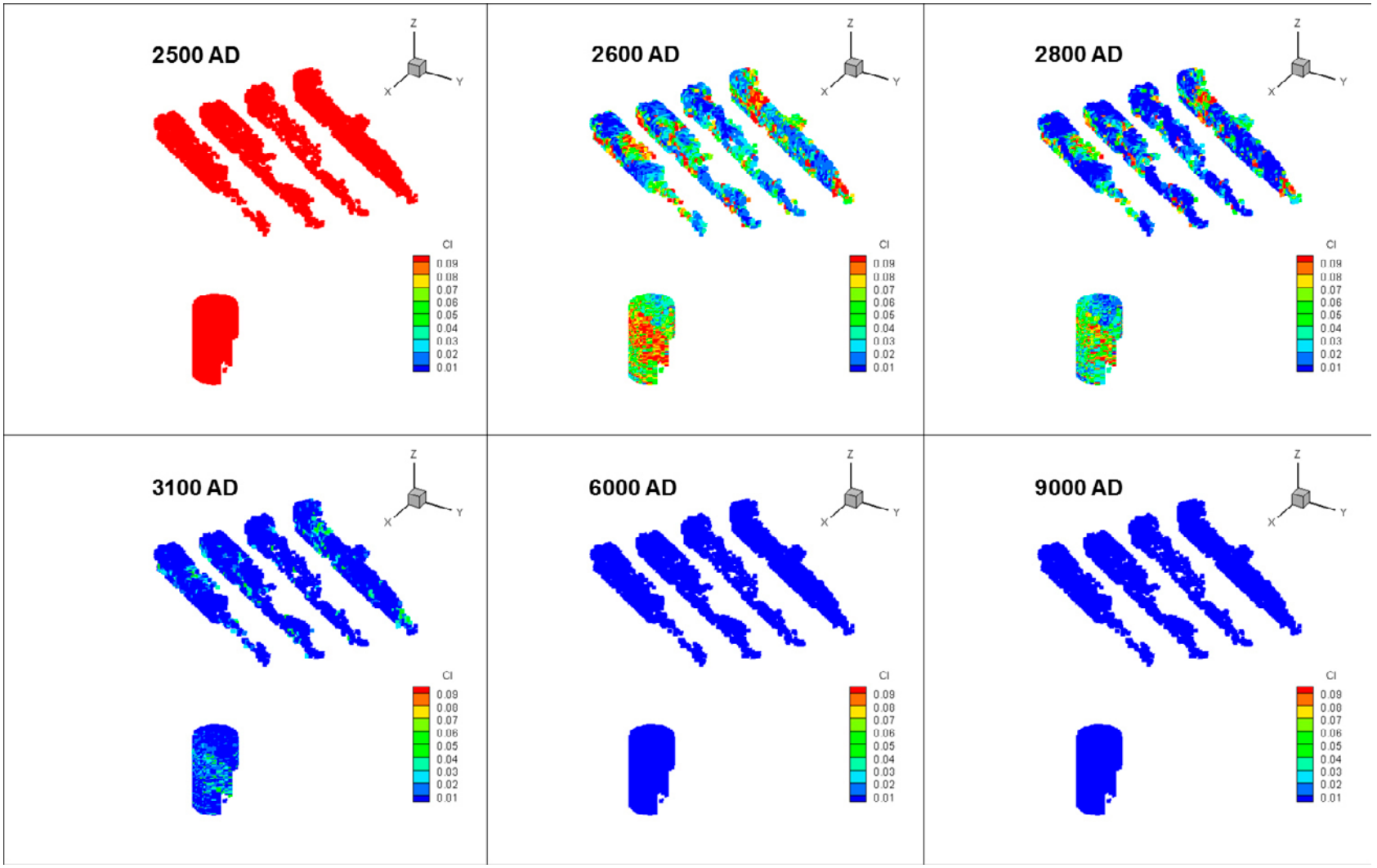


***Figure 3-1.*** *Distribution of chloride concentrations (mol/L) at SFR1 repository depth computed for the temperate period over a period time of 6,500 years.*

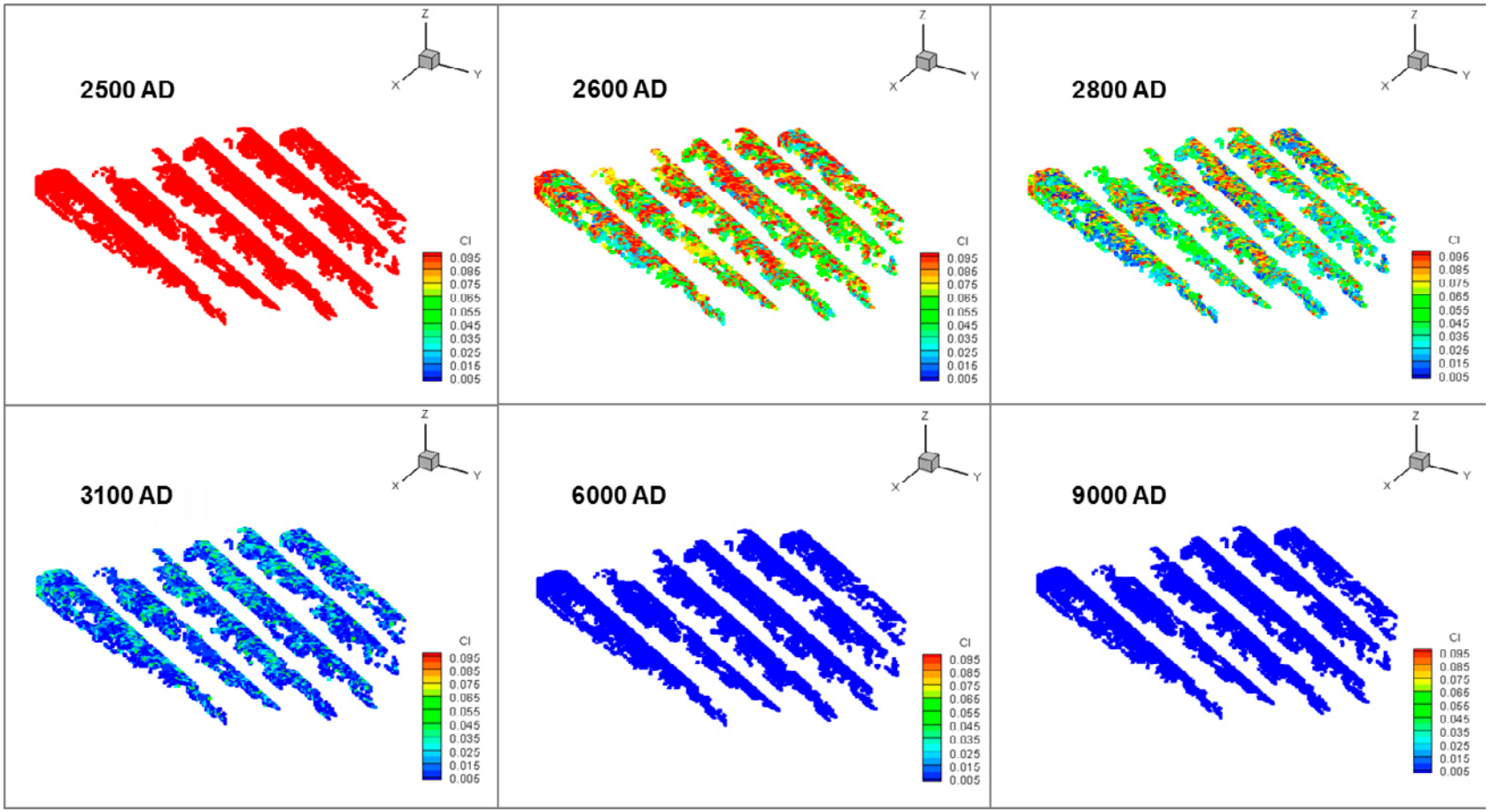


***Figure 3-2.*** *Distribution of chloride concentrations (mol/L) at SFR3 repository depth computed for the temperate period over a period time of 6,500 years.*

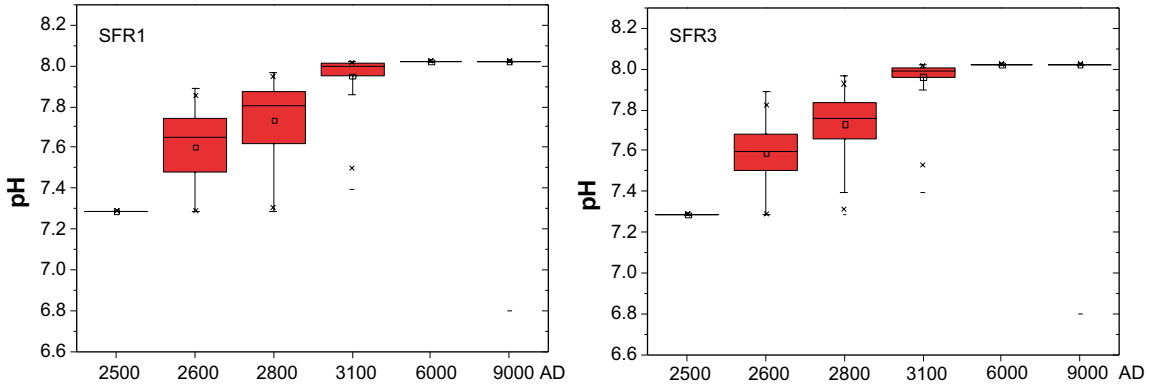


***Figure 3-3.*** *Box-and- whiskers plots showing the statistical distribution of pH at repository depth for the temperate period. The statistical measures are the median, the 25th and 75th percentile (box), the mean (square), the 5th and 95th percentile ("whiskers") and the maximum and the minimum values.*

From 3100 AD to the end of the simulation time pH attains a steady state with a value around 8. The range of pH variation computed for the temperate period, agrees with the values measured at present at SFR (7–8) in the bedrock water samples (Nilsson et al. 2011). The abundance of calcite in the fractures permits to predict a minimum risk for overestimating the pH-buffering conditions (Sandström et al. 2014).

Although Eh values measured on-site are not always reliable, they clearly evidence that anoxic conditions prevail at present in the host rocks (Auqué et al. 2013). The evolution of the redox conditions computed at repository depth shows that anoxic conditions will remain over the considered time frame controlled by equilibrium conditions with $Fe(OH)_3$ (Figure 3-4). The hydrological model predicts that, during the Temperate Period, meteoric water will occupy progressively more position of the repository with time as a direct consequence of the regional uplift. However, a change in the reducing characteristics of the infiltration water is not expected, as these waters will interact, first with the soils and later with fracture filling minerals and they will be depleted in oxygen.

The most probable values of Eh defined by Auqué et al. (2013) are in the range from –250 mV to –200 mV. Our computed values for Eh are limited between –180 and –250 mV evolving at lower values from 2500 to 6000 AD for the Base Case in SFR1 (Figure 3-7) and in SFR3 (Figure 3-8). The results show that in both repositories, the anoxic conditions will be preserved for the whole temperate period and perfectly fit the range of the available field measurements (Auqué et al. 2013). It is worthwhile noting that the adopted methodology and the spatial analysis of the results allow getting insight into the different geochemical conditions that affect different positions of the repository. The model results indicate that during the temperate period, the repository will be increasingly affected by more diluted water that will dissolve calcite and Fe(III) oxyhydroxide; the pH and Eh values will slightly change controlled by these geochemical processes. Redox conditions, now prevailing at repository depth, will remain over the whole simulation period and could be extended to the end of the extended temperate period, as a change in the hydrological conditions, mainly in the infiltration points, is not expected.

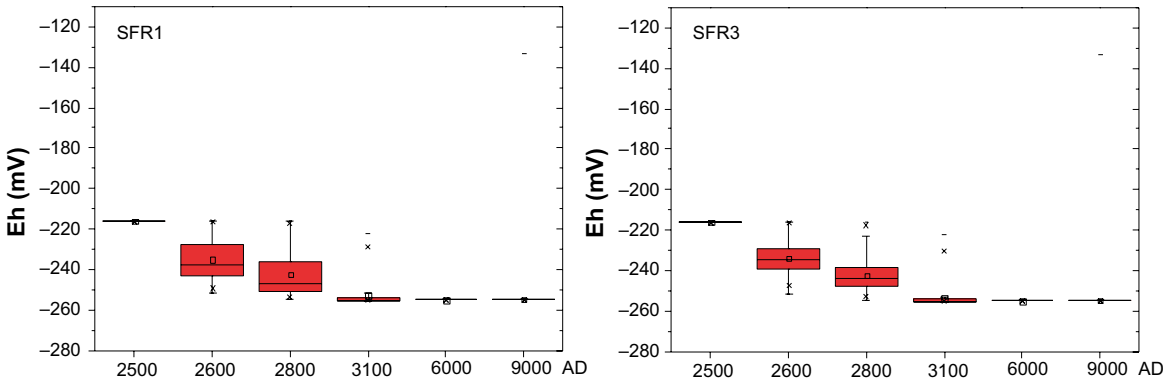


***Figure 3-4.*** *Box-and- whiskers plots showing the statistical distribution of Eh at repository depth for the temperate period. The statistical measures are the median, the 25th and 75th percentile (box), the mean (square), the 5th and 95th percentile ("whiskers") and the maximum and the minimum values.*

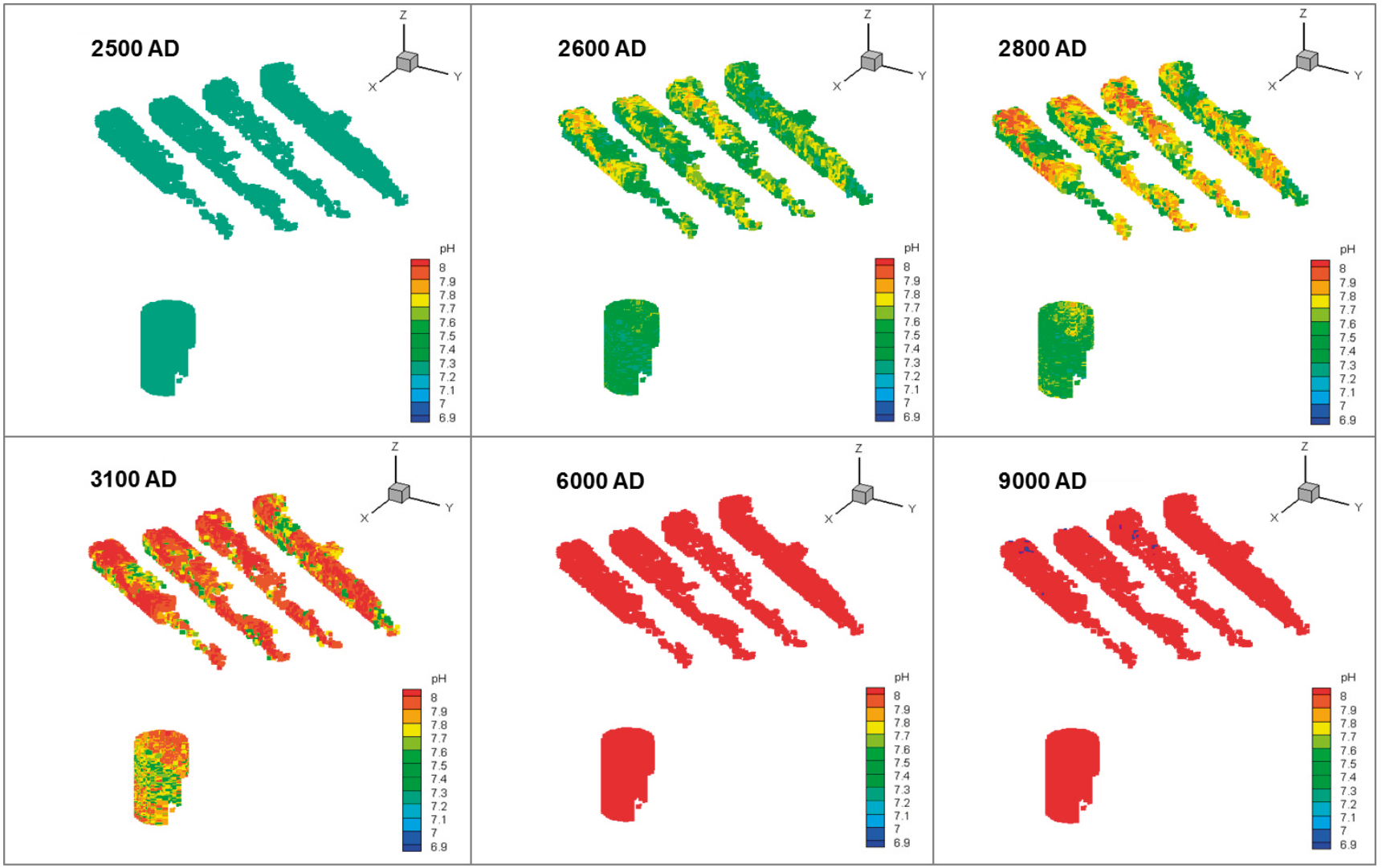


***Figure 3-5.*** *Distribution of pH at SFR1 repository depth for the temperate period over a period time of 6,500 years.*

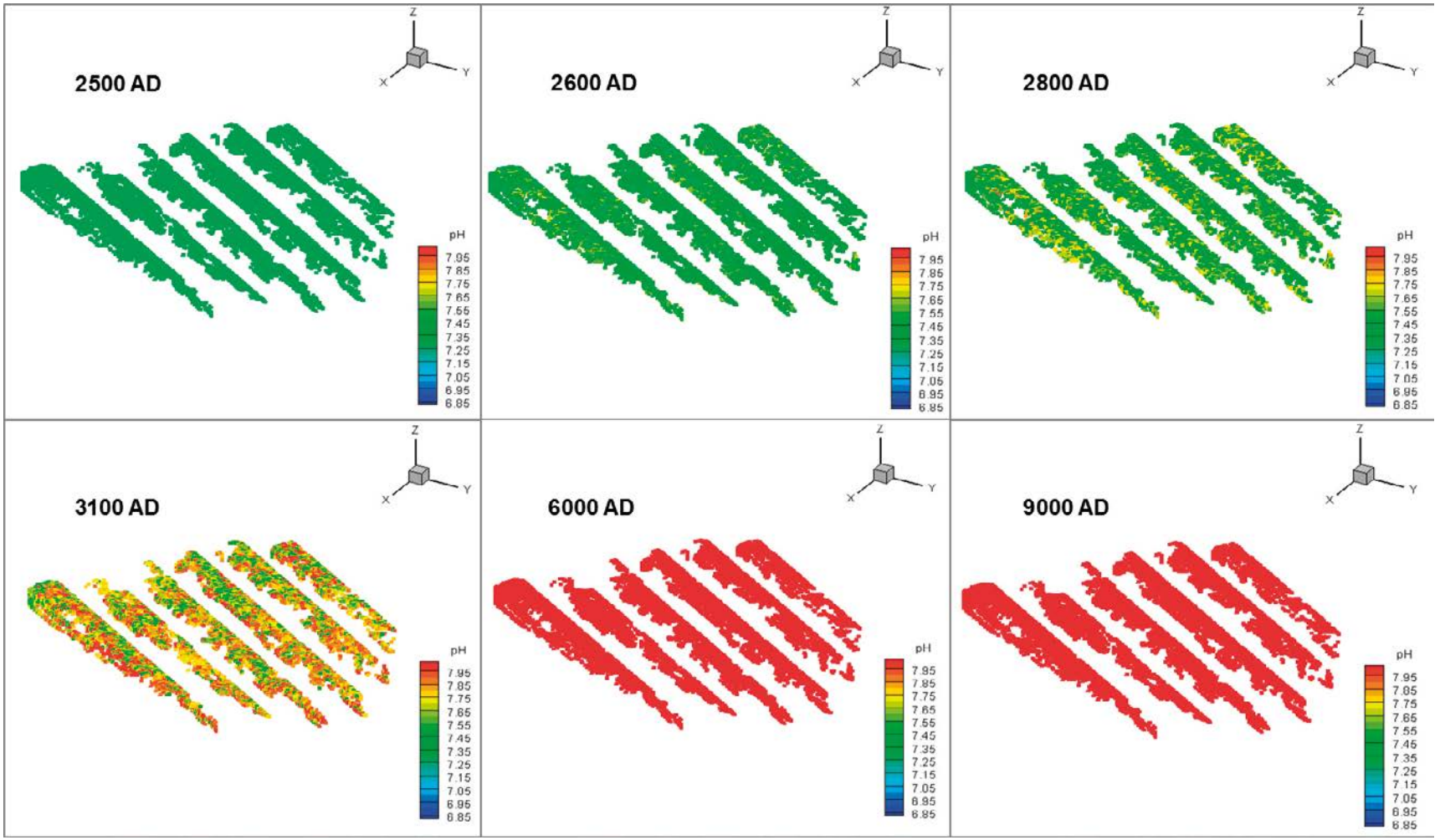


***Figure 3-6.*** *Distribution of pH at SFR3 repository depth for the temperate period over a period time of 6,500 years.*

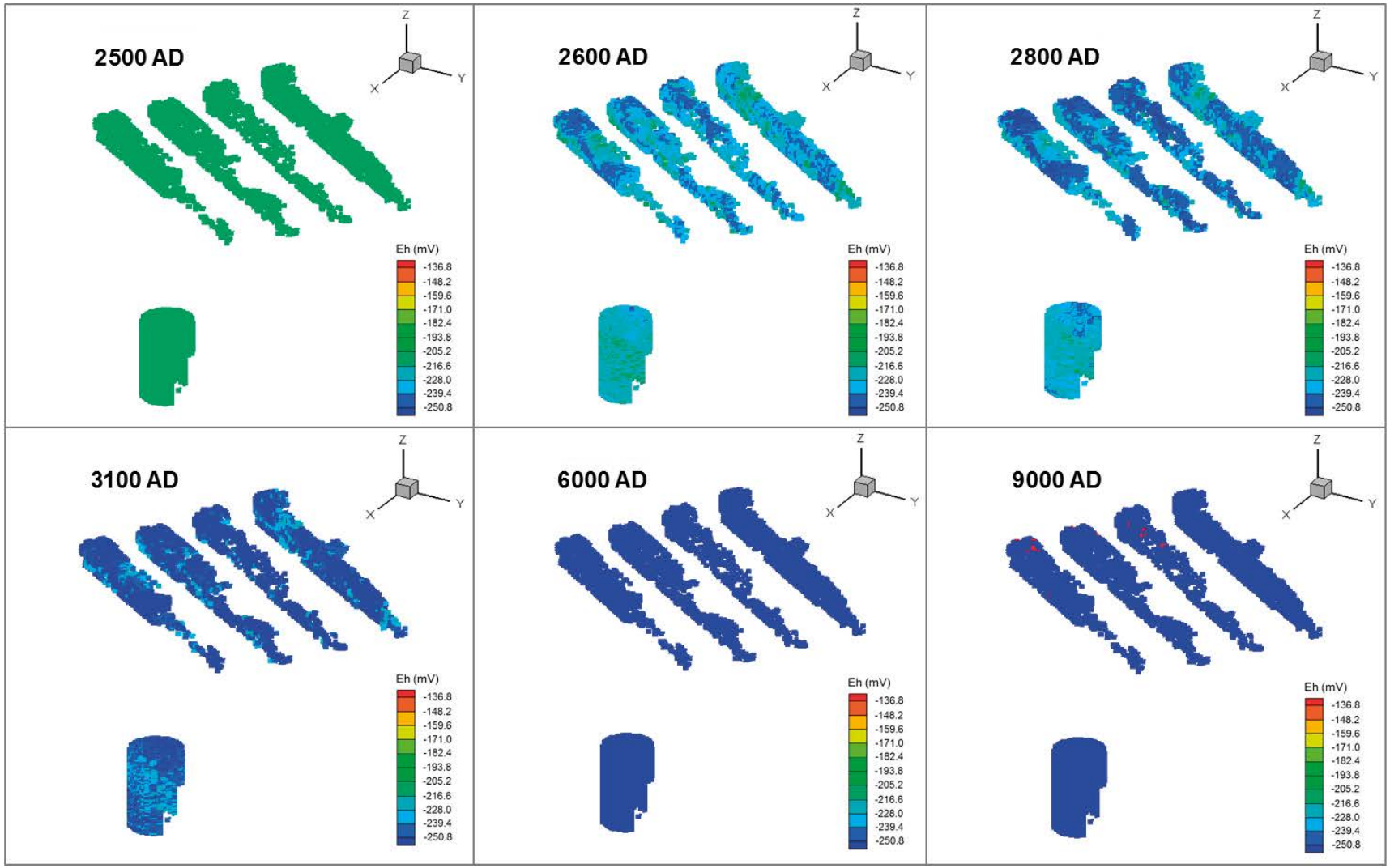


***Figure 3-7.*** *Distribution of Eh (mV) at SFR1 repository depth for the temperate period over a period time of 6,500 years.*

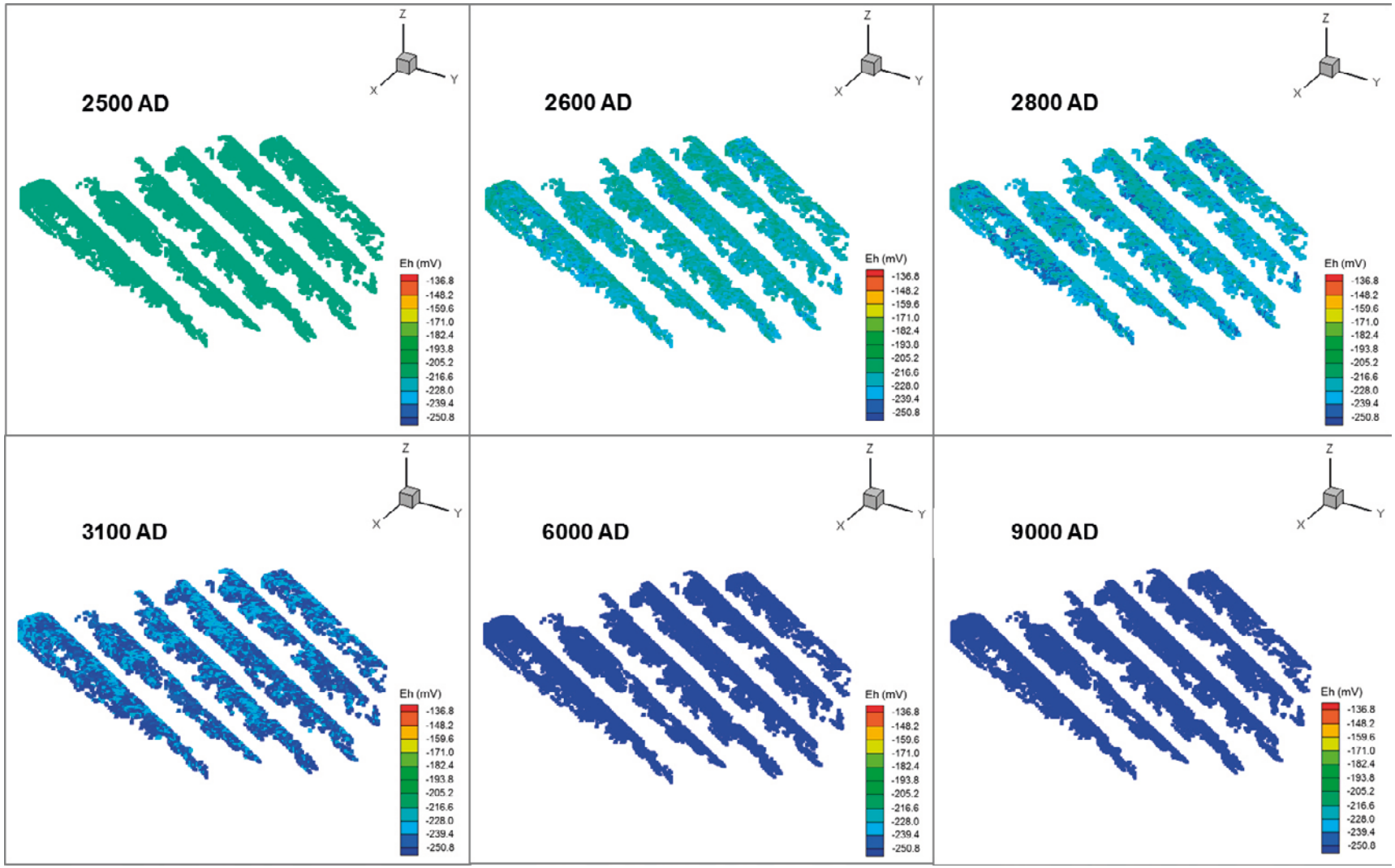


***Figure 3-8.*** *Distribution of Eh (mV) at SFR3 repository depth for the temperate period over a period time of 6,500 years.*

For the Variant Case, where we assume redox conditions controlled by mineral equilibrium with $FeS_{(am)}$, pH values obtained at repository depth do not change significantly with respect to those of the Base Case (Tables A3-1, A3-2, A3-3, A3-4, Appendix 3). The simulated pH values are not sensitive with respect to the Fe-bearing mineral choses to be in equilibrium in the groundwaters. From the comparison of the results for both cases (Figure 3-9 and Figure 3-4) it is possible to conclude that Eh values slightly depend on the mineral phase selected for redox control (Fe(III) oxyhydroxide or Fe(II) sulphide). As both minerals are present in the fracture fillings and there are no geochemical arguments that can be used to postulate which mineral will mainly regulates the redox potentials of groundwaters, the whole range of computed Eh for both cases should be considered, i.e. from –215 to –275 mV (between –215 and –265 mV for the Base Case and from –215 to –275 for the Variant Case (see Appendix 3)).

The evolution of the computed concentrations of major cations (Figure 3-12) shows the same trend as chloride. As a result of infiltration, the groundwater at repository depth becomes progressively more diluted and lower cation concentrations are expected at the end of the simulated period. The cations that contribute more to the charge concentrations are Na and Ca, and to a much lower extent, Mg and K (see also Tables A3-1, A3-2, A3-3 and A3-4, Appendix 3). It is worth noting that cation exchange reactions have not been included in the numerical simulations for the Base and Variant Cases.

Sulphide concentrations in groundwaters are mainly controlled by the interplay between of microbial, chemical (dissolution/precipitation) and hydraulic processes. The evolution of microbial activity and microbially-mediated are not explicitly included in our calculations. However, our geochemical model considers fast thermodynamic equilibrium between $SO_4$ and $HS^-$, which implicitly assumes microbially-mediated reactions.

Under anoxic conditions, dissolved Fe(II) is normally present and the maximum sulphide concentrations are controlled by precipitation of Fe(II) sulphide. Fe concentrations are in the expected range of concentrations taken into account the geochemical constraints of the different geochemical cases (Base Case: $7.32\cdot10^{-6}$–$8.43\cdot10^{-8}$ M, Variant Case: $1.23\cdot10^{-5}$–$1.12\cdot10^{-5}$ M). As expected, higher iron concentrations have been computed when amorphous Fe(II) sulphide is considered to be in equilibrium instead of hematite (see log K values in Table 2-6). As there are not reference values reported by Auqué et al. (2013) for this aqueous species, the concentration range that includes both geochemical cases ($8.4\cdot10^{-8}$ M–$1.23\cdot10^{-5}$ M) could be considered as indicative of the variability in Fe concentrations that could be expected in the groundwaters.

The calculated sulphide concentrations are in the range of $7.3\cdot10^{-6}$ M and $8.4\cdot10^{-8}$ M for the Base Case (Tables A3-1, A3-3, Appendix 3) and from $1.23\cdot10^{-5}$ M to $1.11\cdot10^{-5}$ M for the Variant Case (Tables A3-2, A3-4, Appendix 3).

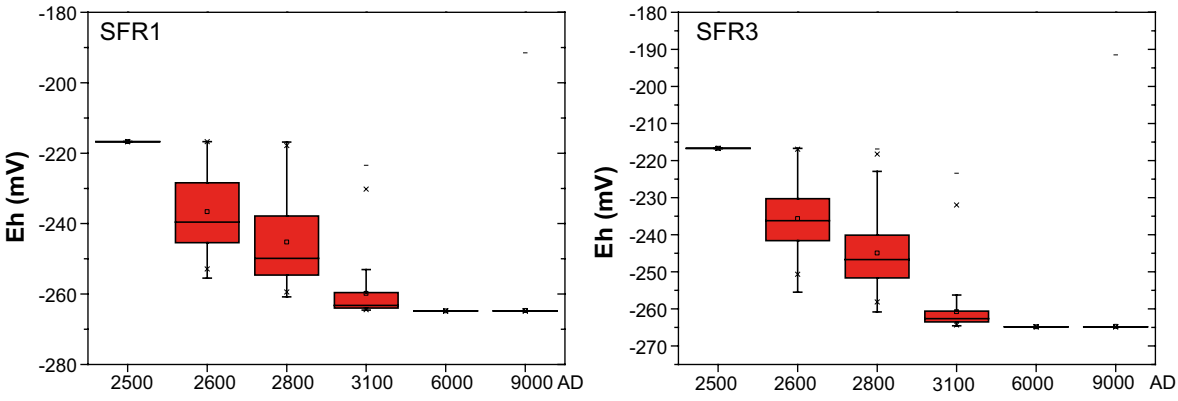


***Figure 3-9.*** *Box-and- whiskers plots showing the statistical distribution of Eh at repository depth for the Variant Case for the temperate period. The statistical measures are the median, the 25th and 75th percentile (box), the mean (square), the 5th and 95th percentile ("whiskers") and the maximum and the minimum values.*

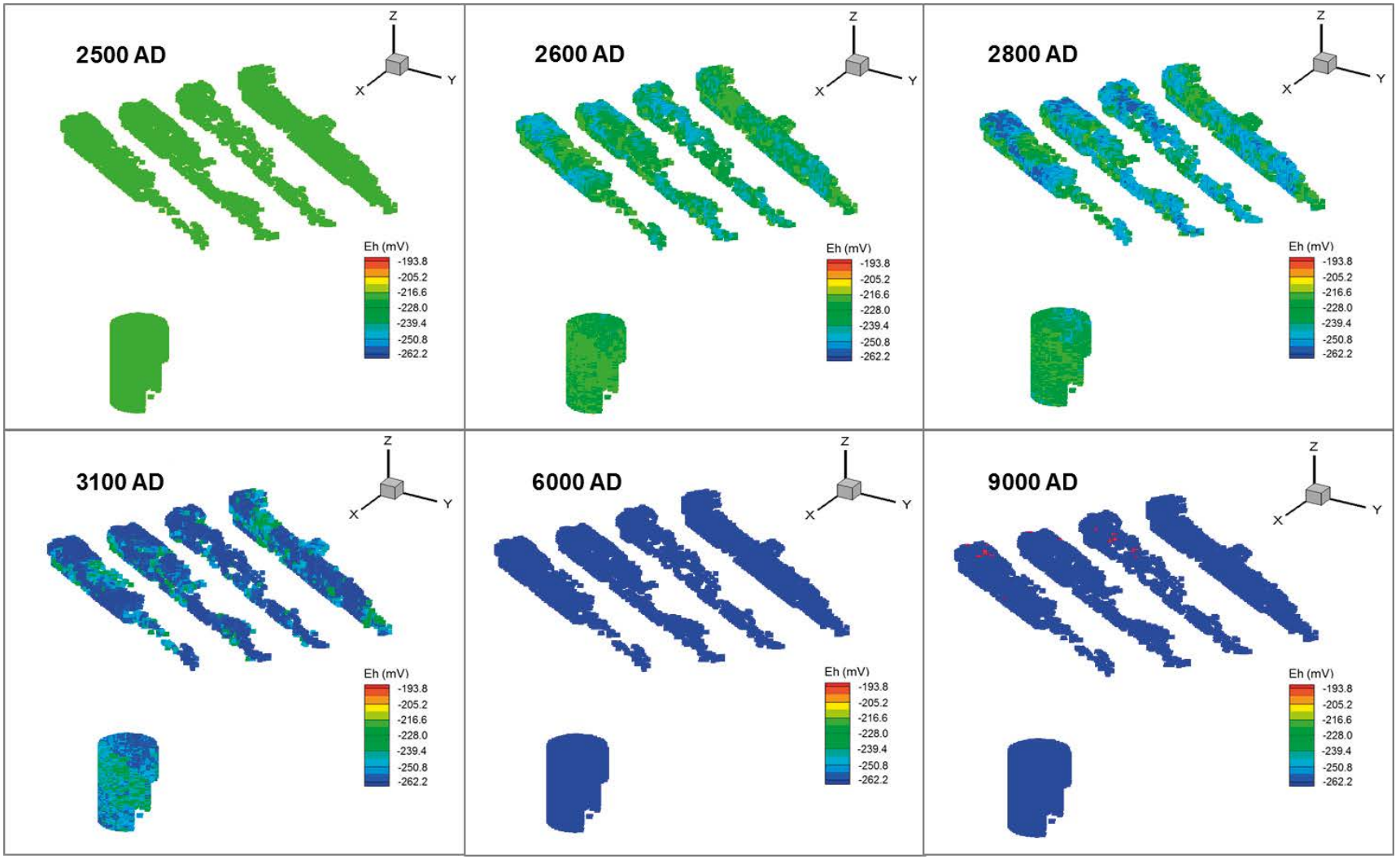


***Figure 3-10.*** *Distribution of Eh (mV) for the variant case at SFR1 repository depth for the temperate period over a period time of 6,500 years.*

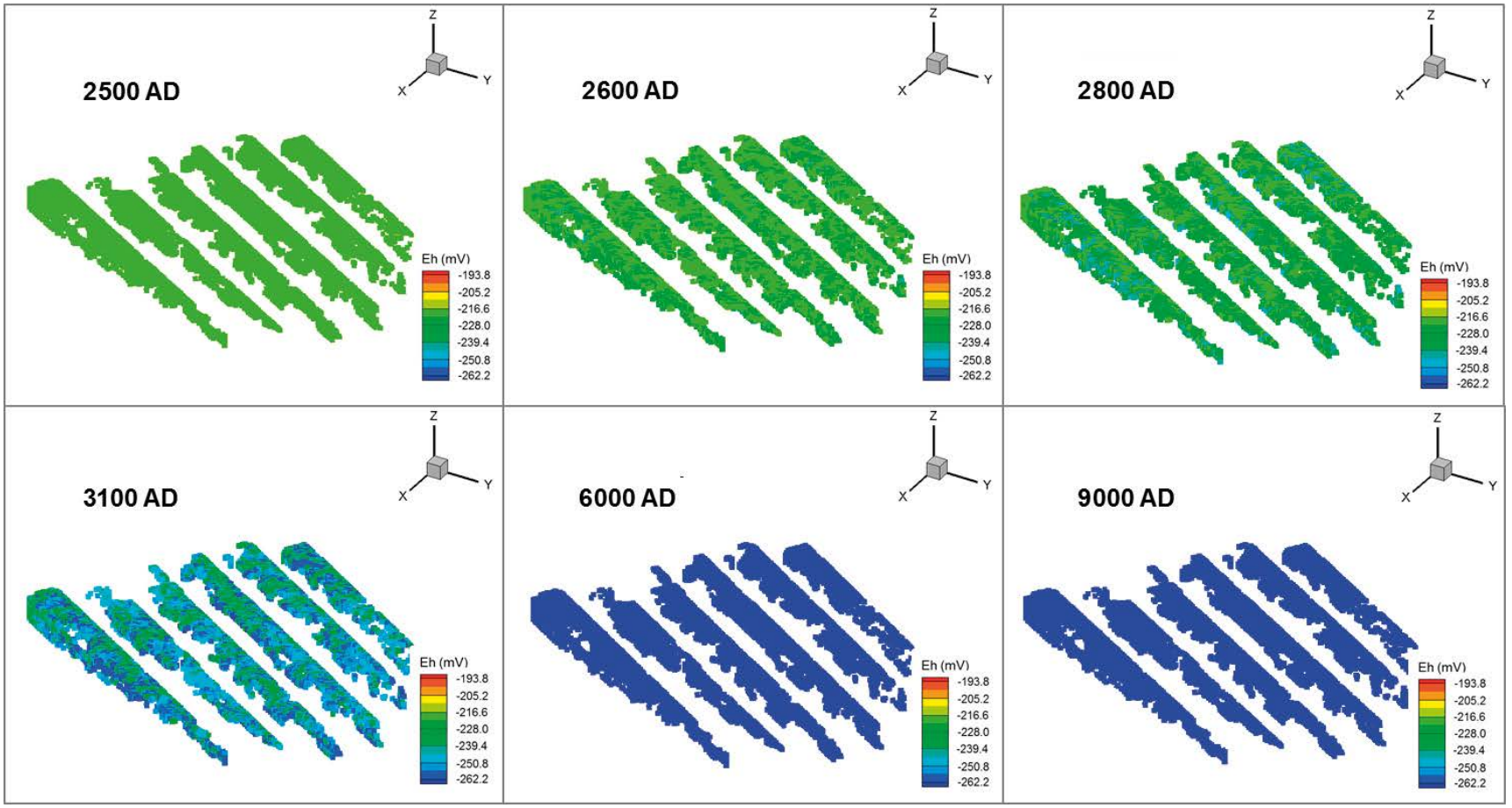


***Figure 3-11.*** *Distribution of Eh (mV) for the variant case at SFR3 repository depth for the temperate period over a period time of 6,500 years.*

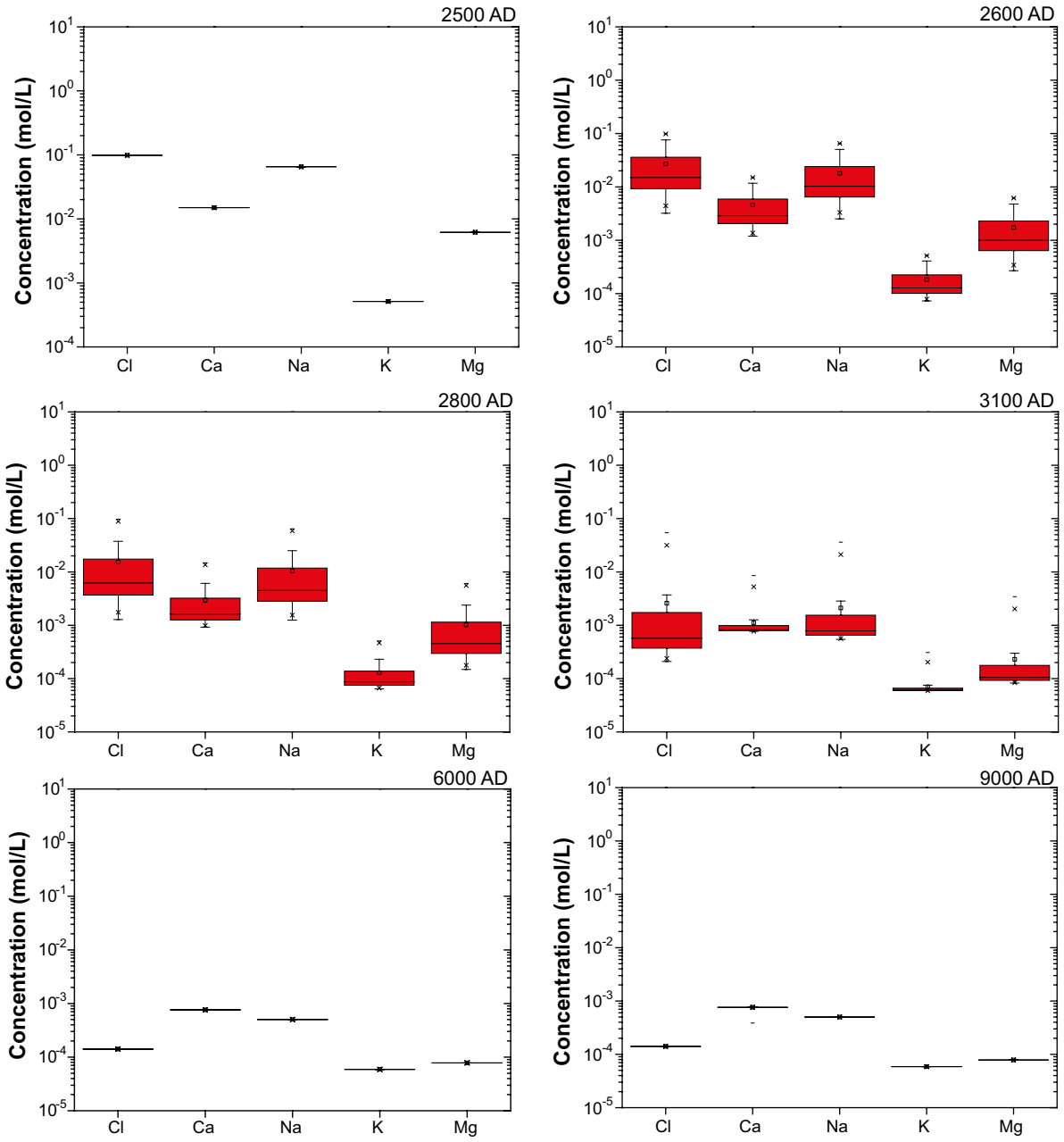


***Figure 3-12.*** *Box-and- whiskers plots showing the statistical distribution of major cations at repository depth for the temperate period (Base Case). The statistical measures are the median, the 25$^{th}$ and 75$^{th}$ percentile (box), the mean (square), the 5$^{th}$ and 95$^{th}$ percentile ("whiskers") and the maximum and the minimum values.*

## 3.3 Uncertainty analysis

### 3.3.1 Montecarlo simulations

***The impact of travel time uncertainties on kinetic dissolution of silicate***

In Section 2.4.3, silicate minerals have been mentioned to be present in the fracture filling at SFR. In general terms, the effect of the kinetic dissolution of these minerals is the addition of cations and silica to groundwaters. Moreover, these geochemical reactions consume protons and increase the pH of the solutions (Brantley et al. 2008).

In a typical subsurface environment, the hydrological conditions in combination with the rate of mineral weathering determine the final composition of groundwaters. Besides mineralogy, several factors influence the dissolution of silicate minerals. For instance, the influence of pH on the dissolution rate of silicates has been widely reported in the literature (Langmuir 1997). In all the aforementioned cases, the rate of dissolution shows a minimum at neutral pH and the rate increases both at lower and higher pH values. Other parameters that control these mineral-water reactions are the reactive surface areas and the reaction time. Both parameters are recognized as sources of uncertainty in all natural environments and their impact on reaction rate measurements has traditionally been reported by experimentalists.

The objective of this Monte Carlo simulations is to assess the impact of hydrodynamic uncertainties (i.e. travel times) on kinetically driven reactions such as silicate dissolution. As in the considered medium kinetic rates are typically very slow, using expert judgment, a distribution of travel times was defined as follows:

1) the distribution of travel times of the recharge flow path computed at 5000 AD using the layout TD08a has been multiplied by a factor of 100.
2) the resulting distribution has been fitted using a lognormal distribution. This fit is shown in Figure 3-13.

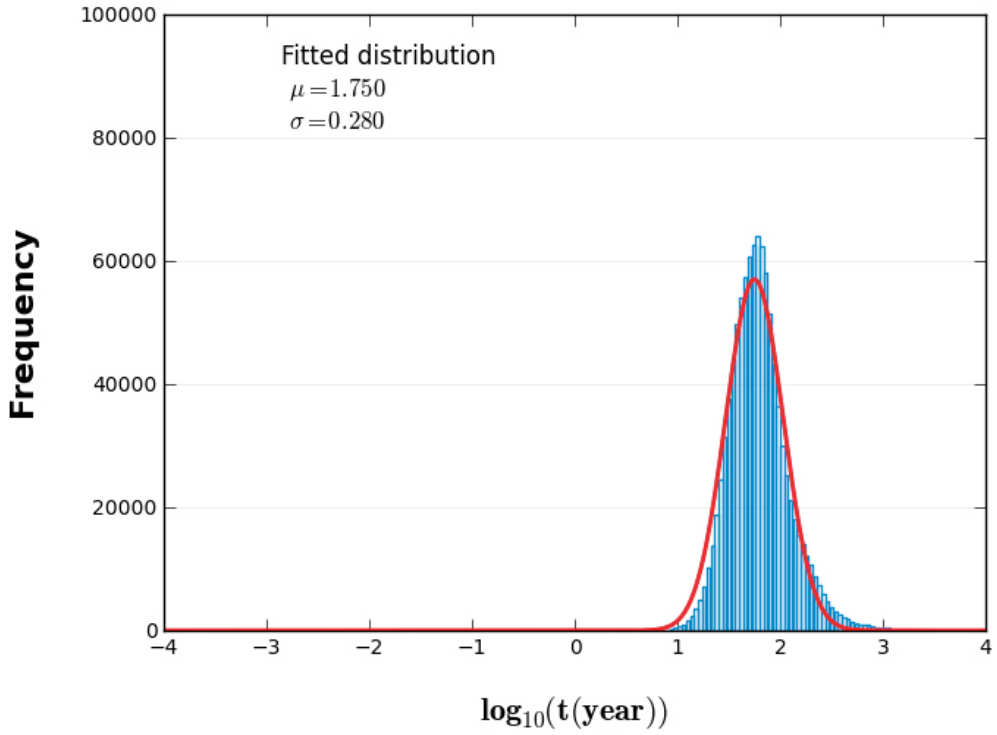


***Figure 3-13.*** *Probability Distribution Function (PDF) for travel times used in the sensitivity analyses.*

The calculations were conducted by adding the kinetic dissolution reactions listed in the Table 2-9 to the reactive transport simulation defined for the Base Case. We assumed specific surface areas of 874 $m^2/L$, 0.63 $m^2/L$, 0.3 $m^2/L$ and 0.52 $m^2/L$, for chlorite, albite, illite and K-feldspar, respectively. Due to the lack of specific information about mineral abundance and granulometry of the SFR fracture fillings, these values have been taken as reference from a similar study performed in Olkiluoto (Finland), where a quantitative mineralogical study was performed in the fracture fillings (Trinchero et al. 2014b). Each time that a travel time value is sampled by Monte Carlo, a PHREEQC simulation is run and an output file is obtained at a final time of 9000 AD at repository level for the fixed reactive surfaces above mentioned. All chemical parameters were kept static, no statistical variation of chemical reaction parameters was used. A total number of 100 realizations were performed using the MC-PHREEQC software with travel time varying between 1 and 25 years according to the PDF shown in Figure 3-13.

In order to test the impact of hydrodynamic uncertainties, the reactive transport simulation of the Base Case (without kinetic dissolution of silicates) was also run with 100 realizations and the obtained results included in Figure 3-14 as reference values.

The calculated pH for the geochemical case that considers kinetic dissolution of chlorite (BC + Chlorite diss., Figure 3-14), display a slight and constant increase with respect to the Base Case. The kinetic dissolution of chlorite slightly modifies pH, even considering the longest groundwater residence times. Taking into account that chlorite has been reported as one of the most abundant minerals in the fracture fillings, these results permit to rule out the possibility of a peak of high pH due to water-chlorite interaction during infiltration.

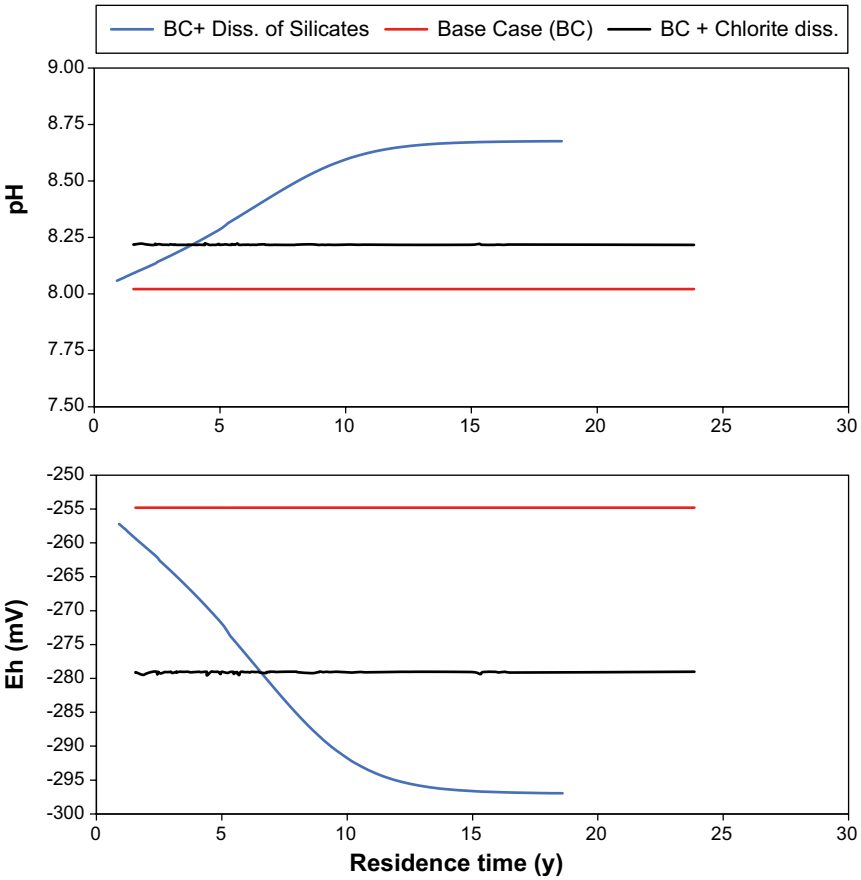


***Figure 3-14.*** *Results of the 100 realizations: pH and Eh computed values at repository depth at 9000 AD for different residence times of groundwaters in the fractures.*

In contrast, kinetic dissolution of albite, illite and K-feldspar (*i.e* BC+ Diss of Silicates) is sensitive to residence time of groundwaters and pH increases up to 8.7 for residence times higher than 10 years (Figure 3-14). Due to the interdependency of pH and Eh, computed redox conditions vary consequently with the pH values to more reducing characteristics (Figure 3-14) with Eh values around –300 mV if higher residence time values are assumed. This Eh falls in the lower limit of the range reported by Auqué et al. (2013) for the temperate period (–135 mV to –300 mV). Based on the present composition of evolved groundwaters, it could be concluded that the highest pH values computed in the Monte Carlo simulations are not representative of probable geochemical cases as these pH values are rarely observed in the site at present.

As a consequence of silicate dissolution, Si, Al and other cations are released into the waters and maximum silica and Al concentrations will be, in turn, controlled by precipitation of $SiO_{2(am)}$ and kaolinite. In Figure 3-15, the evolution of Si and Al is plotted as a function of residence times. A silica concentration of $1.41 \cdot 10^{-4}$ M has been computed for the Base and Variant Case at a final time of 9000 AD (see Appendix 3). The range of concentration given by Auqué et al. (2013) for the temperate period is between $5 \cdot 10^{-4}$ and $3 \cdot 10^{-4}$ M. These concentrations correspond to the values obtained for short residence times (Figure 3-15). Chlorite dissolution process has a modest influence on the Si computed concentrations. In contrast, kinetic dissolution of albite, illite and K-feldspar could produce a significant release of Si especially when residence times are longer than 10 years.

Aluminium release due to chlorite dissolution is computed as an active process with concentrations that increases significantly with respect to the Base Case at 9000 AD and remains without variations over time (Figure 3-15). Lower Al concentrations are obtained at short travel times for the geochemical case that includes kinetic dissolution of silicates. At higher travel times, aluminium contents increase significantly and clearly highlight the high impact that residence times could have on the final composition of groundwaters if kinetic reactions are involved. The aluminium concentrations are stabilized by reaching equilibrium conditions with kaolinite.

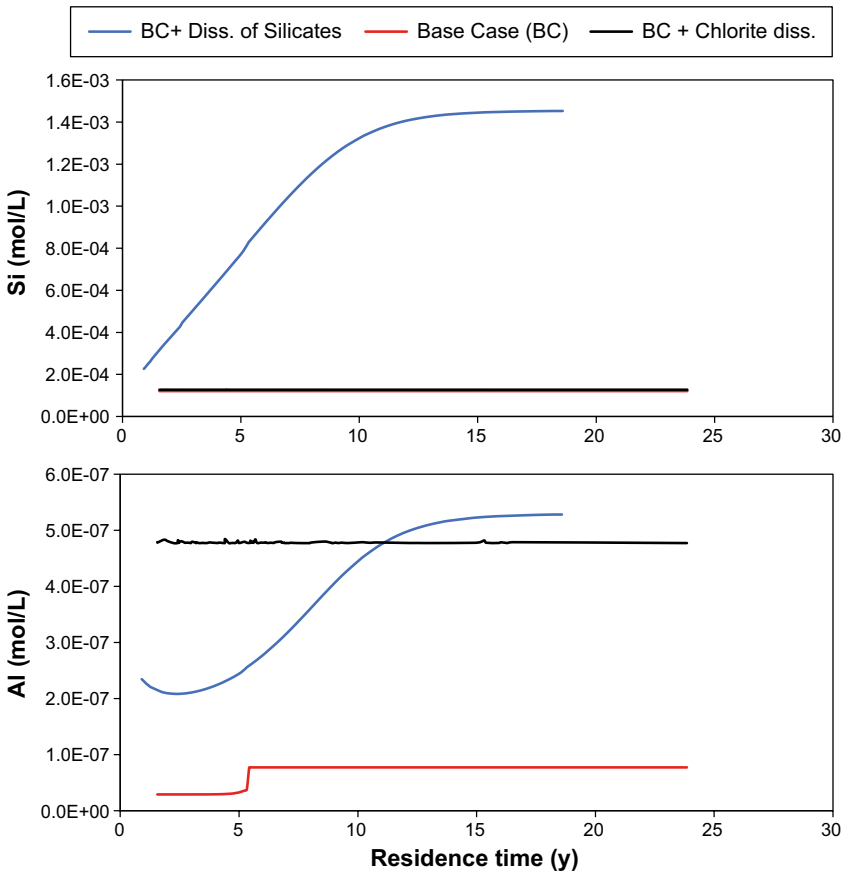


***Figure 3-15.*** *Results of the 100 realizations: Si and Al concentrations at repository depth at 9000 AD for different residence time of groundwaters in the fractures.*

### *The role of clay as cation exchangers*

As discussed in Section 2.4.5, clays present in the fracture can contribute to cation exchange reaction that could modify the chemical composition of the groundwaters. In order to model these reactions, a value for the cation exchange capacity and an estimation of the amount of clay minerals is needed. Several approaches based on experimental measurements can be used to define these parameters. However, the distribution of clay minerals along the fracture is usually assumed to be constant and homogenously distributed. This assumption is not realistic as natural systems are characterized by a high spatial variability. In this case and, in a similar way as that previously described for kinetic dissolution of silicates, the reactive transport simulation defined for the Base Case was modified by adding cation exchange reactions with clays (illite). This Monte Carlo simulation consists of 100 realizations where the number of sites/L is treated as a random variable with uniform distribution, ranging from 5 to 80 moles of sites/L based on expert judgment. In this case, residence times is fixed to that used in the Base and Variant Cases and the results are analyzed at the final time of 9000 AD at repository depth.

The evolution of major cations (Figure 3-16) displays an increase in Na concentration in groundwaters due to release processes from the fracture fillings to the waters at CEC higher than 20 mol of sites/L. Sodium concentrations computed in the groundwater for the Base Case at 9000 AD (without any exchange reaction) is $5 \cdot 10^{-4}$ M (Figure 3-12). The results of the Monte Carlo simulations show that sodium concentrations will remain around this value for CEC lower than 20 mol of sites/L. If higher values of CEC are assumed, Na concentration at 9000 AD would reach $3 \cdot 10^{-3}$ M. This value corresponds to the lower concentrations reported by Auqué et al. (2013), for the temperate period ($1 \cdot 10^{-2}$ M and $3 \cdot 10^{-3}$ M).

Potassium concentrations show a distinctive behavior with respect to Na with a peak value around 10 mol of sites/L. For CEC higher than 20 mol of sites/L, the concentration of K decreases sharply to a value of $2.35 \cdot 10^{-5}$ mol/L. Computed K concentration for the Base Case simulations at 9000 AD is $5.88 \cdot 10^{-5}$ M (Figure 3-12), a similar value to that obtained for high CEC values ( Figure 3-16). Auqué et al. (2013) reported K concentrations in the range of $1 \cdot 10^{-2}$ and $1 \cdot 10^{-4}$ M for the temperate period.

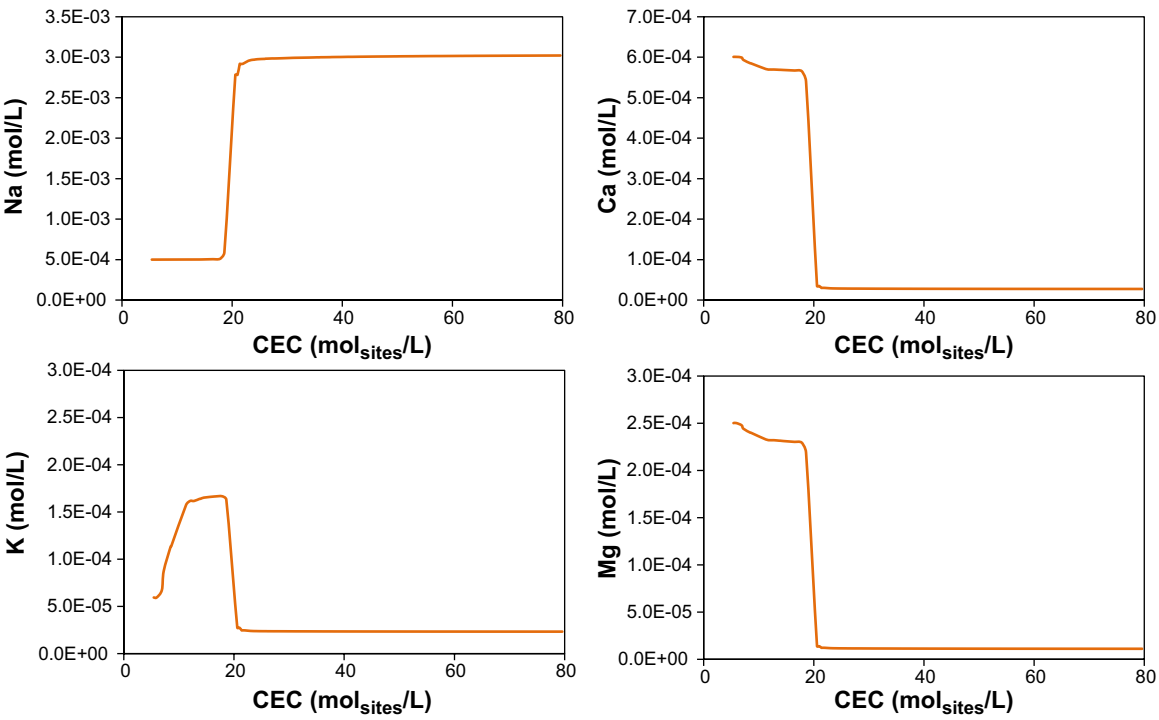


***Figure 3-16.*** *Sensitivity analysis of CEC of clays in the fractures. Computed data at 9000 AD at repository level.*

Divalent ions (i.e Ca and Mg) are preferentially adsorbed in comparison to monovalent ions (Na and K). Ca and Mg display a similar behavior with a progressive decrease in concentrations at CEC values ranging between 5 and 20 mol of sites/L (Figure 3-16). Above this value the groundwaters concentrations decrease at very low values. If high CEC are assumed, Ca is preferentially retained in the exchanger and groundwater becomes undersaturated with respect to calcite, which in turn, dissolves to attain new equilibrium conditions**.** This reaction produces the sharp increase of pH observed in Figure 3-17. Both, pH and Eh are sensitive to the CEC of clays, with a clear impact for values higher than 20 mol of sites/L (Figure 3-17). Computed concentrations of Ca and Mg at 9000 AD for the Base Case are $7.61 \cdot 10^{-4}$ and $7.82 \cdot 10^{-5}$ M, respectively (Figure 3-12). Auqué et al. (2013) reported values from $6 \cdot 10^{-3}$ to $4 \cdot 10^{-4}$ M for Ca and ranging between $5 \cdot 10^{-4}$ and $8 \cdot 10^{-5}$ M for Mg.

In summary, these results have highlighted a number of key points that have significance in the framework of this safety assessment. These points can be summarized as follows:

- If enough amount of exchanger sites is available in the fractures (above 20 mol of site/L), exchange reactions with clays will be able to increase the cation charge of infiltrating meteoric water through desorption of Na initially present in the exchangers. At low CEC values the impact of this reaction is negligible.
- The behavior of Ca and Mg are correlated and related to the high affinity of exchanger by divalent cations. During infiltration of meteoric waters and at low CEC values, a progressive scavenging of Ca and Mg is computed. Above a CEC value of 20 mol of site/L, both divalent elements are strongly retained in the exchangers. If a very high CEC is available in the fractures, the removal of Ca from the groundwater could trigger calcite dissolution reactions and pH values could increase up to 9. As a consequence, Eh could decrease at around –300 mV in groundwaters in contact with the fractures. As this high pH has never been measured at the site, it can be concluded that clays present in the fracture are not abundant enough to produce CEC higher than 20 mol of site/L.
- Clay minerals could have an active role in the final composition of groundwaters. However, a comparison between the computed results with the range of concentrations reported by Auqué et al. (2013), seems to indicate that clays with high CEC are not available in this geochemical system.

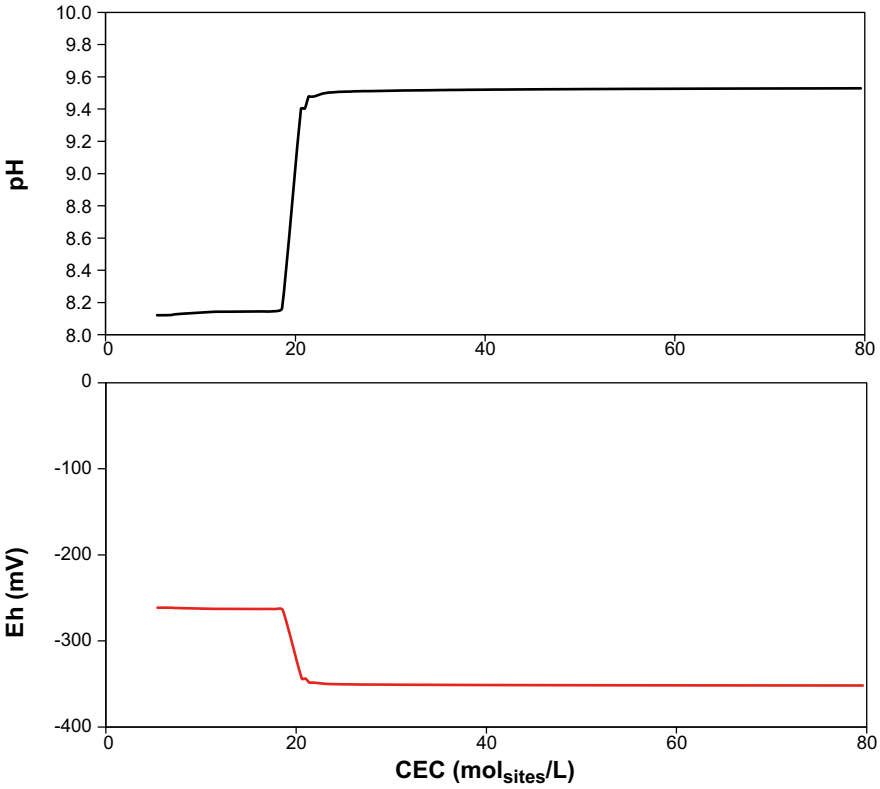


***Figure 3-17.*** *Sensitivity analysis of CEC of clays in the fractures. Reported results at 9000 AD at repository level.*

## 3.4 Concluding remarks for the temperate period

The analysis of the spatial distribution of key geochemical parameters (i.e. maps at repository depth) has pointed out the capability of the methodology to provide indications of the different geochemical conditions that affect different positions of the repository at different times.

The results indicate that groundwater pH at repository level will evolve from 7.3 to 8 in a period of 600 years from 2500 AD. The hydrological model predicts that the signature of meteoric water at repository depht will increase with time. However, changes in the reducing characteristics of the infiltration water is not expected, as these waters will interact, first with the soils and later with fracture minerals and they will be depleted in oxygen before arriving at repository level. Reducing conditions are observed for the whole simulated period as a consequence of the mineral control (either hematite or $FeS_{(am)}$).

The signature of altered meteoric water is evident in the whole domain, being a direct consequence of preferential flow. The salinity at the SFR repository during the temperate period ranges between 6 and $1 \cdot 10^{-2}$ g/L. The evolution of the computed concentrations of major cations shows the same trend of chloride with a major contribution of Na and Ca and low concentrations of Mg and K.

The results of the sensitivity analyses show that high residence times of groundwater would impact on chemical composition of the water due to kinetic dissolution reactions that will increase pH and release Si and Al to the waters. The range of expected values, assuming a wide range of residence times, is provided by the Monte Carlo simulations. The whole results computed for this sensitivity case support the fact that kinetic dissolution of silicate is a geochemical process that could be an active role on the control of the chemical composition of groundwater mainly at long groundwater residence time.

The assessment of the role of clays as exchanger in the fractures has allowed inferring a limited extent of these processes in the SFR system.

# 4 Temporal and Spatial evolution of groundwaters for the periglacial period

The periglacial period has been simulated using the methodological approach already described for the temperate period (Section 2.4). The same geochemical model is assumed with a Base Case under equilibrium conditions with calcite and hematite and a Variant Case where the presence of $FeS_{(am)}$ instead of hematite is assumed in the fracture fillings. The underlying hydrogeological conditions are described by the set of particle trajectories analyzed in detail in Section 2.3.2.

Uncertainties related to the initial state for this period have been accounted for the use of two different boundary infiltrating water denoted as "lake or glacial water" (Table 2-7). In all simulations for the periglacial period, "evolved" waters computed at the end of the temperate period, have been initially linked to each hydrochemical zone and defined as fracture waters at the initial state (Table 2-7).

## 4.1 Results

### 4.1.1 Periglacial period (lake boundary water)

The chemical evolution of groundwater reaching the repository during the periglacial period displays only slight changes in the pH and Eh conditions compared to those computed at the end the Temperate Period. The pH values decrease from 8 to around 7.5 for the Base and the Variant Case (Figure 4-1).

Anoxic conditions are preserved over 10 ky but a trend to higher Eh values is observed from the beginning to the end of the computed time period. The values evolved from –243 to –78 mV and from –271 to –245 mV for the Base Case and the Variant Case respectively (Figure 4-2 and Figure 4-3).

In Figure 4-4 and Figure 4-5, the temporal and spatial evolution of chloride concentrations is shown. Due to its conservative behavior, chloride is a useful indicator of the progression of the hydrogeological conditions. As it can be observed in these figures, main changes occur in a period time of 1,000 y while water infiltrating from the taliks arrives progressively to repository depth.

A similar pattern is observed for the evolution major cation concentrations in the groundwaters. Calcium concentrations increase from $7.61 \cdot 10^{-4}$ to $1.34 \cdot 10^{-3}$ M because the prescribed boundary waters have higher concentrations than those of the fracture water and, in addition, during the interaction with the mineral fractures calcite is dissolved. Na, K, and Mg contents evolve from the initial concentrations in the fracture groundwaters to those of the infiltrating water. Precipitation of secondary phases is not attained in the simulated time period and no other processes are involved in the uptake/release of these elements.

In agreement with the evolution of chloride concentrations, the pH and Eh (Figure 4-6, Figure 4-7, Figure 4-10, Figure 4-11, Figure 4-12 and Figure 4-13) progressively change with the arrival of talik waters evolved in contact with the fracture minerals. In any case, circumneutral pH and anoxic conditions are maintained during the simulated time period at all the positions of the repository.

During the periglacial period, travel times are longer than those for the temperate period but, as the conceptual model only consider chemical reaction under equilibrium conditions, the results are mainly controlled by the composition of the infiltrating water and the buffer effect of matrix waters. This fact determine minor changes in the composition of groundwaters during this period compared to those computed at the final of the temperate period. These results show a good agreement with the Ca and Cl concentrations proposed by Auqué et al. (2013) for the periglacial period. In the case of Na, K and Mg, and as already stated for the temperate period, the lower concentrations computed for this climatic period fall close to the minimum concentrations defined by Auqué et al. (2013) because mixing process coupled to the reactive transport simulations are not included in the conceptual model.

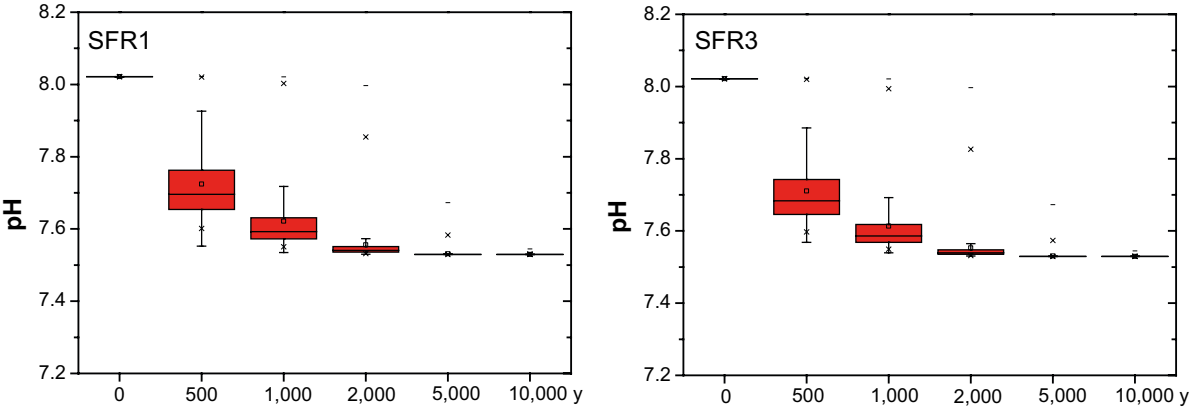


***Figure 4-1.*** *Box-and- whiskers plots showing the statistical distribution of pH at repository depth for the Base Case and for the periglacial period (lake boundary water). The statistical measures are the median, the 25th and 75th percentile (box), the mean (square), the 5th and 95th percentile ("whiskers") and the maximum and the minimum values.*

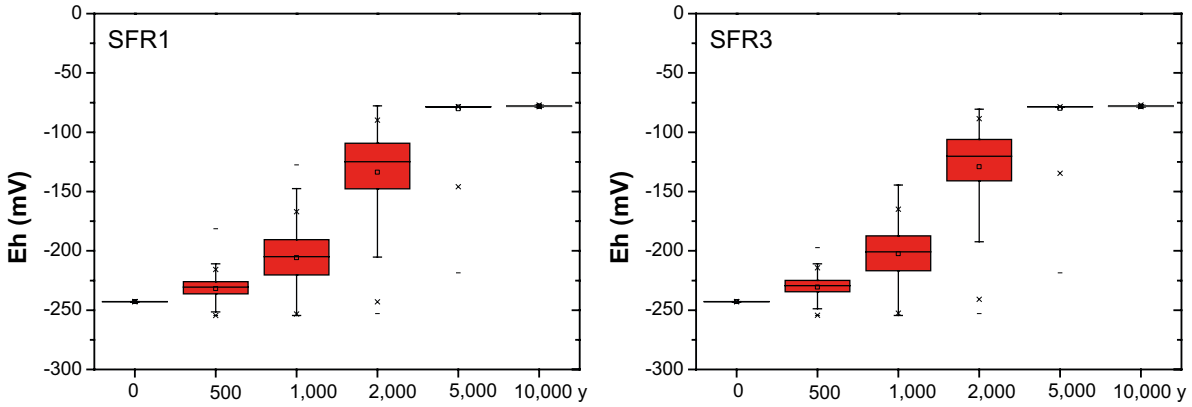


***Figure 4-2.*** *Box-and- whiskers plots showing the statistical distribution of Eh (mV) at repository depth for the Base Case and for the periglacial period (lake boundary water). The statistical measures are the median, the 25th and 75th percentile (box), the mean (square), the 5th and 95th percentile ("whiskers") and the maximum and the minimum values.*

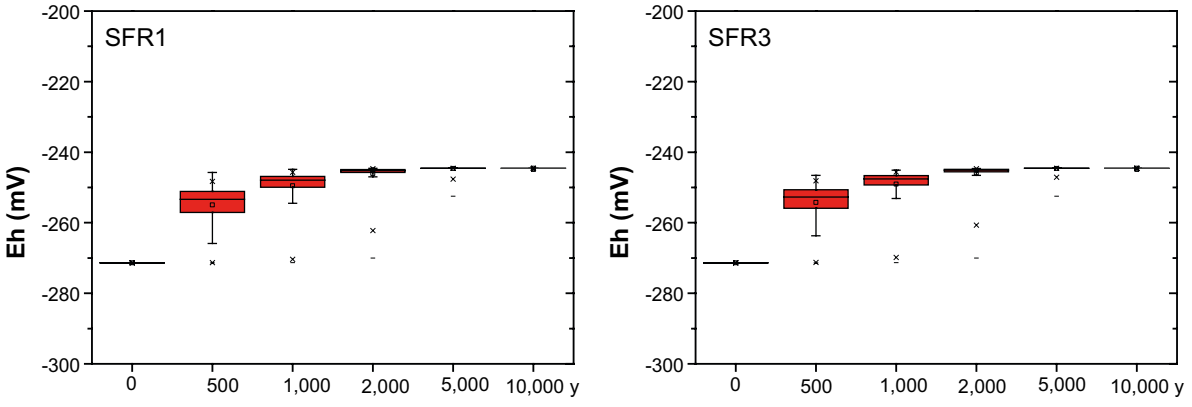


***Figure 4-3.*** *Box-and- whiskers plots showing the statistical distribution of Eh (mV) at repository depth for the Variant Case and for the periglacial period (lake boundary water). The statistical measures are the median, the 25th and 75th percentile (box), the mean (square), the 5th and 95th percentile ("whiskers") and the maximum and the minimum values.*

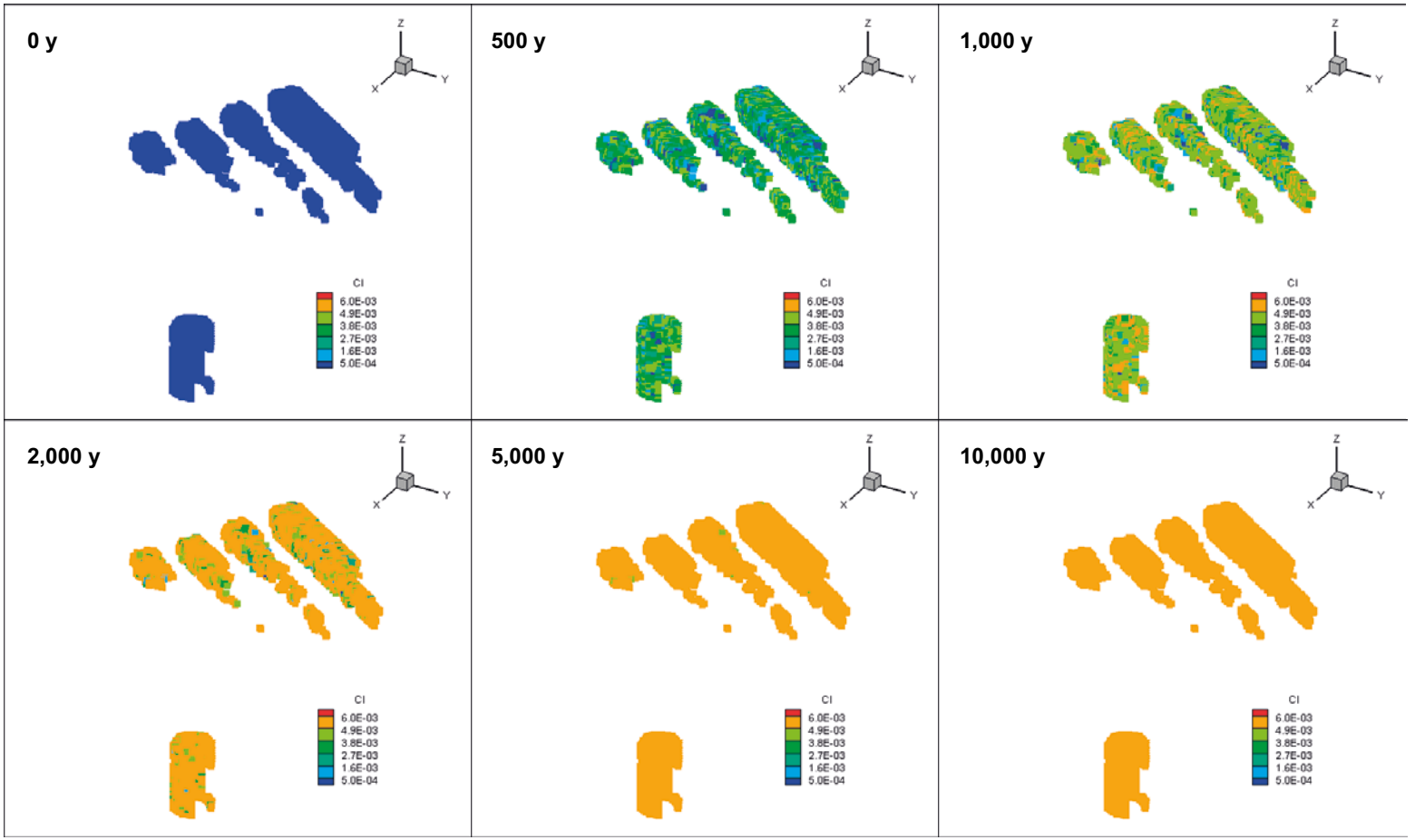


***Figure 4-4.*** *Temporal evolution of chloride for the Base Case of the periglacial period (lake boundary water) at SFR1 repository depth over a period time of 10,000 years.*

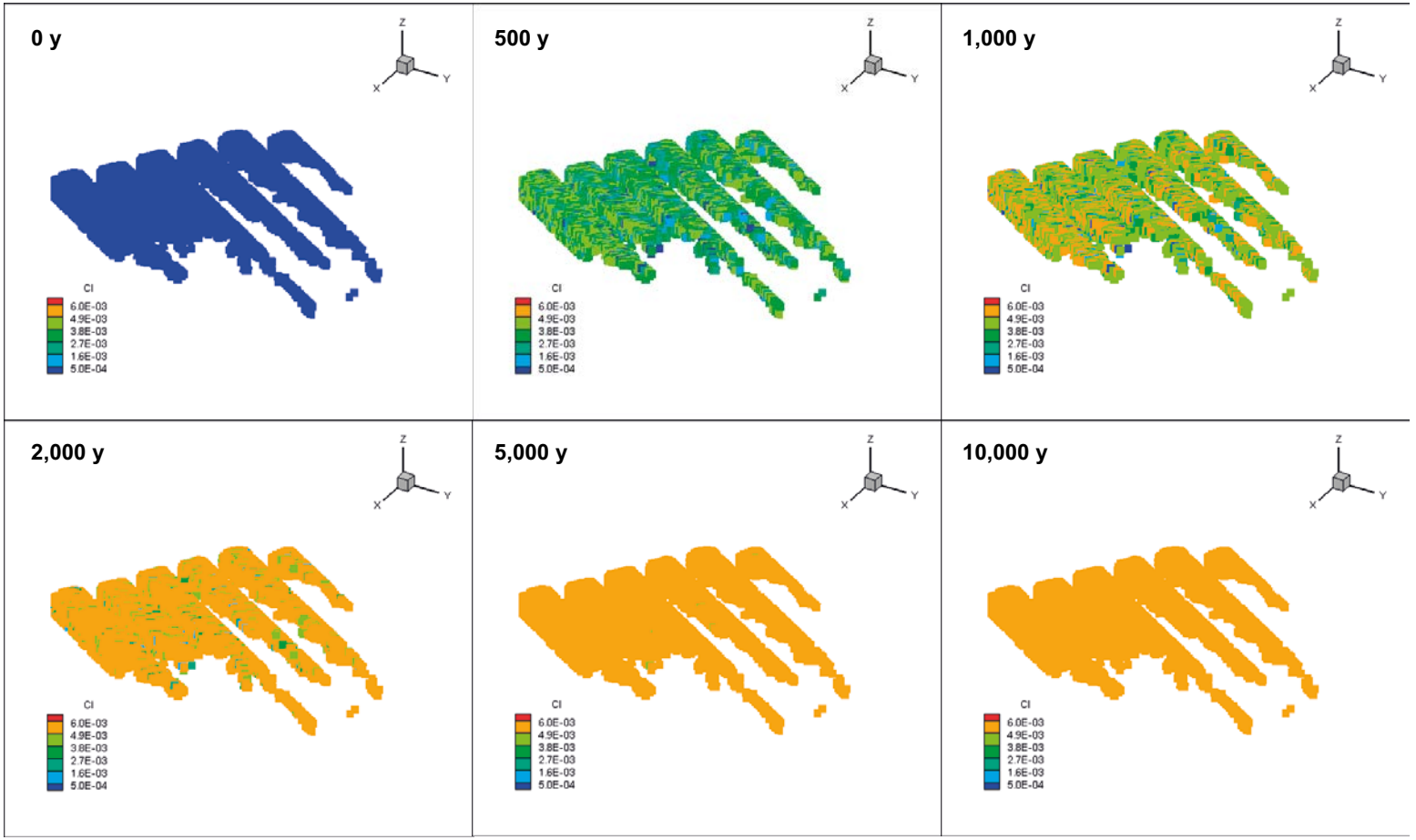


***Figure 4-5.*** *Temporal evolution of chloride for the Base Case of the periglacial period (lake boundary water) at SFR3 repository depth over a period time of 10,000 years.*

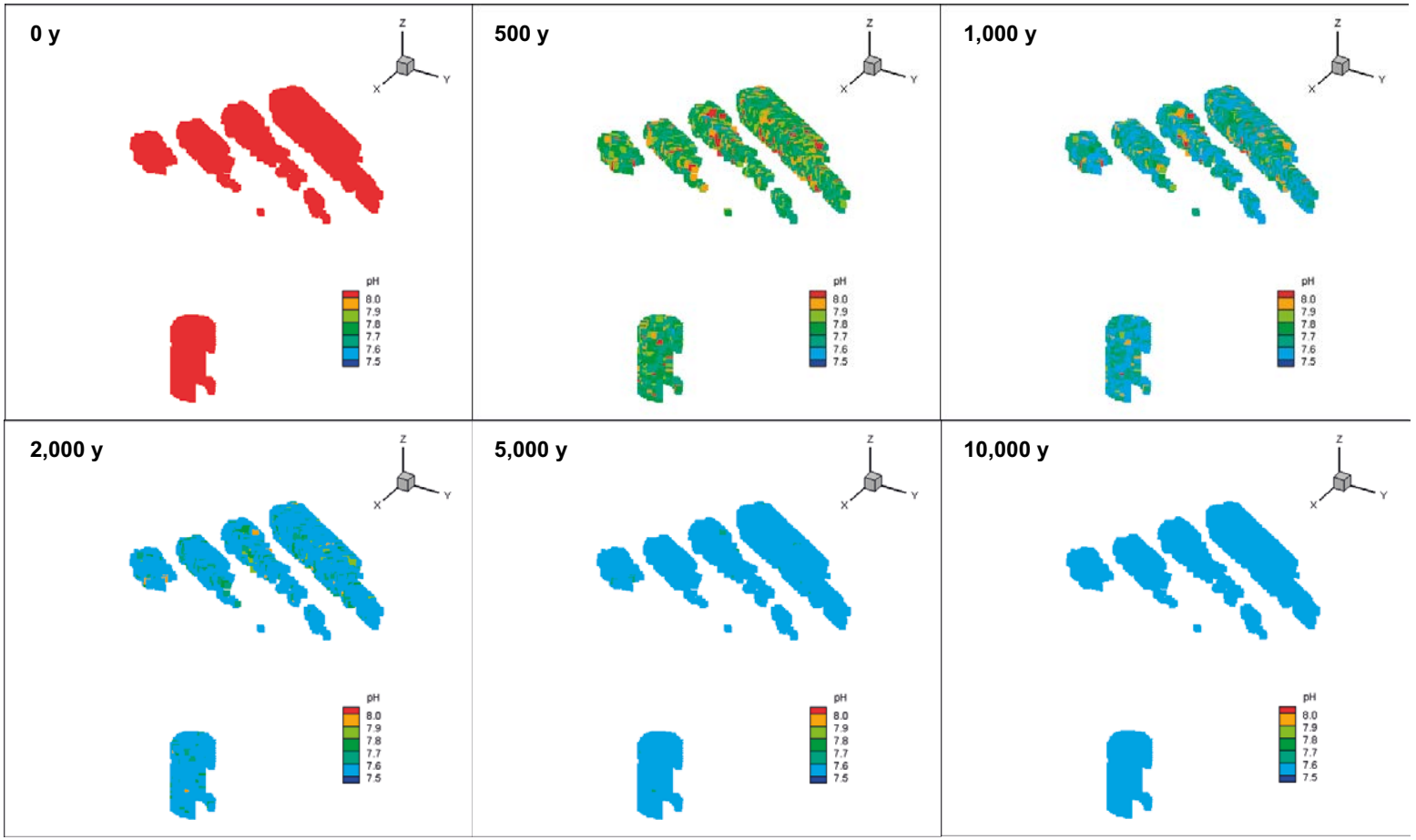


***Figure 4-6.*** *Temporal evolution of pH for the Base Case of the periglacial period (lake boundary water) at SFR1 repository depth over a period time of 10,000 years.*

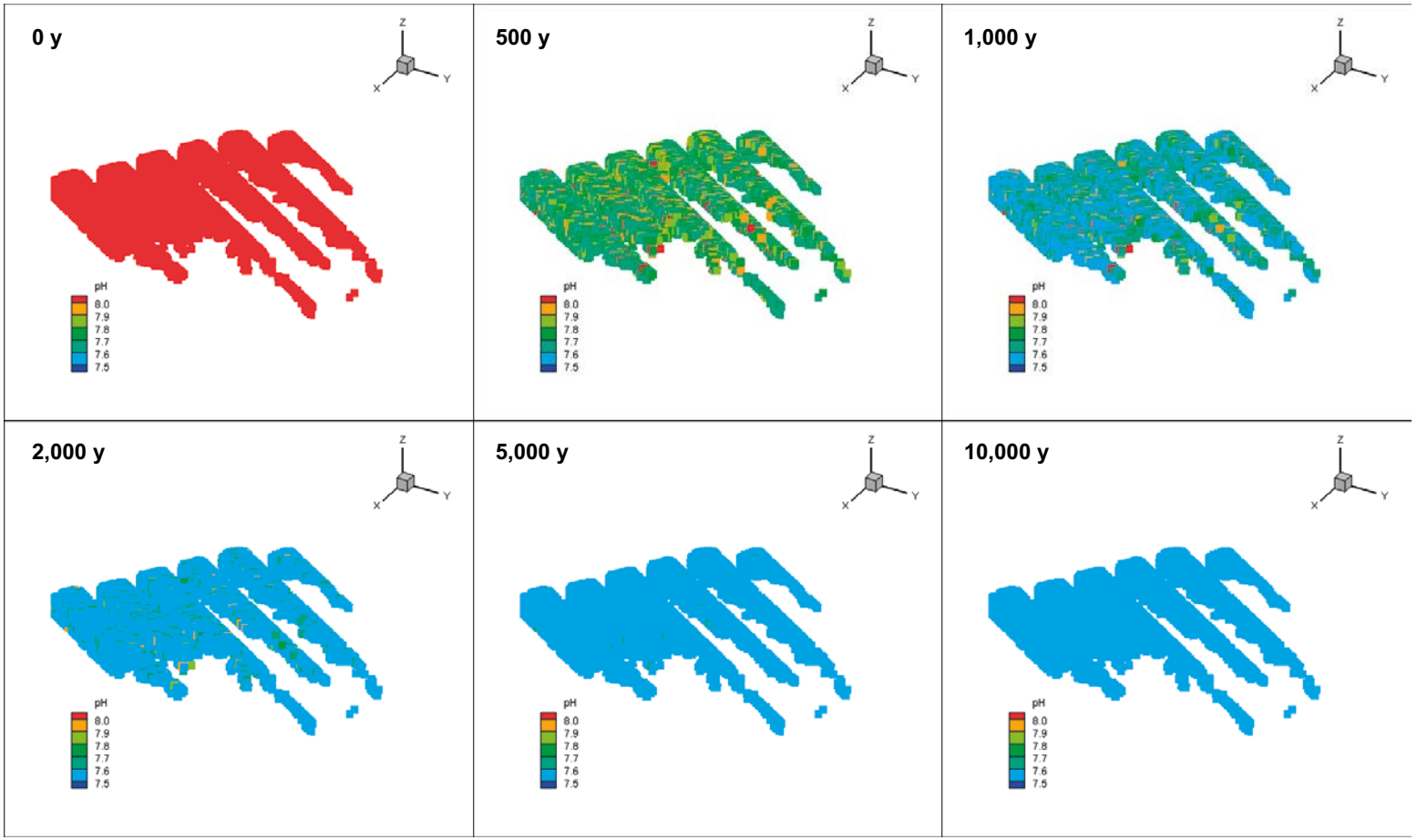


***Figure 4-7.*** *Temporal evolution of pH for the Base Case of the periglacial period (lake boundary water) at SFR3 repository depth over a period time of 10,000 years.*

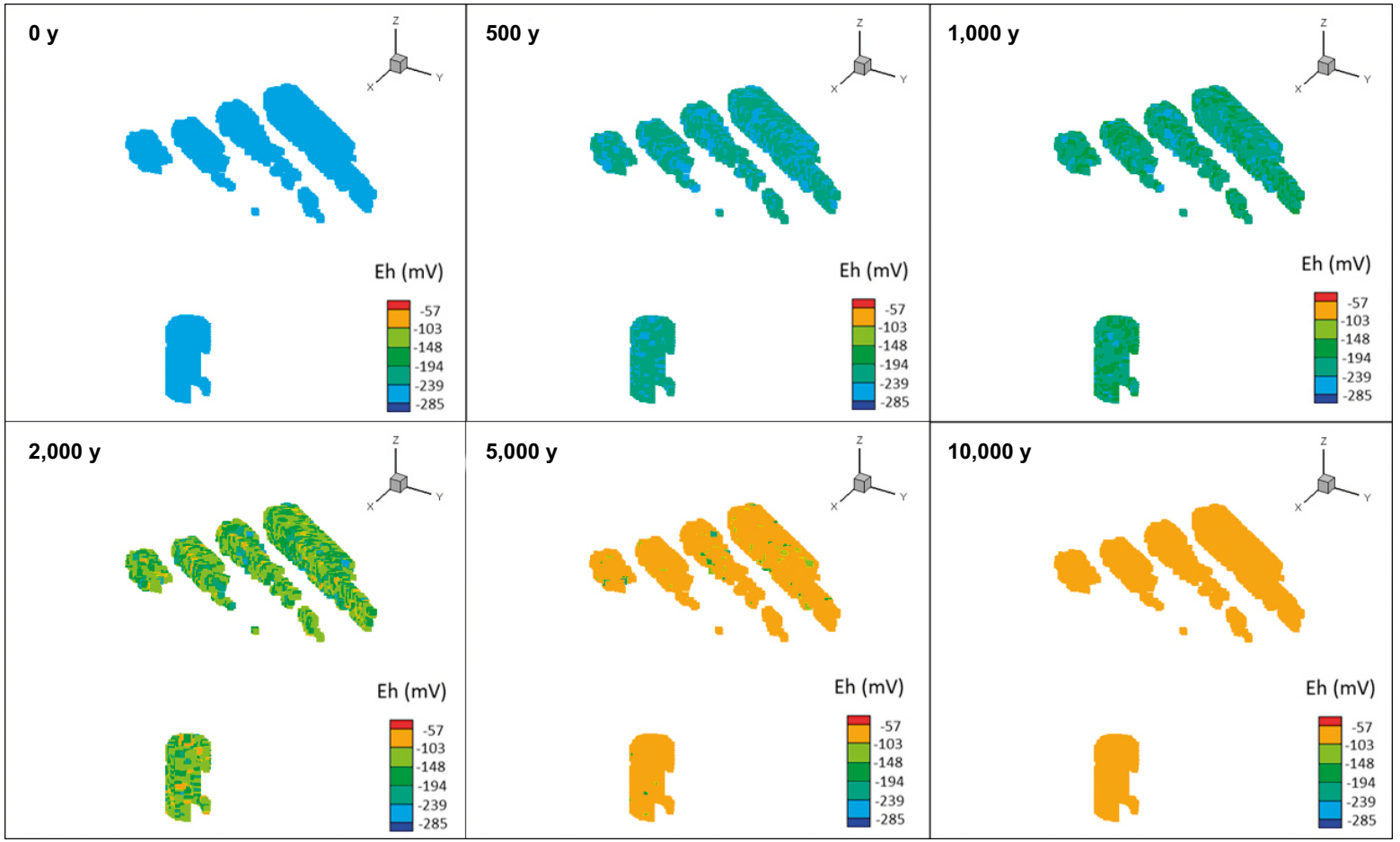


***Figure 4-8.*** *Temporal evolution of Eh (mV) for the Base Case of the periglacial period (lake boundary water) at SFR1 repository depth over a period time of 10,000 years.*

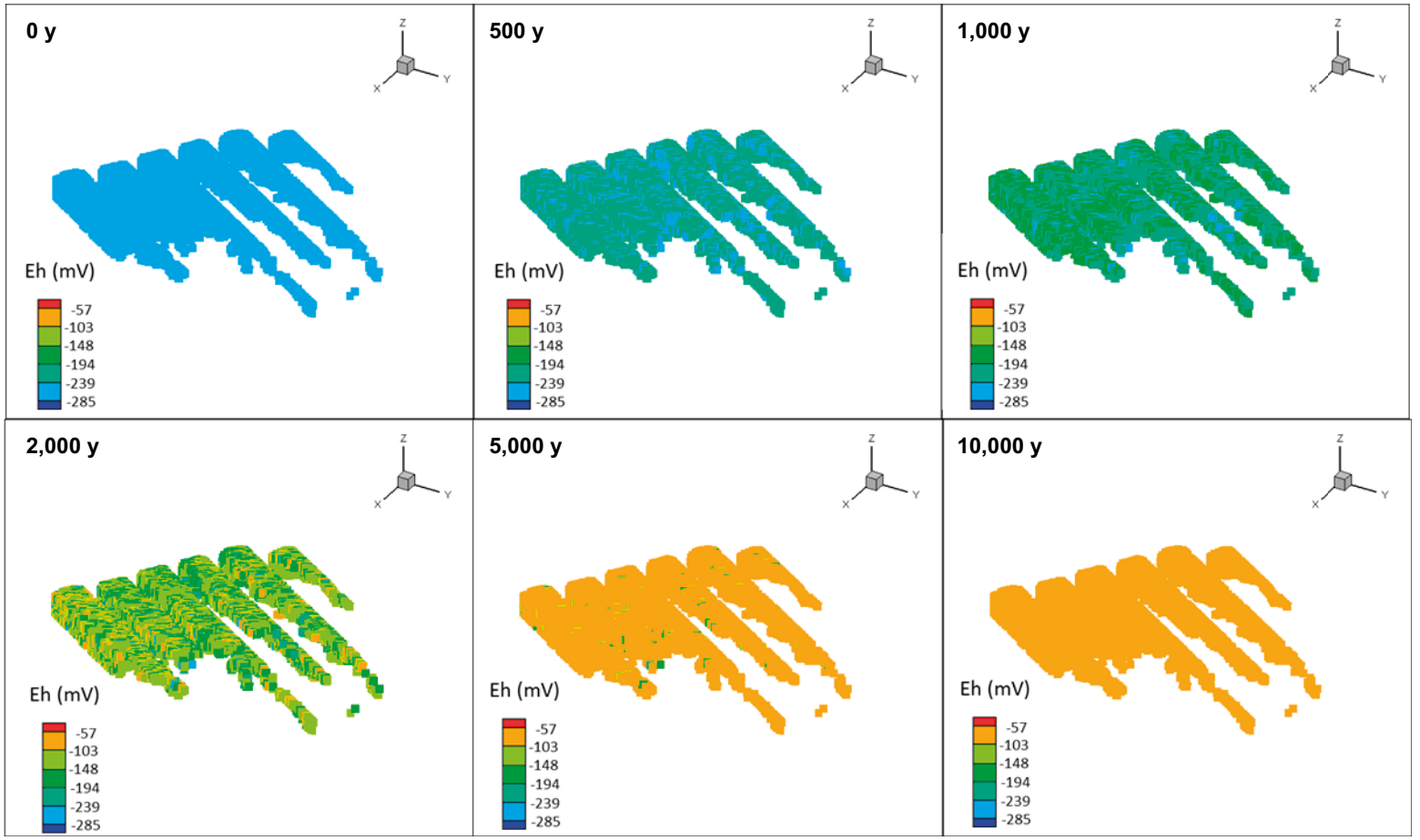


***Figure 4-9.*** *Temporal evolution of Eh (mV) for the Base Case of the periglacial period (lake boundary water) at SFR3 repository depth over a period time of 10,000 years.*

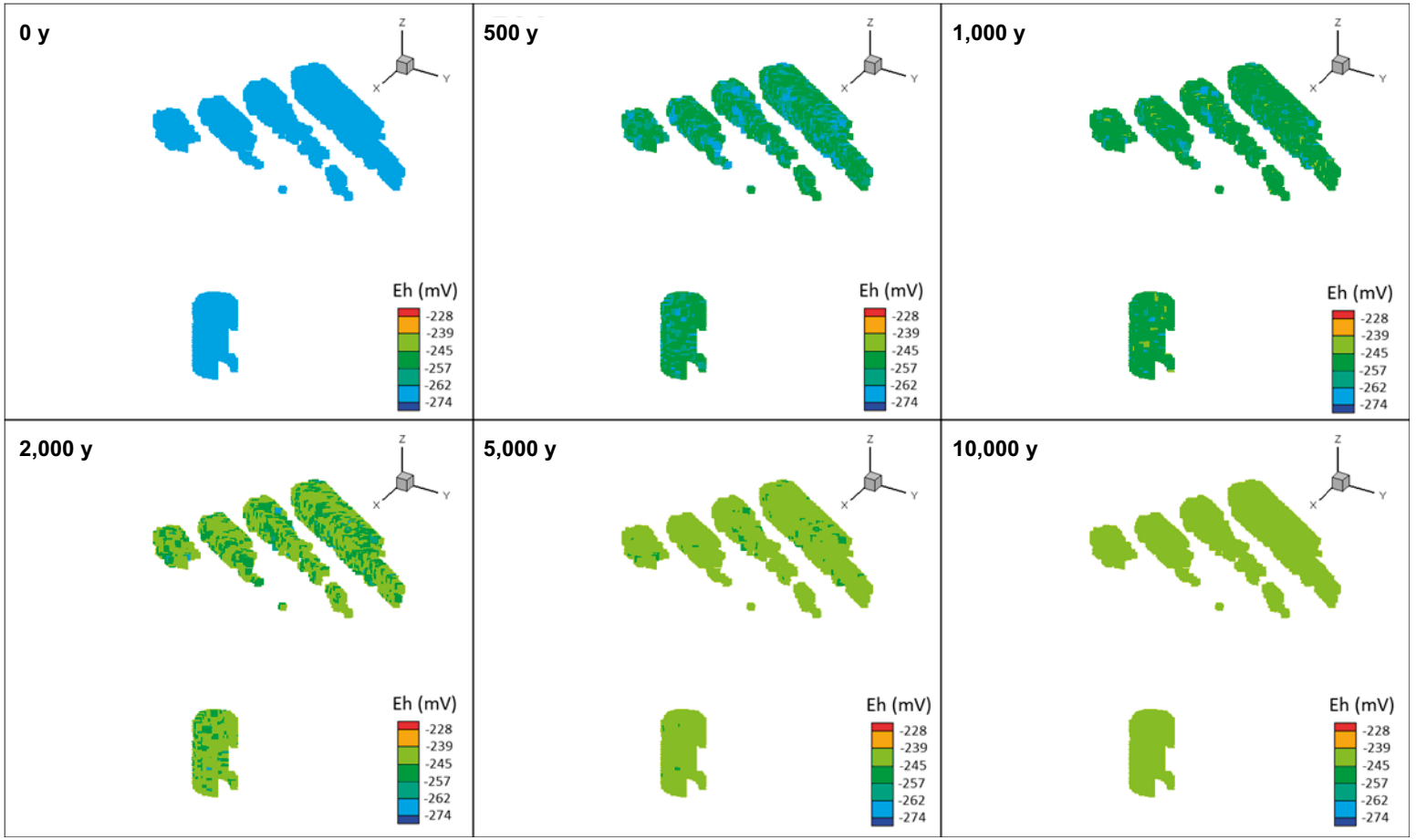


***Figure 4-10.*** *Temporal evolution of Eh (mV) for the Variant Case of the periglacial period (lake boundary water) at SFR1 repository depth over a period time of 10,000 years.*

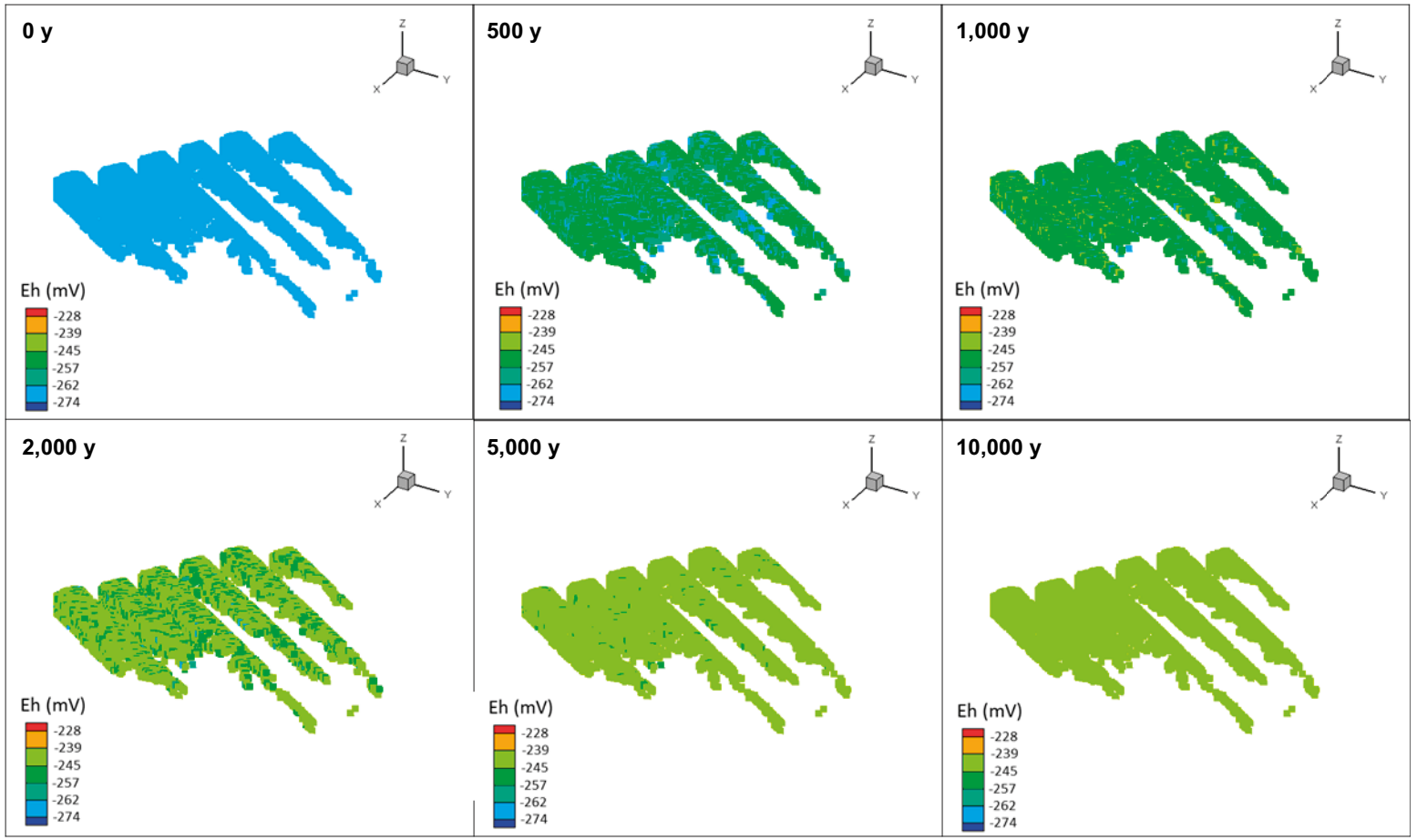


***Figure 4-11.*** *Temporal evolution of Eh (mV) for the Variant Case of the periglacial period (lake boundary water) at SFR3 repository depth over a period time of 10,000 years.*

### 4.1.2 Periglacial Period (glacial boundary water)

The computed results this case where very diluted waters are prescribed as infiltrating waters show that the range of the calculated salinities decreases with respect to those obtained for the end of the temperate period ( Figure 4-12 for SFR1 and Figure 4-13 for SFR3). Under the hydrogeological conditions assumed for this geochemical period, salinity at repository level is expected to decrease from $1.2 \cdot 10^{-4}$ M to $2 \cdot 10^{-5}$ M in a period time of 10,000 y in SFR1 and SFR3 (Figure 4-12 and Figure 4-13). Salinity values expressed as TDS (g/L) are included in Tables A3-5, A3-6, A3-7 and A3-8, Appendix 3.

Infiltration of these very diluted waters triggers calcite dissolution processes in the fracture and increases pH from 8.2 to 9.4 in groundwaters at repository level (Figure 4-14). The computed range of pH variation is slightly different for the Variant Case (equilibrium conditions with $FeS_{(am)}$) with respect to the Base Case (Figure 4-15).

The temporal and spatial evolution of pH values in SFR1 and SF3 is shown in Figure 4-16 and Figure 4-17.

In our calculations redox conditions are controlled by equilibrium with hematite or $FeS_{(am)}$, depending on the geochemical case. Along these equilibrium reactions, the Eh values are fixed at each cell in the fractures when the pH is defined by calcite equilibrium reaction. This interdependence of pH and Eh determinate that changes produced by the increase of pH due to calcite dissolution processes modify the Eh values computed under equilibrium conditions with hematite or $FeS_{(am)}$. This process is clearly observed if the Eh values plotted in Figure 4-18 and Figure 4-19 are compared to Figure 4-14 and Figure 4-15, respectively. The values for the Base Case are slightly higher than those reported for the Variant Case (the latter assumes equilibrium conditions with $FeS_{(am)}$). The increase of Eh values observed after 2,000 years for the Base Case is a consequence of the progressive depletion of the buffer effect of the matrix. The rock matrix is accessed by diffusion and have a large potential reducing capacity. In any case, reducing conditions are computed under the assumed geochemical conditions for all the considered simulation cases.

Temporal changes in redox conditions are expected throughout a period of 2,000 years as consequence of calcite dissolution during water infiltration. From this time and onward, the Eh remains stable around a value of –304 mV for the Base Case (Figure 4-20 and Figure 4-21) and –352 mV for the Variant Case (Figure 4-22) as calcite dissolution is stopped. As both geochemical cases have been defined to be probable from a geochemical point of view, the whole range of Eh variation for the periglacial period can be estimated between –271 mV and –352 mV.

Major groundwater components as Na, K, Ca and Mg will follow the salinity trend (see Tables A3-5, A3-6, A3-7 and A3-8, Appendix 3). Sodium, K and Mg concentrations vary from $5 \cdot 10^{-4}$ M – $7.39 \cdot 10^{-6}$ M, $5.88 \cdot 10^{-5}$ M – $1.02 \cdot 10^{-5}$ M, and $7.82 \cdot 10^{-5}$ M – $4.11 \cdot 10^{-6}$ M, respectively. These low concentrations are a direct consequence of dilution processes (cation exchange reactions have not been included in the calculations). In contrast, Ca which is controlled by dissolution/precipitation of calcite is less affected by periglacial conditions and display a range of variation between $7.61 \cdot 10^{-4}$ M and $1.85 \cdot 10^{-4}$ M.

The evolution of iron and sulfur species is controlled in our model by the same reactions described for the Temperate Period. The computed Fe concentrations for the Variant Case ($6.56 \cdot 10^{-6}$ M – $6.33 \cdot 10^{-6}$ M) are higher than Fe concentrations computed in equilibrium with hematite ($4.92 \cdot 10^{-8}$ M – $4.06 \cdot 10^{-11}$ M) (Tables A3-5, A3-6, A3-7, A3-8, Appendix 3).

Sulphide concentrations under the assumption of equilibrium with respect to Fe(II) sulphide (from $1.26 \cdot 10^{-4}$ M to $2.8 \cdot 10^{-4}$ M) are also higher that those computed for the Base Case (from $4.39 \cdot 10^{-9}$ M to $1.08 \cdot 10^{-6}$ M).

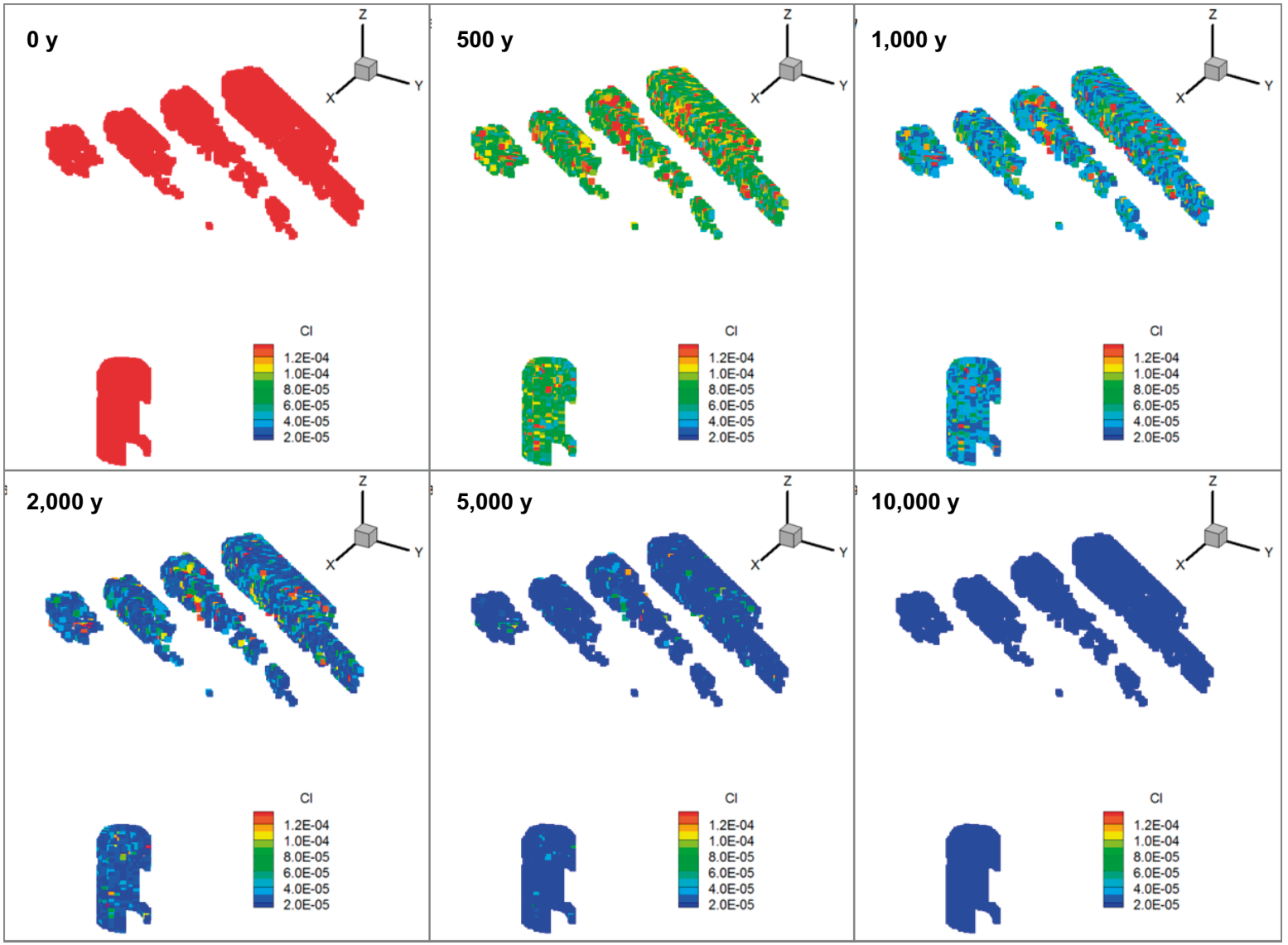


***Figure 4-12.*** *Distribution of chloride concentrations (mol/L) for the Base and Variant cases (glacial boundary water) of the periglacial period at SFR1 repository depth for a period time of 10,000 years.*

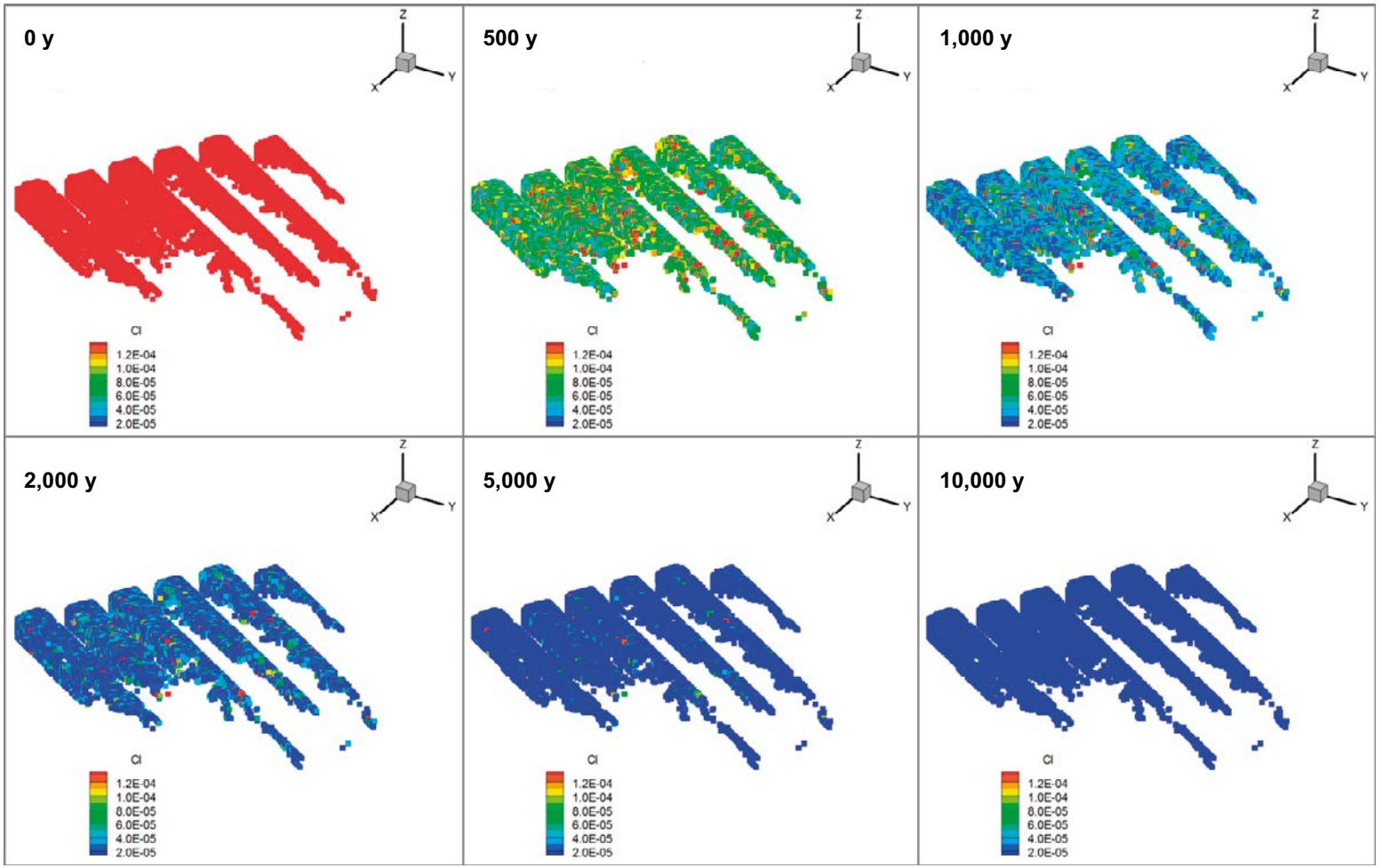


***Figure 4-13.*** *Distribution of chloride concentrations (mol/L) for the Base and Variant cases (glacial boundary water) of the periglacial period at SFR3 repository depth for a period time of 10,000 years.*

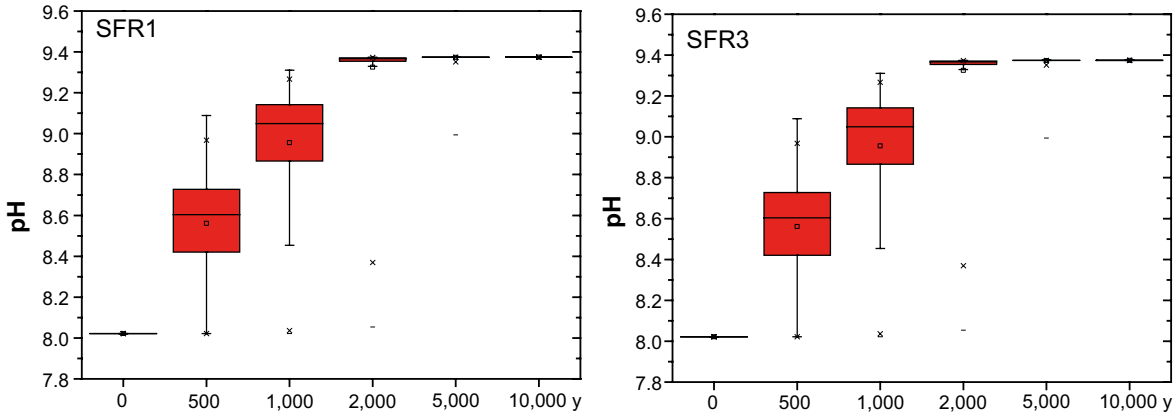


***Figure 4-14.*** *Box-and- whiskers plots showing the statistical distribution of pH at repository depth for the Base Case and for the periglacial period (glacial boundary water). The statistical measures are the median, the 25th and 75th percentile (box), the mean (square), the 5th and 95th percentile ("whiskers") and the maximum and the minimum values.*

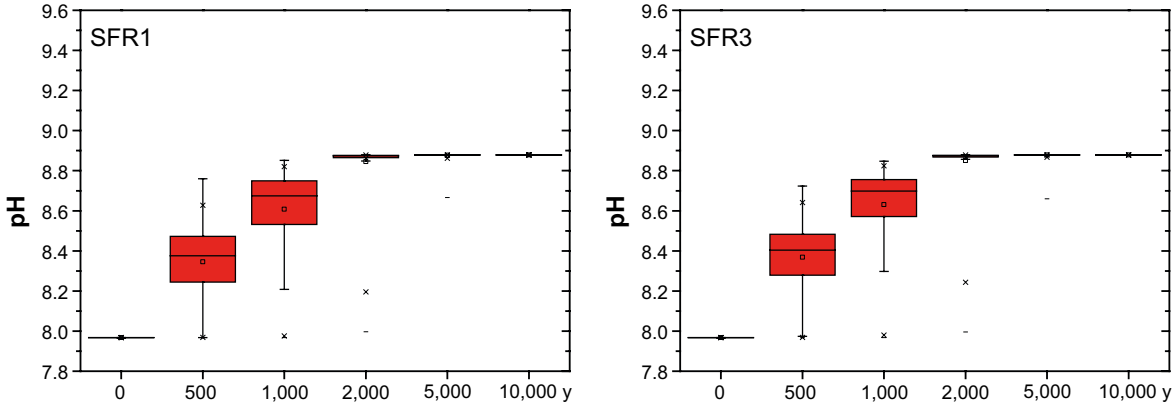


***Figure 4-15.*** *Box-and- whiskers plots showing the statistical distribution of pH at repository depth for the Variant Case and for the periglacial period (glacial boundary water). The statistical measures are the median, the 25th and 75th percentile (box), the mean (square), the 5th and 95th percentile ("whiskers") and the maximum and the minimum values.*

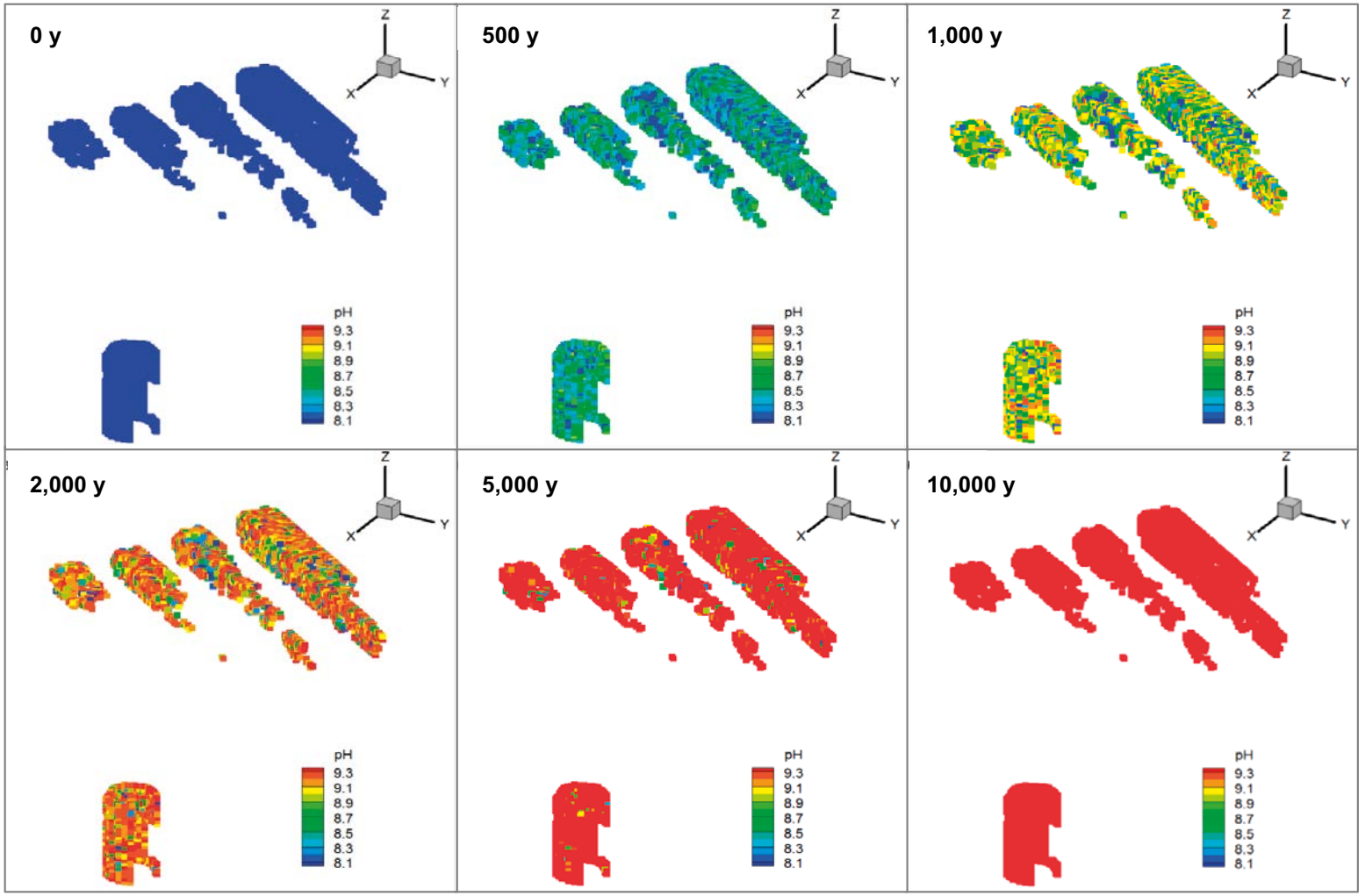


***Figure 4-16.*** *Distribution of pH for the Base Case of the periglacial period (glacial boundary water) at SFR1 repository depth over a period time of 10,000 years.*

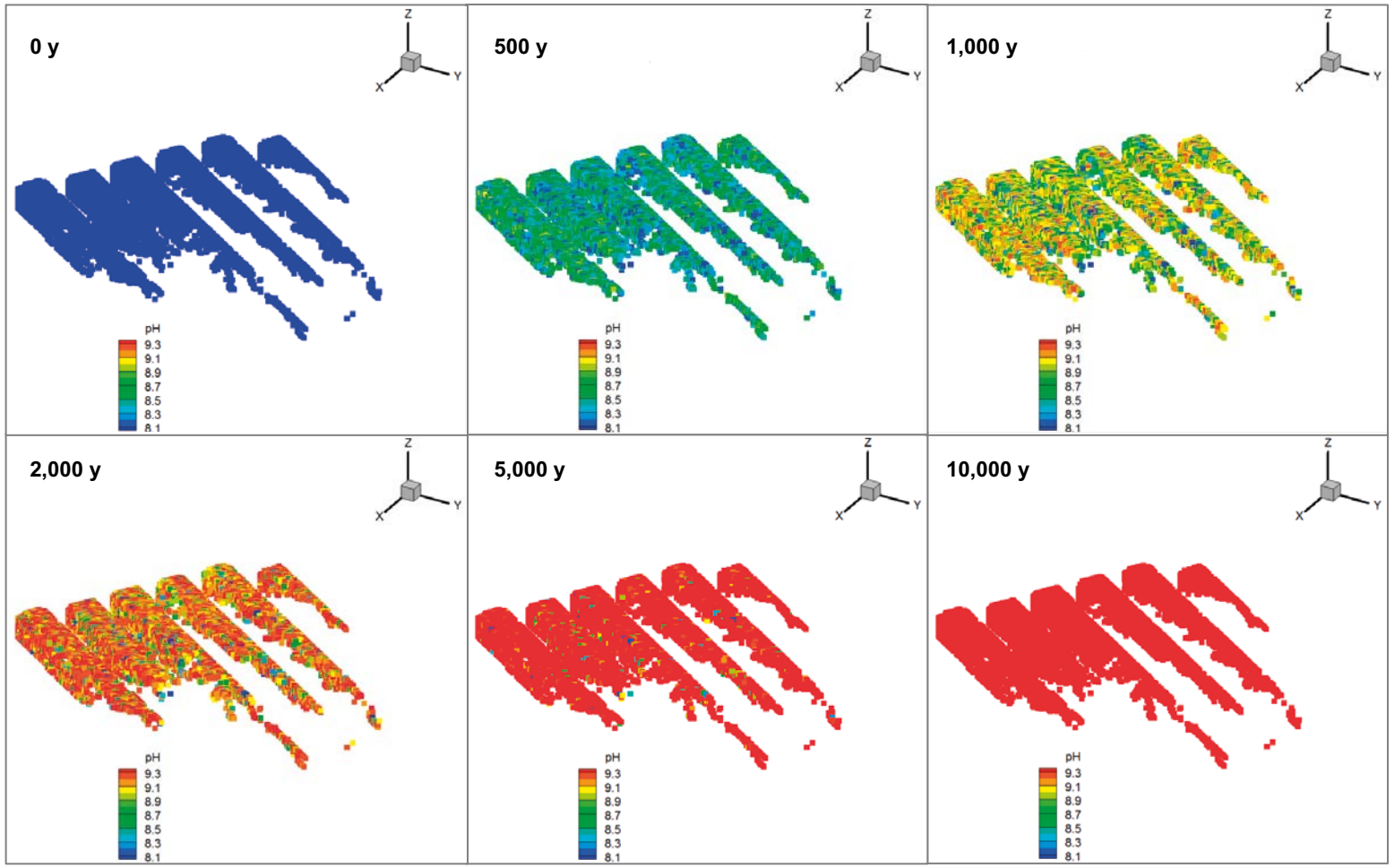


***Figure 4-17.*** *Distribution of pH for the Base Case of the periglacial period (glacial boundary water) at SFR3 repository depth over a period time of 10,000 years.*

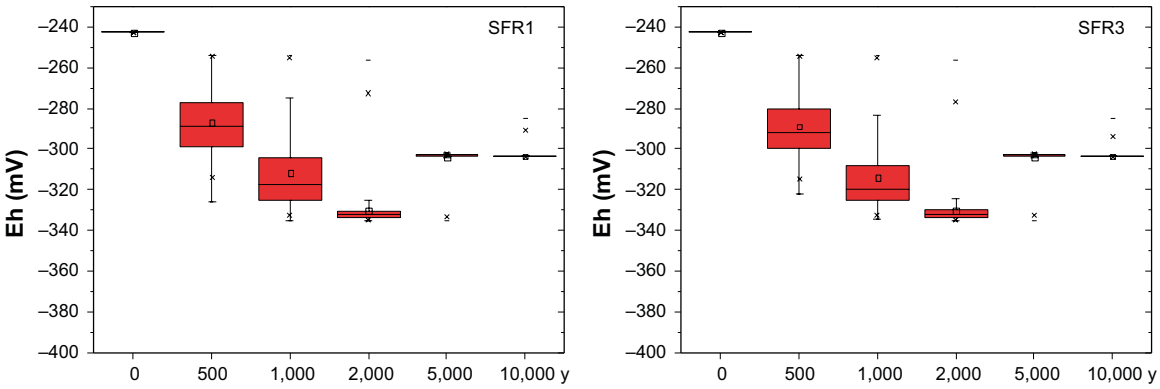


***Figure 4-18.*** *Box-and- whiskers plots showing the statistical distribution of Eh(mV) at repository depth for the Base Case and for the periglacial period(glacial boundary water). The statistical measures are the median, the 25th and 75th percentile (box), the mean (square), the 5th and 95th percentile ("whiskers") and the maximum and the minimum values.*

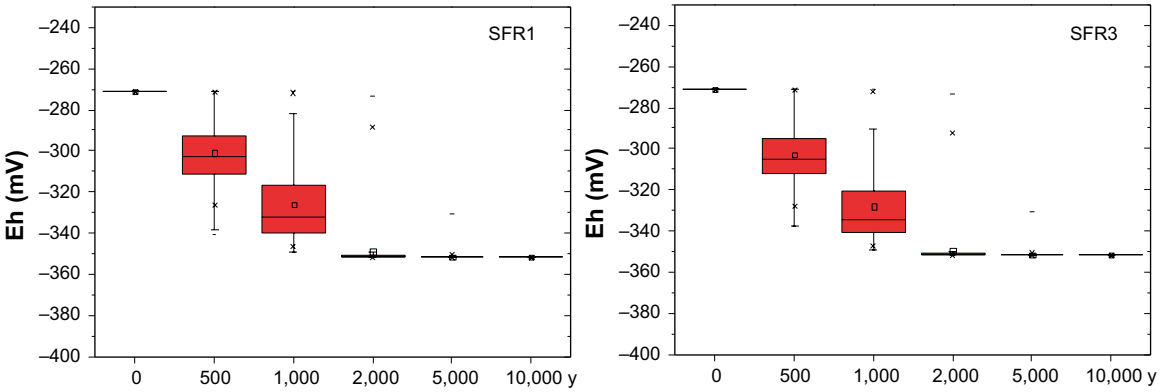


***Figure 4-19.*** *Box-and- whiskers plots showing the statistical distribution of Eh(mV) at repository depth for the Variant Case and for the periglacial period(glacial boundary waters). The statistical measures are the median, the 25th and 75th percentile (box), the mean (square), the 5th and 95th percentile ("whiskers") and the maximum and the minimum values.*

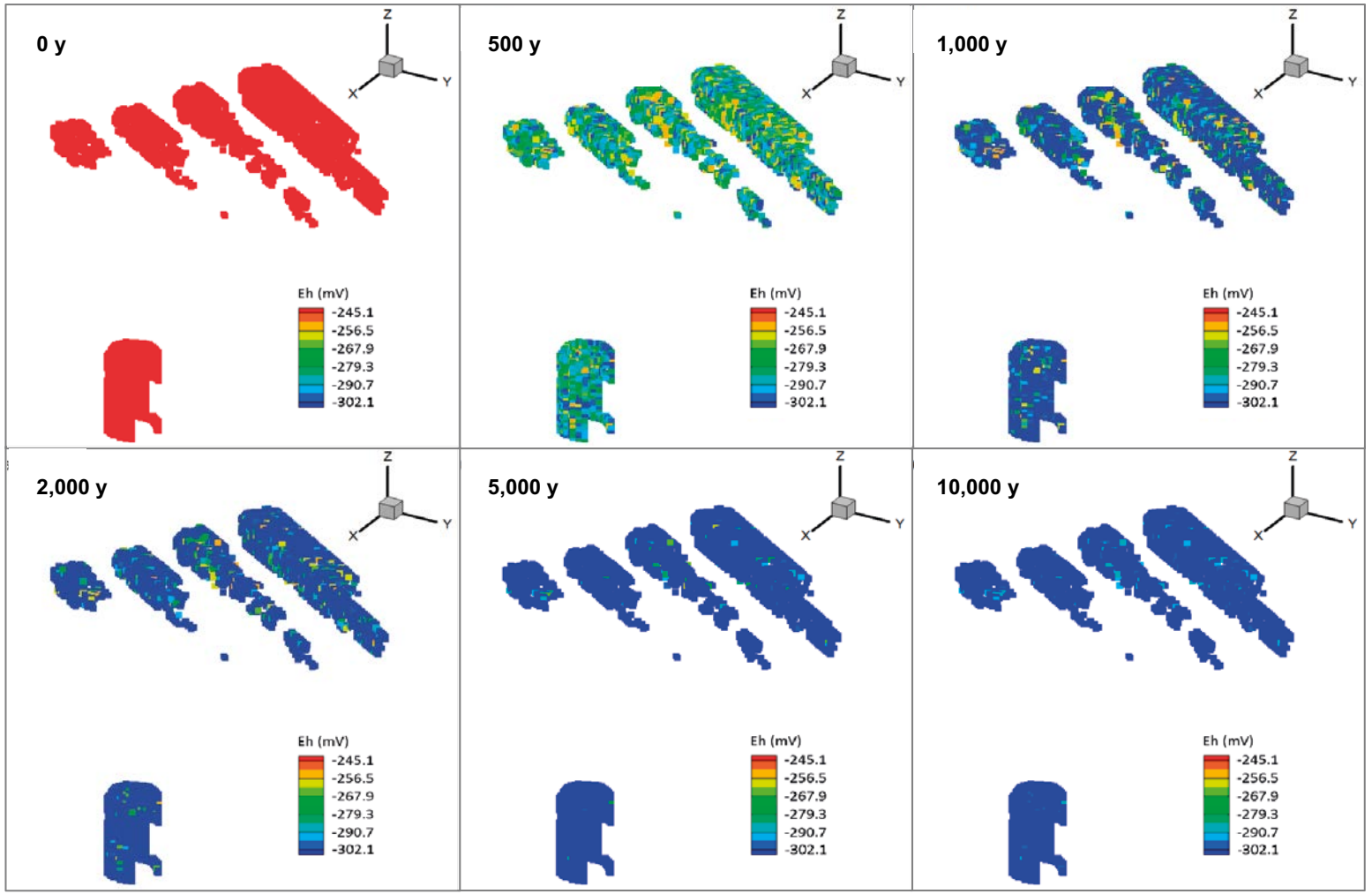


***Figure 4-20.*** *Temporal evolution of Eh(mV) of the periglacial period (glacial boundary water) for the Base Case at SFR1 repository depth over a period time of 10,000 years.*

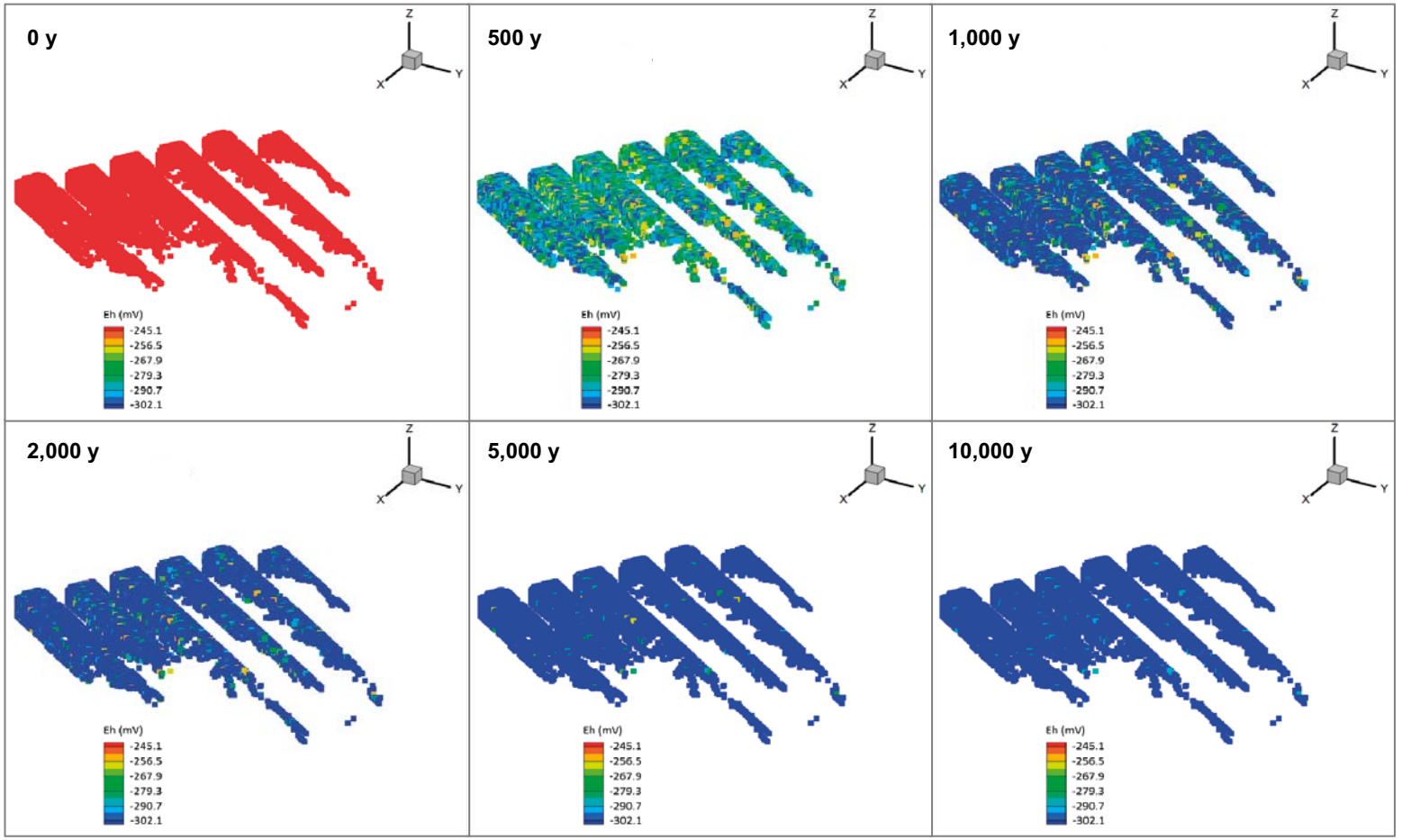


***Figure 4-21.*** *Temporal evolution of Eh(mV) of the periglacial period (glacial boundary water) for the Base Case at SFR3 repository depth over a period time of 10,000 years.*

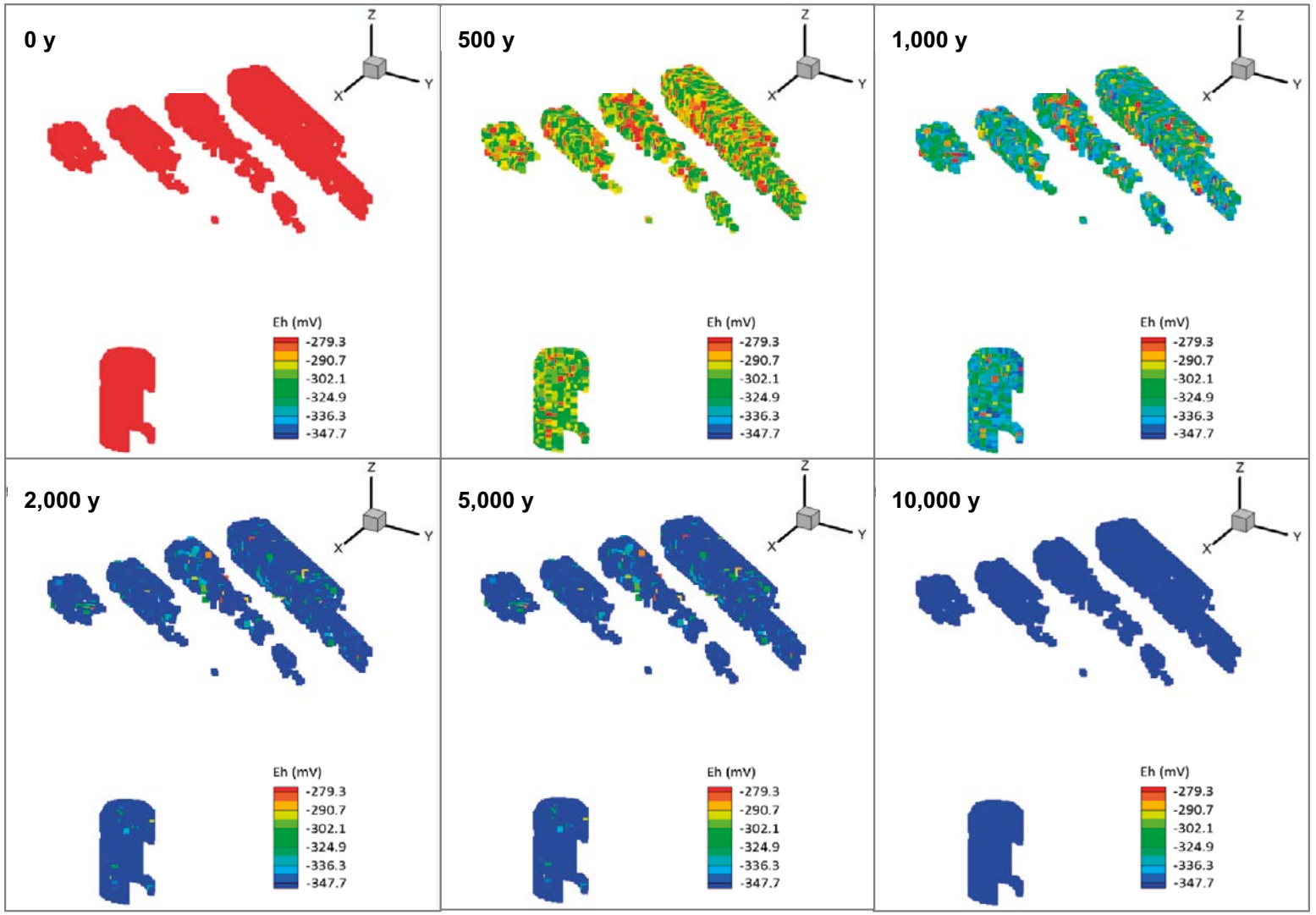


***Figure 4-22.*** *Temporal evolution of Eh (mV) for the Variant Case of the periglacial period (glacial boundary water) at SFR1 repository depth over a period time of 10,000 years.*

# 5 Uncertainties and model simplifications

The results presented in this report are affected by different sources of uncertainties. Some of these uncertainties have already been addressed by means of Monte Carlo simulations (see Section 3.3); others are qualitatively discussed in this section.

## 5.1 Recharge paths and travel times

As pointed out in Section 2.1.3, the reactive transport calculations are heavily dependent on the groundwater flow models, from which they take all the hydrogeological information; i.e. recharge paths and related travel times. It turns out that the results of our calculations inherit all the uncertainties that stem from the hydrogeological conceptual model.

In Öhman et al. (2014), a sensitivity analysis is included to assess the combined effect of bedrock heterogeneity and the related parameterization uncertainty. This was done considering 17 "Bedrock cases" where the bedrock parameterization was changed based on different HCD structures and different DFN realizations. In the reactive transport calculations, only the results of BASE_CASE1_DFN_R85 are considered. According to Öhman et al. (2014), this bedrock has, on average, "median flow percentiles". It turns out that, loosely speaking; the distribution of travel times used in our calculations can be considered representative of the expected (average) flow conditions. "Extreme" Bedrock cases, with faster or slower flow patterns, would lead to respectively faster and slower propagations of the "infiltration signature" at repository depth.

Moreover, it should be recognized that neither the temperate nor the periglacial hydrogeological simulations had the analysis of recharge patterns as a major performance measure. It turns out that the recharge paths and related travel times delineated by the groundwater flow models are affected by additional epistemic uncertainty, which is indeed propagated to the results of the reactive transport calculations.

## 5.2 Matrix diffusion processes

Exchange processes between the fractures and the surrounding matrix are represented in a simplified way; using a first order approximation. The reason for using this approach lies in the limitation of PHREEQC to efficiently simulate matrix diffusion processes in an explicit way.

The first-order approximation implicitly assumes that that the solute is always instantaneously mixed in the porewater of the matrix. This assumption is rigorously valid only when the characteristic time for diffusion is faster than the characteristic advective time in the fracture.

As pointed out by Haggerty and Gorelick (1995), the first-order approximation tends to underestimate the time taken by the system to reach equilibrium. This means that our models underestimate the time taken by the "infiltration signature" to propagate until repository depth.

## 5.3 Geochemical processes

Equilibrium assumptions, generalized over the whole studied rocks, it is a model simplification. However, this assumption sounds reasonable taking into account the reported minerals in the fracture fillings and the composition of the present groundwaters in the SFR site. The approach used to calculate Eh conditions simplifies the behavior of the real system imposing, alternatively, equilibrium conditions with hematite or $FeS_{(am)}$. This uncertainty has been dealt combining the computed results for the Base and Variant Cases to provide a range of variation for most relevant parameters, but being able to explain separately the two possible cases.

Other processes different from dissolution-precipitation reactions under equilibrium conditions, like cation exchange and kinetic dissolution of silicates, have not been included in the simulations of the Base and Variant Cases. They have been treated as sensitivity cases in Section 3.3.

# 6 Summary and Conclusions

The hydrogeological evolution of the groundwater in the area of the SFR repository, has been modelled by implementing a large-scale reactive transport model. The main objective was focused on the quantitative estimation of the chemical composition of groundwater during the temperate and periglacial periods. From a methodological point of view, the numerical approach integrates the results flow models to a set of one-dimensional reactive transport simulations using FASTREACT. For each modelling period (temperate and periglacial periods), a snapshot of the velocity field is taken from the hydrogeological model and one million particles are injected at repository depth and backtracked to the surface to delineate the infiltration paths and corresponding travel times.

The model conceptualization assumes that the hydrochemical evolution of the groundwater at repository depth is the result of infiltration processes from the surface of the domain to the repository. The infiltration occurs in an extended and complex network of fractures and the infiltrating waters, in turn, undergo geochemical reactions with the rock and minerals, namely calcite and hematite/$FeS_{(am)}$ precipitation/dissolution. In all the reactive transport simulations denoted as "Base Case" hematite is assumed to be the main iron mineral present in the fracture filling. An additional geochemical case, denoted as "Variant Case", has been defined where $FeS_{(am)}$, instead of hematite, is considered as the mineral controlling redox conditions. The role of other geochemical reactions, such as kinetic dissolution of aluminosilicates and cation exchange processes, have been assessed by performing Monte Carlo simulations.

Mass exchange between the transmissive zones and the low permeable matrix was simulated using a dual porosity approach for the temperate and periglacial periods.

## 6.1 Temperate period

During this climatic period, infiltration of meteoric water due to the progressive displacement of the Baltic shore line will mainly define the chemical composition of groundwaters in contact with the SFR repository. As a consequence of that, salinity will change and decrease. The computed chloride concentrations and TDS values show a progressive decrease driven by infiltration processes that occur at the surface. This "dilution" occurs in a period time of 600 from 2500 AD and is slightly counterbalanced by the release of evolved water from the matrix.

The results, computed over a time frame of 9,000 years (from 2500 AD), point out the strong buffering effect of mineral dissolution that control pH values in a range of 7.3–8.2 in groundwaters at repository level for this climatic period at both SFR1 and SFR3. Even considering that the signature of meteoric water arriving at repository depth will increase with time, our results predict that redox condition will remain with reducing characteristics during the whole temperate period. Buffering effect of fracture minerals will produce oxygen depletion in groundwaters. This is direct consequence of buffering effect of mineral such as hematite or $FeS_{(am)}$present in the fracture fillings and assumed to control redox under equilibrium conditions.

The behavior of major cations  is controlled by dilution processes due to the infiltration of meteoric origin waters and shows the same trend already observed for salinity. The cations contributing with the highest charge concentrations in the groundwater are Na and Ca, and to a much lower extend, Mg and K.

Sensitivity analyses provided information about the effect of other geochemical reactions as kinetic dissolution of silicates and cation exchange reactions. Our results suggest that uncertainties associated to residence times would impact on chemical composition of the water by increasing pH and releasing Si and Al into the groundwaters. This sensitivity analysis permitted us to define the range of variation of these elements in a wide range of residence times.

The assessment of the role of clays as exchanger in the fractures has allowed inferring a limited extent of these processes in the SFR system.

## 6.2 Periglacial period

The reactive transport simulations of the Periglacial period are affected by important sources of uncertainty associated with the definition of the hydrogeochemical initial state of the system.

Consistently with the Temperate calculations, all the numerical studies have been carried out assuming the presence of either calcite/hematite (Base case) or calcite/$FeS_{(am)}$ (Variant Case) in the fracture filling material.

The obtained results for the periglacial period performed with a lake boundary water, show that the chemical composition of groundwaters at repository depth will not be substantially modified by the infiltration of water from the taliks. Only slight changes has been computed in terms of pH, Eh, salinity and major cations for this period.

In contrast, infiltration of glacial water could have an evident impact on the evolution of the groundwater composition at repository depth. Longer residence times with respect to the temperate period are predicted for this period, and in a period of around 1 ky the salinity substantially decrease at repository deph.

The pH and Eh values are calculated to change between 8.2–9.4 and –271 mV and –352 mV, respectively. Major groundwater components follow the salinity trend.

# References

SKB's (Svensk Kärnbränslehantering AB) publications can be found at www.skb.se/publications. References to SKB's unpublished documents are listed separately at the end of the reference list. Unpublished documents will be submitted upon request to document@skb.se.


**Auqué, L F, Gimeno M J, Acero P, Gómez J, 2013.** Compositions of groundwater for SFR and its extension, during different climate cases, SR-PSU, SKB R-13-16, Svensk Kärnbränslehantering AB.

**Bodén A, Lundin J, 2007.** SFR kontrollprogram. Bergkontroll. Bergkontrollgruppens årsrapport 2006. Huvudrapport. Doknr 2448900-001, Vattenfall Power Consultant AB. (In Swedish.)

**Bradbury M H, Baeyens B, 2000.** A generalised sorption model for the concentration dependent uptake of caesium by argillaceous rocks. Journal of Contaminant Hydrology 42, 141–163.

**Brantley S L, Kubicki J D, White A F (eds), 2008.** Kinetics of water–rock interaction. New York: Springer.

**Curtis P, Markström I, Petersson J, Triumf C-A, Isaksson H, Mattsson H, 2011.** Site investigation SFR. Bedrock geology. SKB R-10-49, Svensk Kärnbränslehantering AB.

**de Vries L M, Trinchero P, Molinero J, 2012.** MCPhreeqc: extending geochemical modelling with automatic stochastic simulations. EGU General Assembly 2012 Vienna, 6355.

**Duro, L, Grivé M, Cera E, Domènech C, Bruno J, 2006.** Update of a thermodynamic database for radionuclides to assist solubility limits calculation for performance assessment. SKB TR-06-17, Svensk Kärnbränslehantering AB.

**French H M, 2007.** The periglacial environment. 3rd ed. Chichester: Wiley.

**Gimeno M J, Auqué L, Gómez J, Acero P, 2011.** Site investigation SFR. Water–rock interaction and mixing modelling in the SFR. SKB P-11-25, Svensk Kärnbränslehantering AB.

**Grivé M, Domènech C, Montoya V, García D, Duro L, 2010.** Determination and assessment of the concentration limits to be used in SR-Can. Supplement to TR-06-32. SKB R-10-50, Svensk Kärnbränslehantering AB.

**Haggerty R, Gorelick S M, 1995.** Multiple-rate mass transfer for modeling diffusion and surface reactions in media with pore-scale heterogeneity. Water Resources Research 31, 2383–2400.

**Hummel W, Berner U, Curti E, Pearson F J, Thoenen T, 2002.** Nagra/PSI Chemical thermodynamic data base 01/01. Boca Raton: Universal Publishers.

**Langmuir D, 1997.** Aqueous environmental geochemistry. Upper Saddle River, NJ: Prentice Hall.

**Lowson R T, Comarmod M-C J, Rajaratnam G, Brown P L, 2005.** The kinetics of the dissolution of chlorite as a function of pH and at 25°C. Geochimica et Cosmochimica Acta 69, 1687–1699.

**Löfgren M, Sidborn M, 2010.** Statistical analysis of results from the quantitative mapping of fracture minerals in Forsmark. Site descriptive modelling – complementary studies. SKB R-09-30, Svensk Kärnbränslehantering AB.

**Löfman J, Poteri A, Pitkänen P, 2010.** Modelling of salt water upconing in Olkiluoto. Posiva Working Report 2010-25, Posiva Oy, Finland.

**Malmström M E, Berglund S, Jarsjö J, 2008.** Combined effect of spatially variable flow and mineralogy on the attenuation of acid mine drainage in groundwater. Applied Geochemistry 23, 1419–1436.

**Nilsson A-C, Tullborg E-L, Smellie J, Gimeno M J, Gómez J B, Auqué L F, Sandström B, Pedersen K, 2011.** SFR site investigation. Bedrock hydrogeochemistry. SKB R-11-06, Svensk Kärnbränslehantering AB.

**Odén M, Follin S, Öhman J, Vidstrandt P, 2014.** SR-PSU Bedrock hydrogeology. Groundwater flow modelling methodology, setup and results. SKB R-13-25, Svensk Kärnbränslehantering AB.

**Parkhurst D L, Appelo C A J, 1999.** User's guide to PHREEQC (version 2): a computer program for speciation, batch-reaction, one-dimensional transport, and inverse geochemical calculations. Water-Resources Investigations Report 99-4259, U.S. Geological Survey, Denver, Colorado.

**Salas J, Gimeno M J, Auqué L F, Molinero J, Gómez J, Juárez I, 2010.** SR-Site – hydrogeochemical evolution of the Forsmark site. SKB TR-10-58, Svensk Kärnbränslehantering AB.

**Sandström B, Tullborg E-L, 2009.** Episodic fluid migration in the Fennoscandian Shield recorded by stable isotopes, rare earth elements and fluid inclusions in fracture minerals at Forsmark, Sweden. Chemical Geology 266, 135–151.

**Sandström B, Tullborg E-L, 2011.** Site investigation SFR. Fracture mineralogy and geochemistry of borehole sections sampled for groundwater chemistry and Eh. Results from boreholes KFR01, KFR08, KFR10, KFR19, KFR7A and KFR105. SKB P-11-01, Svensk Kärnbränslehantering AB.

**Sandström B, Tullborg E-L, de Torres T, Ortiz J E, 2006.** The occurrence and potential origin of asphaltite in bedrock fractures, Forsmark, central Sweden. GFF 128, 233–242.

**Sandström B, Tullborg E-L, Smellie J, MacKenzie A B, Suksi J, 2008.** Fracture mineralogy of the Forsmark site. SDM-Site Forsmark. SKB R-08-102, Svensk Kärnbränslehantering AB.

**Sandström B, Tullborg E-L, Larson S Å, Page L, 2009.** Brittle tectonothermal evolution in the Forsmark area, central Fennoscandian Shield, recorded by paragenesis, orientation and $^{40}Ar/^{39}Ar$ geochronology of fracture minerals. Tectonophysics 478, 158–174.

**Sandström B, Annersten H, Tullborg E-L, 2010.** Fracture-related hydrothermal alteration of metagranitic rock and associated changes in mineralogy, geochemistry and degree of oxidation: a case study at Forsmark, central Sweden. International Journal of Earth Sciences 99, 1–25.

**Sandström B, Tullborg E-L, Sidborn M, 2014.** Iron hydroxide occurrence and redox capacity in bedrock fractures in the vicinity of SFR. SKB R-12-11, Svensk Kärnbränslehantering AB.

**Shapiro A M, Cvetkovic V D , 1988.** Stochastic analysis of solute arrival time in heterogeneous porous media. Water Resources Research 24, 1711–1718.

**SKB, 2008.** Site decription of Forsmark at completion of the site investigation phase. SDM-Site Forsmark. SKB TR-08-05, Svensk Kärnbränslehantering AB.

**SKB, 2013.** Site description of the SFR area at Forsmark at completion of the site investigation phase. SDM-PSU Forsmark. SKB TR-11-04, Svensk Kärnbränslehantering AB.

**SKB, 2014a.** Safety analysis for SFR. Long-term safety. Main report for the safety assessment SR-PSU. SKB TR-14-01, Svensk Kärnbränslehantering AB.

**SKB, 2014b.** Geosphere process report for the safety assessment SR-PSU. SKB TR-14-05, Svensk Kärnbränslehantering AB.

**SKB, 2014c.** Data report for the for the safety assessment SR-PSU. TR-14-10, Svensk Kärnbränslehantering AB.

**SKB, 2014d.** Climate and climate-related issues for the safety assessment SR-PSU. SKB TR-13-05, Svensk Kärnbränslehantering AB.

**Stephens M B, Fox A, La Pointe P, Simeonov A, Isaksson H, Hermansson J, Öhman J, 2007.** Geology Forsmark. Site descriptive modelling Forsmark stage 2.2. SKB R-07-45, Svensk Kärnbränslehantering AB.

**Stigsson M, Follin S, Andersson J, 1998.** On the simulation of variable density flow at SFR, Sweden. SKB R-99-08, Svensk Kärnbränslehantering AB.

**Svensson U, 2010.** Darcy Tools version 3.4. Verification, validation and demonstration. SKB R-10-71, Svensk Kärnbränslehantering AB

**Sverdrup H U, 1990.** The kinetics of base cation release due to chemical weathering. Lund: Lund University Press.

**Trinchero P, Molinero J, Román-Ross G, 2014a.** FASTREACT – A streamline-based approach for the solution of multicomponent reactive transport problems. SKB R-10-45, Svensk Kärnbränslehantering AB.

**Trinchero P, Román-Ross G, Maia F, Molinero J, 2014b.** Posiva safety case hydrogeochemical evolution of the Olkiluoto site. Posiva Working Report 2014-09, Posiva Oy, Finland.

**Tröjbom M, Söderbäck B, 2006.** Chemical characteristics of surface systems in the Forsmark area. Visualisation and statisticasl evaluation of data from shallow groundwater, precipitation, and regolith. SKB R-06-19, Svensk Kärnbränslehantering AB.

**van Genuchten M T, 1985.** A general approach for modeling solute transport in structured soils. IAH Memoirs 17, 513–526.

**Vidstrand P, Follin S, Öhman J, 2014.** SR-PSU Hydrogeological modelling. TD13 – Periglacial climate conditions. SKB P-14-06, Svensk Kärnbränslehantering AB.

**Öhman J, Follin S, Odén M, 2014.** SR-PSU Hydrogeological modelling. TD11 – Temperate climate conditions. SKB P-14-04, Svensk Kärnbränslehantering AB.

### Unpublished documents

| SKBdoc id, version | Title | Issuer, year |
|---|---|---|
| 1261302 ver 1.0 | Thermodynamic database_TDB_SKB-2009 | SKB, 2013 |

# Appendix 1

## Input files used for the parameterization of the FASTREACT reference simulations

As specified in Section 2.2, the numerical study presented in this report has been carried out using the FASTREACT methodology. This approach consists in the collection of information on advective transport and the formulation of travel time PDFs. This is usually done by means of particle tracking simulations. In this appendix we provide details about the different particle tracking simulations used to parameterize the different FASTREACT models.

### 1. Temperate period simulations

The simulations have been performed using the hydrogeological base case "TD11 BASE_CASE1_ DFN_R85" and the repository layout denoted as *TD11*.

The files, which correspond to the recharge locations for the two facilities at different time, are those stored in the ProjectPlace folders denoted as:

- TD11_c01_BASE_CASE1_DFN_R85_L1BC_RECHARGE_SFR1_(2013-02-20).zip
- TD11_c01_BASE_CASE1_DFN_R85_L1BC_RECHARGE_Extension_(2013-02-20).zip

The first compressed folder contains these six files:

- BASE_CASE1_DFN_R85_L1BC_2000AD_All_SFR1_D__Exit_loc.dat
- BASE_CASE1_DFN_R85_L1BC_2500AD_All_SFR1_D__Exit_loc.dat
- BASE_CASE1_DFN_R85_L1BC_3000AD_All_SFR1_D__Exit_loc.dat
- BASE_CASE1_DFN_R85_L1BC_3500AD_All_SFR1_D__Exit_loc.dat
- BASE_CASE1_DFN_R85_L1BC_5000AD_All_SFR1_D__Exit_loc.dat
- BASE_CASE1_DFN_R85_L1BC_9000AD_All_SFR1_D__Exit_loc.dat

The second compressed folder contains these six files:

- BASE_CASE1_DFN_R85_L1BC_2000AD_All_SFR2_D__Exit_loc.dat
- BASE_CASE1_DFN_R85_L1BC_2500AD_All_SFR2_D__Exit_loc.dat
- BASE_CASE1_DFN_R85_L1BC_3000AD_All_SFR2_D__Exit_loc.dat
- BASE_CASE1_DFN_R85_L1BC_3500AD_All_SFR2_D__Exit_loc.dat
- BASE_CASE1_DFN_R85_L1BC_5000AD_All_SFR2_D__Exit_loc.dat
- BASE_CASE1_DFN_R85_L1BC_9000AD_All_SFR2_D__Exit_loc.dat

The format of these files is shown in the following screenshot.

| Wall_ID | Wall_q(m/s) | Release_X | Release_Y | Relea_Z | Time (s) | F-quot(s/m) | Exit_q(m/s) | A(m2) | Exit___X | Exit___Y | Exit__Z | Path_L (m) | Cell_ID |
|---|---|---|---|---|---|---|---|---|---|---|---|---|---|
| Z3118603 | 0.41786E-10 | 1632843.9 | 6701847.9 | -74.00 | 0.32248E+09 | 0.44195E+13 | 0.11041E-09 | 64. | 1632949.7 | 6701755.4 | -6.50 | 0.2140E+03 | 6276529 |
| X2875080 | 0.13875E-09 | 1632857.9 | 6701998.0 | -83.00 | 0.17957E+09 | 0.61514E+12 | 0.38717E-09 | 64. | 1632965.6 | 6701735.7 | -6.50 | 0.4477E+03 | 6272276 |
| Z3110645 | 0.35977E-08 | 1632816.9 | 6701065.2 | -74.00 | 0.99200E+08 | 0.35395E+12 | 0.67802E-09 | 64. | 1632931.1 | 6701601.8 | -6.50 | 0.2798E+03 | 6271695 |
| Z3554776 | 0.89016E-10 | 1632916.0 | 6701960.9 | -78.00 | 0.16494E+09 | 0.10758E+13 | 0.84411E-09 | 64. | 1632955.9 | 6701779.9 | -6.50 | 0.3414E+03 | 6271586 |
| Y3362679 | 0.52606E-12 | 1633051.2 | 6701976.5 | -99.50 | 0.77130E+09 | 0.43779E+13 | 0.21365E-08 | 64. | 1632959.6 | 6701815.5 | -6.00 | 0.3255E+03 | 1007324 |

The following columns have been analyzed and used to parameterize the FASTREACT reference simulations:

- Column 10, 11, 12. These columns provide the recharge location of each trajectory.
- Column 6. This column provides the total advective travel time of each trajectory.

## 2. Periglacial simulations

The simulation is representative of the shallow permafrost and the bedrock base case. This information has been directly provided by the hydrogeological modellers via peer-to-peer file sharing, so it is not possible to keep track of the orginal file.

The format of these files is shown in the following screenshot.

| Wall__ID | Wall_q(m/s) | Release_X | Release_Y | Relea_Z | Time (s) | F-quot(s/m) | FWS (m2) | Exit_q(m/s) | A(m2) | Exit____X | Exit____Y | Exit__Z | Path_L (m) | Cell_ID |
|---|---|---|---|---|---|---|---|---|---|---|---|---|---|---|
| X4251098 | 0.33839E-08 | 1632841.3 | 6701849.6 | -75.00 | 0.11002E+10 | 0.33346E+13 | 0.27196E+07 | 0.16747E-07 | 1024. | 1629704.2 | 6698631.6 | 8.00 | 0.6419E+04 | 3388418 |
| Y4452918 | 0.21609E-10 | 1633062.3 | 6701970.6 | -83.00 | 0.28157E+10 | 0.99378E+13 | 0.27881E+07 | 0.33190E-08 | 1024. | 1629132.7 | 6698807.0 | 6.00 | 0.7845E+04 | 2942327 |
| X4519392 | 0.67272E-08 | 1632818.2 | 6701869.1 | -73.00 | 0.17135E+10 | 0.13086E+14 | 0.27593E+07 | 0.30091E-08 | 1024. | 1628917.0 | 6698944.9 | 7.00 | 0.7087E+04 | 1785608 |
| Z4836689 | 0.15900E-09 | 1632822.1 | 6701940.2 | -70.00 | 0.14432E+10 | 0.36497E+13 | 0.23978E+07 | 0.15726E-07 | 1024. | 1629660.0 | 6698621.8 | 6.00 | 0.6783E+04 | 2945503 |
| Y4473632 | 0.56022E-08 | 1632869.7 | 6701832.6 | -79.00 | 0.14577E+10 | 0.30358E+13 | 0.26106E+07 | 0.60590E-08 | 1024. | 1629059.4 | 6698929.8 | 11.00 | 0.7136E+04 | 1408726 |
| Z4246339 | 0.17239E-08 | 1632783.2 | 6701886.7 | -72.00 | 0.12611E+10 | 0.19830E+13 | 0.29255E+07 | 0.64623E-08 | 1024. | 1628944.0 | 6698927.6 | 8.00 | 0.7519E+04 | 3386546 |

The following columns have been analyzed and used to parameterize the FASTREACT reference simulations:

- Column 11, 12, 13. These columns provide the recharge location of each trajectory.
- Column 6. This column provides the total advective travel time of each trajectory.

# Appendix 2

## Some details about the first-order approximation

In the past decades, a large body of literature has examined in great detail the implications of first-order approaches when modelling diffusion and surface reactions. The first-order approximation was first introduced by Van Genuchten thirty years ago (van Genuchten 1985). In this work, the author compared breakthrough curves computed using this approximation with analytical solutions. The conclusion was that, although the first-order approach always preserves the first two moments of the breakthrough curves (i.e. total recovered mass and mean arrival time), the match with the exact solution greatly varies depending on the underlying transport parameters and geometries.

Ten year later, Haggerty and Gorelick (1995) modelled laboratory batch experiments of solute uptake in Borden sand using a single-rate (i.e. first-order approximation) and a multiple-rate mass transfer model (the latter is proved to provide the exact solution to the mass transfer problem) (Figure A2-1). The authors concluded that "Both models give essentially the same prediction at times less than 3 days and far from equilibrium. However the single sphere model [i.e. first-order approximation] predicts that 99.9% of equilibrium is achieved approximately five times sooner than the composite model [i.e. actual solution]".

Recently, the first-order approximation was used to simulate matrix diffusion processes in a numerical work focused on assessing the hydrogeological evolution at the Olkiluoto site (Trinchero et al. 2014b). The authors thoroughly discussed the implications of this approximation. They pointed out that the use of the first-order approach implies that the solute is always instantaneously mixed in the porewater of the matrix. The authors argued that this assumption is rigorously valid only when the characteristic time for diffusion is faster than the characteristic advective time in the fracture. When this condition is not fulfilled, the first-order approximation tends to underestimate the time taken by the system to reach equilibrium. In other words, when using the first-order approximation, the time taken by infiltration processes to propagate until repository depth is under-estimated.

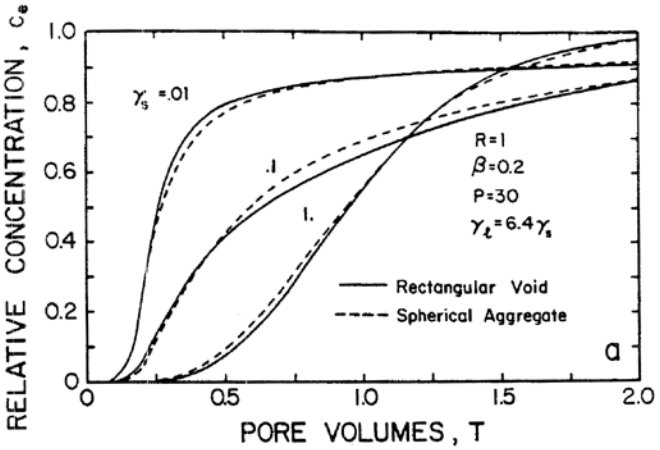


***Figure A2-1.*** *Breakthrough curves obtained with the first-order rate model and the exact solution (van Genuchten 1985).*

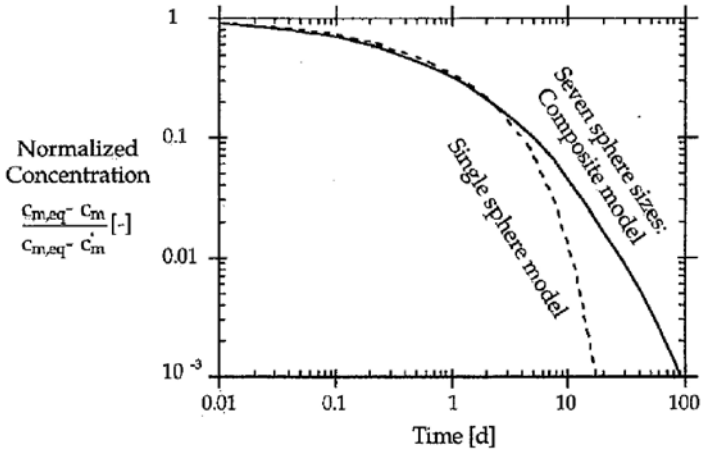


***Figure A2-2.*** *Batch experiment of solute uptake modelled using a single-rate and a multi-rate model (Haggerty and Gorelick 1995).*

# Appendix 3

## Tables of the statistical results

**Table A3-1. Temperate period: Base Case of SFR 1. All concentrations and alkalinity are in mol/L, the TDS is in g/L and the Eh is reported in mV.**

| Temperate Period 2500 AD | | | | | | | | | | | | | | | | | |
|---|---|---|---|---|---|---|---|---|---|---|---|---|---|---|---|---|---|
| | pH | Eh | Cl | TDS | Alkalinity | Ca | C | Na | K | Mg | S | S(VI) | S(–II) | Fe | Fe(II) | Fe(III) | Si | Al |
| Mean | 7.29 | –216.00 | 9.87E–02 | 2.13 | 1.47E–03 | 1.50E–02 | 1.55E–03 | 6.52E–02 | 5.13E–04 | 6.17E–03 | 3.65E–03 | 3.61E–03 | 4.21E–05 | 7.32E–06 | 7.32E–06 | 9.33E–15 | 1.83E–04 | 5.88E–08 |
| Max | 7.29 | –216.00 | 9.87E–02 | 2.13 | 1.47E–03 | 1.50E–02 | 1.55E–03 | 6.52E–02 | 5.13E–04 | 6.17E–03 | 3.65E–03 | 3.61E–03 | 4.21E–05 | 7.32E–06 | 7.32E–06 | 9.33E–15 | 1.83E–04 | 5.88E–08 |
| q3 | 7.29 | –216.00 | 9.87E–02 | 2.13 | 1.47E–03 | 1.50E–02 | 1.55E–03 | 6.52E–02 | 5.13E–04 | 6.17E–03 | 3.65E–03 | 3.61E–03 | 4.21E–05 | 7.32E–06 | 7.32E–06 | 9.33E–15 | 1.83E–04 | 5.88E–08 |
| Median | 7.29 | –216.00 | 9.87E–02 | 2.13 | 1.47E–03 | 1.50E–02 | 1.55E–03 | 6.52E–02 | 5.13E–04 | 6.17E–03 | 3.65E–03 | 3.61E–03 | 4.21E–05 | 7.32E–06 | 7.32E–06 | 9.33E–15 | 1.83E–04 | 5.88E–08 |
| q1 | 7.29 | –216.00 | 9.87E–02 | 2.13 | 1.47E–03 | 1.50E–02 | 1.55E–03 | 6.52E–02 | 5.13E–04 | 6.17E–03 | 3.65E–03 | 3.61E–03 | 4.21E–05 | 7.32E–06 | 7.32E–06 | 9.33E–15 | 1.83E–04 | 5.88E–08 |
| Min | 7.29 | –216.00 | 9.87E–02 | 2.13 | 1.47E–03 | 1.50E–02 | 1.55E–03 | 6.52E–02 | 5.13E–04 | 6.17E–03 | 3.65E–03 | 3.61E–03 | 4.21E–05 | 7.32E–06 | 7.32E–06 | 9.33E–15 | 1.83E–04 | 5.88E–08 |

| Temperate Period 2600 AD | | | | | | | | | | | | | | | | | |
|---|---|---|---|---|---|---|---|---|---|---|---|---|---|---|---|---|---|
| | pH | Eh | Cl | TDS | Alkalinity | Ca | C | Na | K | Mg | S | S(VI) | S(–II) | Fe | Fe(II) | Fe(III) | Si | Al |
| Mean | 7.60 | –234.65 | 2.69E–02 | 0.58 | 1.64E–03 | 4.60E–03 | 1.71E–03 | 1.81E–02 | 1.82E–04 | 1.73E–03 | 1.09E–03 | 1.08E–03 | 1.16E–05 | 1.76E–06 | 1.76E–06 | 7.24E–15 | 1.38E–04 | 7.26E–08 |
| Max | 7.94 | –216.01 | 9.87E–02 | 2.13 | 1.76E–03 | 1.50E–02 | 1.79E–03 | 6.52E–02 | 5.13E–04 | 6.17E–03 | 3.65E–03 | 3.61E–03 | 4.21E–05 | 7.32E–06 | 7.32E–06 | 9.33E–15 | 1.83E–04 | 7.69E–08 |
| q3 | 7.72 | –227.19 | 3.60E–02 | 0.78 | 1.70E–03 | 5.91E–03 | 1.75E–03 | 2.41E–02 | 2.24E–04 | 2.30E–03 | 1.42E–03 | 1.40E–03 | 1.55E–05 | 2.30E–06 | 2.30E–06 | 7.72E–15 | 1.44E–04 | 7.55E–08 |
| Median | 7.64 | –236.71 | 1.61E–02 | 0.35 | 1.67E–03 | 3.04E–03 | 1.73E–03 | 1.10E–02 | 1.33E–04 | 1.07E–03 | 7.08E–04 | 7.01E–04 | 7.05E–06 | 9.24E–07 | 9.24E–07 | 6.92E–15 | 1.31E–04 | 7.45E–08 |
| q1 | 7.48 | –241.57 | 1.04E–02 | 0.22 | 1.59E–03 | 2.21E–03 | 1.67E–03 | 7.22E–03 | 1.06E–04 | 7.11E–04 | 5.03E–04 | 4.98E–04 | 4.59E–06 | 5.79E–07 | 5.79E–07 | 6.63E–15 | 1.27E–04 | 7.11E–08 |
| Min | 7.29 | –253.12 | 1.99E–03 | 0.04 | 1.47E–03 | 1.02E–03 | 1.55E–03 | 1.71E–03 | 6.73E–05 | 1.92E–04 | 2.04E–04 | 2.03E–04 | 1.00E–06 | 1.60E–07 | 1.60E–07 | 6.18E–15 | 1.22E–04 | 5.88E–08 |

| Temperate Period 2800 AD | | | | | | | | | | | | | | | | | |
|---|---|---|---|---|---|---|---|---|---|---|---|---|---|---|---|---|---|
| | pH | Eh | Cl | TDS | Alkalinity | Ca | C | Na | K | Mg | S | S(VI) | S(–II) | Fe | Fe(II) | Fe(III) | Si | Al |
| Mean | 7.73 | –242.06 | 1.53E–02 | 0.33 | 1.69E–03 | 2.93E–03 | 1.74E–03 | 1.05E–02 | 1.29E–04 | 1.02E–03 | 6.79E–04 | 6.72E–04 | 6.68E–06 | 9.91E–07 | 9.91E–07 | 6.77E–15 | 1.31E–04 | 7.46E–08 |
| Max | 7.99 | –216.14 | 9.74E–02 | 2.10 | 1.77E–03 | 1.48E–02 | 1.80E–03 | 6.43E–02 | 5.07E–04 | 6.09E–03 | 3.60E–03 | 3.56E–03 | 4.15E–05 | 7.21E–06 | 7.21E–06 | 9.30E–15 | 1.82E–04 | 7.71E–08 |
| q3 | 7.86 | –235.87 | 1.74E–02 | 0.37 | 1.74E–03 | 3.22E–03 | 1.78E–03 | 1.18E–02 | 1.38E–04 | 1.14E–03 | 7.52E–04 | 7.44E–04 | 7.57E–06 | 1.00E–06 | 1.00E–06 | 6.97E–15 | 1.32E–04 | 7.65E–08 |
| Median | 7.79 | –245.74 | 6.73E–03 | 0.14 | 1.72E–03 | 1.69E–03 | 1.77E–03 | 4.83E–03 | 8.92E–05 | 4.86E–04 | 3.73E–04 | 3.70E–04 | 3.04E–06 | 3.82E–07 | 3.82E–07 | 6.44E–15 | 1.25E–04 | 7.61E–08 |
| q1 | 7.62 | –249.45 | 4.17E–03 | 0.09 | 1.66E–03 | 1.33E–03 | 1.73E–03 | 3.14E–03 | 7.74E–05 | 3.27E–04 | 2.82E–04 | 2.80E–04 | 1.94E–06 | 2.56E–07 | 2.56E–07 | 6.30E–15 | 1.24E–04 | 7.43E–08 |
| Min | 7.29 | –254.85 | 8.19E–04 | 0.02 | 1.47E–03 | 8.56E–04 | 1.55E–03 | 9.45E–04 | 6.19E–05 | 1.20E–04 | 1.62E–04 | 1.62E–04 | 5.04E–07 | 1.13E–07 | 1.13E–07 | 6.12E–15 | 1.21E–04 | 5.92E–08 |

**Temperate period 3100 AD**

| | pH | Eh | Cl | TDS | Alkalinity | Ca | C | Na | K | Mg | S | S(VI) | S(–II) | Fe | Fe(II) | Fe(III) | Si | Al |
|---|---|---|---|---|---|---|---|---|---|---|---|---|---|---|---|---|---|---|
| Mean | 7.95 | –252.60 | 2.60E–03 | 0.06 | 1.76E–03 | 1.11E–03 | 1.79E–03 | 2.12E–03 | 7.02E–05 | 2.30E–04 | 2.26E–04 | 2.24E–04 | 1.27E–06 | 2.10E–07 | 2.10E–07 | 6.21E–15 | 1.23E–04 | 7.68E–08 |
| Max | 8.02 | –222.40 | 5.44E–02 | 1.17 | 1.78E–03 | 8.56E–03 | 1.80E–03 | 3.61E–02 | 3.09E–04 | 3.43E–03 | 2.07E–03 | 2.05E–03 | 2.33E–05 | 3.71E–06 | 3.71E–06 | 8.29E–15 | 1.55E–04 | 7.72E–08 |
| q3 | 8.01 | –253.55 | 1.66E–03 | 0.04 | 1.78E–03 | 1.80E–03 | 1.50E–03 | 6.58E–05 | 9.75E–04 | 1.72E–04 | 1.92E–04 | 1.91E–04 | 8.65E–07 | 1.47E–07 | 1.47E–07 | 6.16E–15 | 1.22E–04 | 7.72E–08 |
| Median | 8.00 | –254.99 | 6.14E–04 | 0.01 | 1.77E–03 | 8.27E–04 | 1.80E–03 | 8.11E–04 | 6.10E–05 | 1.07E–04 | 1.55E–04 | 1.54E–04 | 4.16E–07 | 1.04E–07 | 1.04E–07 | 6.11E–15 | 1.21E–04 | 7.71E–08 |
| q1 | 7.95 | –255.05 | 3.72E–04 | 0.01 | 1.76E–03 | 1.79E–03 | 6.52E–04 | 5.99E–05 | 7.93E–04 | 9.25E–05 | 1.46E–04 | 1.46E–04 | 3.12E–07 | 9.43E–08 | 9.43E–08 | 6.10E–15 | 1.21E–04 | 7.69E–08 |
| Min | 7.40 | –255.07 | 1.81E–04 | 0.004 | 1.55E–03 | 7.66E–04 | 1.63E–03 | 5.26E–04 | 5.90E–05 | 8.07E–05 | 1.39E–04 | 1.39E–04 | 2.30E–07 | 8.61E–08 | 8.61E–08 | 6.09E–15 | 1.21E–04 | 6.80E–08 |

**Temperate period 6000 AD**

| | pH | Eh | Cl | TDS | Alkalinity | Ca | C | Na | K | Mg | S | S(VI) | S(–II) | Fe | Fe(II) | Fe(III) | Si | Al |
|---|---|---|---|---|---|---|---|---|---|---|---|---|---|---|---|---|---|---|
| Mean | 8.02 | –254.8 | 1.41E–04 | 0.003 | 1.78E–03 | 7.61E–04 | 1.80E–03 | 5.00E–04 | 5.88E–05 | 7.82E–05 | 1.38E–04 | 1.38E–04 | 2.13E–07 | 8.43E–08 | 8.43E–08 | 6.09E–15 | 1.21E–04 | 2.91E–08 |
| Max | 8.02 | –254.8 | 1.46E–04 | 0.003 | 1.78E–03 | 7.61E–04 | 1.80E–03 | 5.03E–04 | 5.88E–05 | 7.85E–05 | 1.38E–04 | 1.38E–04 | 2.15E–07 | 8.45E–08 | 8.45E–08 | 6.09E–15 | 1.21E–04 | 3.12E–08 |
| q3 | 8.02 | –254.8 | 1.41E–04 | 0.003 | 1.78E–03 | 7.61E–04 | 1.80E–03 | 5.00E–04 | 5.88E–05 | 7.82E–05 | 1.38E–04 | 1.38E–04 | 2.13E–07 | 8.43E–08 | 8.43E–08 | 6.09E–15 | 1.21E–04 | 2.90E–08 |
| Median | 8.02 | –254.8 | 1.41E–04 | 0.003 | 1.78E–03 | 7.61E–04 | 1.80E–03 | 5.00E–04 | 5.88E–05 | 7.82E–05 | 1.38E–04 | 1.38E–04 | 2.13E–07 | 8.43E–08 | 8.43E–08 | 6.09E–15 | 1.21E–04 | 2.90E–08 |
| q1 | 8.02 | –254.8 | 1.41E–04 | 0.003 | 1.78E–03 | 7.61E–04 | 1.80E–03 | 5.00E–04 | 5.88E–05 | 7.82E–05 | 1.38E–04 | 1.38E–04 | 2.13E–07 | 8.43E–08 | 8.43E–08 | 6.09E–15 | 1.21E–04 | 2.90E–08 |
| Min | 8.02 | –254.8 | 1.41E–04 | 0.003 | 1.78E–03 | 7.61E–04 | 1.80E–03 | 5.00E–04 | 5.88E–05 | 7.82E–05 | 1.38E–04 | 1.38E–04 | 2.13E–07 | 8.43E–08 | 8.43E–08 | 6.09E–15 | 1.21E–04 | 2.90E–08 |

**Temperate period 9000 AD**

| | pH | Eh | Cl | TDS | Alkalinity | Ca | C | Na | K | Mg | S | S(VI) | S(–II) | Fe | Fe(II) | Fe(III) | Si | Al |
|---|---|---|---|---|---|---|---|---|---|---|---|---|---|---|---|---|---|---|
| Mean | 8.02 | –254.8 | 1.41E–04 | 0.003 | 1.78E–03 | 7.61E–04 | 1.80E–03 | 5.00E–04 | 5.88E–05 | 7.82E–05 | 1.38E–04 | 1.38E–04 | 2.13E–07 | 8.43E–08 | 8.43E–08 | 6.09E–15 | 1.21E–04 | 2.91E–08 |
| Max | 8.02 | –254.8 | 1.46E–04 | 0.003 | 1.78E–03 | 7.61E–04 | 1.80E–03 | 5.03E–04 | 5.88E–05 | 7.85E–05 | 1.38E–04 | 1.38E–04 | 2.15E–07 | 8.45E–08 | 8.45E–08 | 6.09E–15 | 1.21E–04 | 3.12E–08 |
| q3 | 8.02 | –254.8 | 1.41E–04 | 0.003 | 1.78E–03 | 7.61E–04 | 1.80E–03 | 5.00E–04 | 5.88E–05 | 7.82E–05 | 1.38E–04 | 1.38E–04 | 2.13E–07 | 8.43E–08 | 8.43E–08 | 6.09E–15 | 1.21E–04 | 2.90E–08 |
| Median | 8.02 | –254.8 | 1.41E–04 | 0.003 | 1.78E–03 | 7.61E–04 | 1.80E–03 | 5.00E–04 | 5.88E–05 | 7.82E–05 | 1.38E–04 | 1.38E–04 | 2.13E–07 | 8.43E–08 | 8.43E–08 | 6.09E–15 | 1.21E–04 | 2.90E–08 |
| q1 | 8.02 | –254.8 | 1.41E–04 | 0.003 | 1.78E–03 | 7.61E–04 | 1.80E–03 | 5.00E–04 | 5.88E–05 | 7.82E–05 | 1.38E–04 | 1.38E–04 | 2.13E–07 | 8.43E–08 | 8.43E–08 | 6.09E–15 | 1.21E–04 | 2.90E–08 |
| Min | 8.02 | –254.8 | 1.41E–04 | 0.003 | 1.78E–03 | 7.61E–04 | 1.80E–03 | 5.00E–04 | 5.88E–05 | 7.82E–05 | 1.38E–04 | 1.38E–04 | 2.13E–07 | 8.43E–08 | 8.43E–08 | 6.09E–15 | 1.21E–04 | 2.90E–08 |

**Table A3-2. Temperate period: Variant Case of SFR 1. All concentrations and alkalinity are in mol/L, the TDS is in g/L and the Eh is reported in mV.**

| Temperate Period 2500 AD | | | | | | | | | | | | | | | | | |
|---|---|---|---|---|---|---|---|---|---|---|---|---|---|---|---|---|---|
| | pH | Eh | Cl | TDS | Alkalinity | Ca | C | Na | K | Mg | S | S(VI) | S(–II) | Fe | Fe(II) | Fe(III) | Si | Al |
| Mean | 7.29 | –216.7 | 9.87E–02 | 2.126 | 1.48E–03 | 1.50E–02 | 1.55E–03 | 6.52E–02 | 5.13E–04 | 6.17E–03 | 3.66E–03 | 3.61E–03 | 5.53E–05 | 1.23E–05 | 1.23E–05 | 1.36E–14 | 1.83E–04 | 5.88E–08 |
| Max | 7.29 | –216.7 | 9.87E–02 | 2.126 | 1.48E–03 | 1.50E–02 | 1.55E–03 | 6.52E–02 | 5.13E–04 | 6.17E–03 | 3.66E–03 | 3.61E–03 | 5.53E–05 | 1.23E–05 | 1.23E–05 | 1.36E–14 | 1.83E–04 | 5.88E–08 |
| q3 | 7.29 | –216.7 | 9.87E–02 | 2.126 | 1.48E–03 | 1.50E–02 | 1.55E–03 | 6.52E–02 | 5.13E–04 | 6.17E–03 | 3.66E–03 | 3.61E–03 | 5.53E–05 | 1.23E–05 | 1.23E–05 | 1.36E–14 | 1.83E–04 | 5.88E–08 |
| Median | 7.29 | –216.7 | 9.87E–02 | 2.126 | 1.48E–03 | 1.50E–02 | 1.55E–03 | 6.52E–02 | 5.13E–04 | 6.17E–03 | 3.66E–03 | 3.61E–03 | 5.53E–05 | 1.23E–05 | 1.23E–05 | 1.36E–14 | 1.83E–04 | 5.88E–08 |
| q1 | 7.29 | –216.7 | 9.87E–02 | 2.126 | 1.48E–03 | 1.50E–02 | 1.55E–03 | 6.52E–02 | 5.13E–04 | 6.17E–03 | 3.66E–03 | 3.61E–03 | 5.53E–05 | 1.23E–05 | 1.23E–05 | 1.36E–14 | 1.83E–04 | 5.88E–08 |
| Min | 7.29 | –216.7 | 9.87E–02 | 2.126 | 1.48E–03 | 1.50E–02 | 1.55E–03 | 6.52E–02 | 5.13E–04 | 6.17E–03 | 3.66E–03 | 3.61E–03 | 5.53E–05 | 1.23E–05 | 1.23E–05 | 1.36E–14 | 1.83E–04 | 5.88E–08 |

| Temperate Period 2600 AD | | | | | | | | | | | | | | | | | |
|---|---|---|---|---|---|---|---|---|---|---|---|---|---|---|---|---|---|
| | pH | Eh | Cl | TDS | Alkalinity | Ca | C | Na | K | Mg | S | S(VI) | S(–II) | Fe | Fe(II) | Fe(III) | Si | Al |
| Mean | 7.60 | –236.6 | 2.69E–02 | 0.579 | 1.66E–03 | 4.59E–03 | 1.70E–03 | 1.81E–02 | 1.82E–04 | 1.73E–03 | 1.10E–03 | 1.08E–03 | 2.30E–05 | 1.23E–05 | 1.23E–05 | 6.94E–14 | 1.38E–04 | 7.26E–08 |
| Max | 7.94 | –216.7 | 9.87E–02 | 2.126 | 1.77E–03 | 1.50E–02 | 1.78E–03 | 6.52E–02 | 5.13E–04 | 6.17E–03 | 3.66E–03 | 3.61E–03 | 5.53E–05 | 1.25E–05 | 1.25E–05 | 2.16E–13 | 1.83E–04 | 7.69E–08 |
| q3 | 7.72 | –228.4 | 3.60E–02 | 0.775 | 1.71E–03 | 5.90E–03 | 1.74E–03 | 2.41E–02 | 2.24E–04 | 2.30E–03 | 1.43E–03 | 1.40E–03 | 2.73E–05 | 1.25E–05 | 1.25E–05 | 9.42E–14 | 1.44E–04 | 7.55E–08 |
| Median | 7.64 | –238.6 | 1.61E–02 | 0.347 | 1.68E–03 | 3.04E–03 | 1.72E–03 | 1.10E–02 | 1.33E–04 | 1.07E–03 | 7.20E–04 | 7.01E–04 | 1.82E–05 | 1.23E–05 | 1.23E–05 | 6.74E–14 | 1.31E–04 | 7.45E–08 |
| q1 | 7.48 | –244.0 | 1.04E–02 | 0.224 | 1.61E–03 | 2.21E–03 | 1.67E–03 | 7.22E–03 | 1.06E–04 | 7.11E–04 | 5.14E–04 | 4.98E–04 | 1.55E–05 | 1.22E–05 | 1.22E–05 | 3.41E–14 | 1.27E–04 | 7.11E–08 |
| Min | 7.29 | –258.5 | 1.99E–03 | 0.043 | 1.48E–03 | 1.02E–03 | 1.55E–03 | 1.71E–03 | 6.73E–05 | 1.92E–04 | 2.14E–04 | 2.03E–04 | 1.15E–05 | 1.19E–05 | 1.19E–05 | 1.36E–14 | 1.22E–04 | 5.88E–08 |

| Temperate Period 2800 AD | | | | | | | | | | | | | | | | | |
|---|---|---|---|---|---|---|---|---|---|---|---|---|---|---|---|---|---|
| | pH | Eh | Cl | TDS | Alkalinity | Ca | C | Na | K | Mg | S | S(VI) | S(–II) | Fe | Fe(II) | Fe(III) | Si | Al |
| Mean | 7.74 | –245.22 | 1.53E–02 | 0.330 | 1.70E–03 | 2.93E–03 | 1.74E–03 | 1.05E–02 | 1.29E–04 | 1.02E–03 | 6.90E–04 | 6.72E–04 | 1.80E–05 | 1.19E–05 | 1.19E–05 | 1.11E–13 | 1.31E–04 | 7.46E–08 |
| Max | 7.99 | –216.85 | 9.74E–02 | 2.098 | 1.78E–03 | 1.48E–02 | 1.79E–03 | 6.43E–02 | 5.07E–04 | 6.09E–03 | 3.62E–03 | 3.56E–03 | 5.47E–05 | 1.25E–05 | 1.25E–05 | 2.37E–13 | 1.82E–04 | 7.71E–08 |
| q3 | 7.86 | –237.81 | 1.74E–02 | 0.375 | 1.75E–03 | 3.21E–03 | 1.77E–03 | 1.18E–02 | 1.38E–04 | 1.14E–03 | 7.63E–04 | 7.44E–04 | 1.91E–05 | 1.22E–05 | 1.22E–05 | 1.52E–13 | 1.32E–04 | 7.65E–08 |
| Median | 7.80 | –249.01 | 6.73E–03 | 0.145 | 1.73E–03 | 1.69E–03 | 1.76E–03 | 4.83E–03 | 8.92E–05 | 4.86E–04 | 3.84E–04 | 3.70E–04 | 1.42E–05 | 1.18E–05 | 1.18E–05 | 1.18E–13 | 1.25E–04 | 7.61E–08 |
| q1 | 7.62 | –253.58 | 4.17E–03 | 0.090 | 1.67E–03 | 1.32E–03 | 1.72E–03 | 3.14E–03 | 7.74E–05 | 3.27E–04 | 2.93E–04 | 2.80E–04 | 1.30E–05 | 1.17E–05 | 1.17E–05 | 6.14E–14 | 1.24E–04 | 7.43E–08 |
| Min | 7.29 | –262.27 | 8.19E–04 | 0.018 | 1.48E–03 | 8.51E–04 | 1.55E–03 | 9.45E–04 | 6.19E–05 | 1.20E–04 | 1.73E–04 | 1.62E–04 | 1.13E–05 | 1.14E–05 | 1.14E–05 | 1.38E–14 | 1.21E–04 | 5.92E–08 |

**Temperate Period 3100 AD**

| | pH | Eh | Cl | TDS | Alkalinity | Ca | C | Na | K | Mg | S | S(VI) | S(–II) | Fe | Fe(II) | Fe(III) | Si | Al |
|---|---|---|---|---|---|---|---|---|---|---|---|---|---|---|---|---|---|---|
| Mean | 7.95 | –259.8 | 2.60E–03 | 0.056 | 1.77E–03 | 1.11E–03 | 1.78E–03 | 2.12E–03 | 7.02E–05 | 2.30E–04 | 2.37E–04 | 2.25E–04 | 1.23E–05 | 1.13E–05 | 1.13E–05 | 2.08E–13 | 1.23E–04 | 7.68E–08 |
| Max | 8.02 | –223.4 | 5.44E–02 | 1.172 | 1.79E–03 | 8.55E–03 | 1.79E–03 | 3.61E–02 | 3.09E–04 | 3.43E–03 | 2.08E–03 | 2.05E–03 | 3.59E–05 | 1.24E–05 | 1.24E–05 | 2.51E–13 | 1.55E–04 | 7.72E–08 |
| q3 | 8.01 | –259.6 | 1.73E–03 | 0.037 | 1.79E–03 | 9.80E–04 | 1.79E–03 | 1.55E–03 | 6.61E–05 | 1.77E–04 | 2.06E–04 | 1.94E–04 | 1.20E–05 | 1.13E–05 | 1.13E–05 | 2.42E–13 | 1.22E–04 | 7.72E–08 |
| Median | 7.95 | –259.8 | 2.60E–03 | 0.056 | 1.77E–03 | 1.11E–03 | 1.78E–03 | 2.12E–03 | 7.02E–05 | 2.30E–04 | 2.37E–04 | 2.25E–04 | 1.23E–05 | 1.13E–05 | 1.13E–05 | 2.08E–13 | 1.23E–04 | 7.68E–08 |
| q1 | 7.95 | –263.8 | 4.09E–04 | 0.009 | 1.77E–03 | 7.94E–04 | 1.78E–03 | 6.76E–04 | 6.00E–05 | 9.47E–05 | 1.59E–04 | 1.47E–04 | 1.13E–05 | 1.12E–05 | 1.12E–05 | 1.97E–13 | 1.21E–04 | 7.69E–08 |
| Min | 7.40 | –264.7 | 1.81E–04 | 0.004 | 1.56E–03 | 7.62E–04 | 1.63E–03 | 5.26E–04 | 5.90E–05 | 8.07E–05 | 1.51E–04 | 1.39E–04 | 1.12E–05 | 1.12E–05 | 1.12E–05 | 2.32E–14 | 1.21E–04 | 6.80E–08 |

**Temperate Period 6000 AD**

| | pH | Eh | Cl | TDS | Alkalinity | Ca | C | Na | K | Mg | S | S(VI) | S(–II) | Fe | Fe(II) | Fe(III) | Si | Al |
|---|---|---|---|---|---|---|---|---|---|---|---|---|---|---|---|---|---|---|
| Mean | 8.03 | –264.8 | 1.41E–04 | 0.003 | 1.79E–03 | 7.56E–04 | 1.79E–03 | 5.00E–04 | 5.88E–05 | 7.82E–05 | 1.49E–04 | 1.38E–04 | 1.12E–05 | 1.11E–05 | 1.11E–05 | 2.52E–13 | 1.21E–04 | 3.10E–08 |
| Max | 8.03 | –264.8 | 1.46E–04 | 0.002 | 1.79E–03 | 7.57E–04 | 1.79E–03 | 5.03E–04 | 5.88E–05 | 7.85E–05 | 1.49E–04 | 1.38E–04 | 1.12E–05 | 1.11E–05 | 1.11E–05 | 2.52E–13 | 1.21E–04 | 3.33E–08 |
| q3 | 8.03 | –264.8 | 1.41E–04 | 0.003 | 1.79E–03 | 7.56E–04 | 1.79E–03 | 5.00E–04 | 5.88E–05 | 7.82E–05 | 1.49E–04 | 1.38E–04 | 1.12E–05 | 1.11E–05 | 1.11E–05 | 2.52E–13 | 1.21E–04 | 3.10E–08 |
| Median | 8.03 | –264.8 | 1.41E–04 | 0.003 | 1.79E–03 | 7.56E–04 | 1.79E–03 | 5.00E–04 | 5.88E–05 | 7.82E–05 | 1.49E–04 | 1.38E–04 | 1.12E–05 | 1.11E–05 | 1.11E–05 | 2.52E–13 | 1.21E–04 | 3.10E–08 |
| q1 | 8.03 | –264.8 | 1.41E–04 | 0.003 | 1.79E–03 | 7.56E–04 | 1.79E–03 | 5.00E–04 | 5.88E–05 | 7.82E–05 | 1.49E–04 | 1.38E–04 | 1.12E–05 | 1.11E–05 | 1.11E–05 | 2.52E–13 | 1.21E–04 | 3.10E–08 |
| Min | 8.03 | –264.8 | 1.41E–04 | 0.003 | 1.79E–03 | 7.56E–04 | 1.79E–03 | 5.00E–04 | 5.88E–05 | 7.82E–05 | 1.49E–04 | 1.38E–04 | 1.12E–05 | 1.11E–05 | 1.11E–05 | 2.52E–13 | 1.21E–04 | 3.10E–08 |

**Temperate Period 9000 AD**

| | pH | Eh | Cl | TDS | Alkalinity | Ca | C | Na | K | Mg | S | S(VI) | S(–II) | Fe | Fe(II) | Fe(III) | Si | Al |
|---|---|---|---|---|---|---|---|---|---|---|---|---|---|---|---|---|---|---|
| Mean | 8.02 | –264.65 | 1.41E–04 | 0.003 | 1.79E–03 | 7.55E–04 | 1.79E–03 | 5.00E–04 | 5.88E–05 | 7.82E–05 | 1.49E–04 | 1.38E–04 | 1.12E–05 | 1.12E–05 | 1.12E–05 | 2.52E–13 | 1.21E–04 | 3.10E–08 |
| Max | 8.03 | –191.46 | 1.41E–04 | 0.003 | 1.79E–03 | 7.56E–04 | 1.79E–03 | 5.00E–04 | 5.88E–05 | 7.82E–05 | 1.66E–04 | 1.38E–04 | 2.78E–05 | 2.96E–05 | 2.96E–05 | 2.52E–13 | 1.21E–04 | 3.10E–08 |
| q3 | 8.03 | –264.81 | 1.41E–04 | 0.003 | 1.79E–03 | 7.56E–04 | 1.79E–03 | 5.00E–04 | 5.88E–05 | 7.82E–05 | 1.49E–04 | 1.38E–04 | 1.12E–05 | 1.11E–05 | 1.11E–05 | 2.52E–13 | 1.21E–04 | 3.10E–08 |
| Median | 8.03 | –264.81 | 1.41E–04 | 0.003 | 1.79E–03 | 7.56E–04 | 1.79E–03 | 5.00E–04 | 5.88E–05 | 7.82E–05 | 1.49E–04 | 1.38E–04 | 1.12E–05 | 1.11E–05 | 1.11E–05 | 2.52E–13 | 1.21E–04 | 3.10E–08 |
| q1 | 8.03 | –264.81 | 1.41E–04 | 0.003 | 1.79E–03 | 7.56E–04 | 1.79E–03 | 5.00E–04 | 5.88E–05 | 7.82E–05 | 1.49E–04 | 1.38E–04 | 1.12E–05 | 1.11E–05 | 1.11E–05 | 2.52E–13 | 1.21E–04 | 3.10E–08 |
| Min | 6.85 | –264.81 | 1.41E–04 | 0.003 | 1.09E–03 | 3.85E–04 | 1.42E–03 | 5.00E–04 | 5.88E–05 | 7.82E–05 | 1.49E–04 | 1.38E–04 | 1.12E–05 | 1.11E–05 | 1.11E–05 | 2.48E–14 | 1.21E–04 | 3.10E–08 |

**Table A3-3. Temperate period: Base Case of SFR 3. All concentrations and alkalinity are in mol/L, the TDS is in g/L and the Eh is reported in mV.**

| Temperate Period 2500 AD | | | | | | | | | | | | | | | | | |
|---|---|---|---|---|---|---|---|---|---|---|---|---|---|---|---|---|---|
| | pH | Eh | Cl | TDS | Alkalinidad | Ca | C | Na | K | Mg | S | S(VI) | S(–II) | Fe | Fe(II) | Fe(III) | Si | Al |
| Mean | 7.29 | –216.01 | 9.87E–02 | 2.126 | 1.47E–03 | 1.50E–02 | 1.55E–03 | 6.52E–02 | 5.13E–04 | 6.17E–03 | 3.65E–03 | 3.61E–03 | 4.21E–05 | 7.32E–06 | 7.32E–06 | 9.33E–15 | 1.83E–04 | 5.88E–08 |
| Max | 7.29 | –216.01 | 9.87E–02 | 2.126 | 1.47E–03 | 1.50E–02 | 1.55E–03 | 6.52E–02 | 5.13E–04 | 6.17E–03 | 3.65E–03 | 3.61E–03 | 4.21E–05 | 7.32E–06 | 7.32E–06 | 9.33E–15 | 1.83E–04 | 5.88E–08 |
| q3 | 7.29 | –216.01 | 9.87E–02 | 2.126 | 1.47E–03 | 1.50E–02 | 1.55E–03 | 6.52E–02 | 5.13E–04 | 6.17E–03 | 3.65E–03 | 3.61E–03 | 4.21E–05 | 7.32E–06 | 7.32E–06 | 9.33E–15 | 1.83E–04 | 5.88E–08 |
| Median | 7.29 | –216.01 | 9.87E–02 | 2.126 | 1.47E–03 | 1.50E–02 | 1.55E–03 | 6.52E–02 | 5.13E–04 | 6.17E–03 | 3.65E–03 | 3.61E–03 | 4.21E–05 | 7.32E–06 | 7.32E–06 | 9.33E–15 | 1.83E–04 | 5.88E–08 |
| q1 | 7.29 | –216.01 | 9.87E–02 | 2.126 | 1.47E–03 | 1.50E–02 | 1.55E–03 | 6.52E–02 | 5.13E–04 | 6.17E–03 | 3.65E–03 | 3.61E–03 | 4.21E–05 | 7.32E–06 | 7.32E–06 | 9.33E–15 | 1.83E–04 | 5.88E–08 |
| Min | 7.29 | –216.01 | 9.87E–02 | 2.126 | 1.47E–03 | 1.50E–02 | 1.55E–03 | 6.52E–02 | 5.13E–04 | 6.17E–03 | 3.65E–03 | 3.61E–03 | 4.21E–05 | 7.32E–06 | 7.32E–06 | 9.33E–15 | 1.83E–04 | 5.88E–08 |

| Temperate Period 2600 AD | | | | | | | | | | | | | | | | | |
|---|---|---|---|---|---|---|---|---|---|---|---|---|---|---|---|---|---|
| | pH | Eh | Cl | TDS | Alkalinidad | Ca | C | Na | K | Mg | S | S(VI) | S(–II) | Fe | Fe(II) | Fe(III) | Si | Al |
| Mean | 7.59 | –233.84 | 2.53E–02 | 0.545 | 1.64E–03 | 4.36E–03 | 1.71E–03 | 1.70E–02 | 1.75E–04 | 1.63E–03 | 1.03E–03 | 1.02E–03 | 1.09E–05 | 1.60E–06 | 1.60E–06 | 7.23E–15 | 1.37E–04 | 7.29E–08 |
| Max | 7.94 | –216.01 | 9.87E–02 | 2.126 | 1.76E–03 | 1.50E–02 | 1.79E–03 | 6.52E–02 | 5.13E–04 | 6.17E–03 | 3.65E–03 | 3.61E–03 | 4.21E–05 | 7.32E–06 | 7.32E–06 | 9.33E–15 | 1.83E–04 | 7.69E–08 |
| q3 | 7.68 | –228.94 | 3.11E–02 | 0.670 | 1.68E–03 | 5.20E–03 | 1.74E–03 | 2.08E–02 | 2.02E–04 | 1.99E–03 | 1.24E–03 | 1.23E–03 | 1.34E–05 | 1.94E–06 | 1.94E–06 | 7.54E–15 | 1.40E–04 | 7.51E–08 |
| Median | 7.60 | –234.51 | 1.95E–02 | 0.420 | 1.65E–03 | 3.52E–03 | 1.72E–03 | 1.32E–02 | 1.48E–04 | 1.28E–03 | 8.28E–04 | 8.20E–04 | 8.48E–06 | 1.14E–06 | 1.14E–06 | 7.07E–15 | 1.33E–04 | 7.39E–08 |
| q1 | 7.51 | –239.40 | 1.27E–02 | 0.274 | 1.61E–03 | 2.55E–03 | 1.69E–03 | 8.75E–03 | 1.17E–04 | 8.55E–04 | 5.86E–04 | 5.80E–04 | 5.59E–06 | 7.14E–07 | 7.14E–07 | 6.75E–15 | 1.29E–04 | 7.19E–08 |
| Min | 7.29 | –253.12 | 1.99E–03 | 0.043 | 1.47E–03 | 1.02E–03 | 1.55E–03 | 1.71E–03 | 6.73E–05 | 1.92E–04 | 2.04E–04 | 2.03E–04 | 1.00E–06 | 1.60E–07 | 1.60E–07 | 6.18E–15 | 1.22E–04 | 5.88E–08 |

| Temperate Period 2800 AD | | | | | | | | | | | | | | | | | |
|---|---|---|---|---|---|---|---|---|---|---|---|---|---|---|---|---|---|
| | pH | Eh | Cl | TDS | Alkalinidad | Ca | C | Na | K | Mg | S | S(VI) | S(–II) | Fe | Fe(II) | Fe(III) | Si | Al |
| Mean | 7.73 | –242.00 | 1.30E–02 | 0.280 | 1.70E–03 | 2.59E–03 | 1.75E–03 | 8.93E–03 | 1.18E–04 | 8.72E–04 | 5.95E–04 | 5.90E–04 | 5.69E–06 | 7.98E–07 | 7.98E–07 | 6.70E–15 | 1.29E–04 | 7.50E–08 |
| Max | 7.99 | –216.14 | 9.74E–02 | 2.098 | 1.77E–03 | 1.48E–02 | 1.80E–03 | 6.43E–02 | 5.07E–04 | 6.09E–03 | 3.60E–03 | 3.56E–03 | 4.15E–05 | 7.21E–06 | 7.21E–06 | 9.30E–15 | 1.82E–04 | 7.71E–08 |
| q3 | 7.83 | –237.96 | 1.45E–02 | 0.312 | 1.73E–03 | 2.80E–03 | 1.77E–03 | 9.90E–03 | 1.25E–04 | 9.64E–04 | 6.48E–04 | 6.42E–04 | 6.34E–06 | 8.20E–07 | 8.20E–07 | 6.84E–15 | 1.30E–04 | 7.63E–08 |
| Median | 7.76 | –243.78 | 8.33E–03 | 0.179 | 1.71E–03 | 1.92E–03 | 1.76E–03 | 5.88E–03 | 9.65E–05 | 5.84E–04 | 4.30E–04 | 4.26E–04 | 3.72E–06 | 4.65E–07 | 4.65E–07 | 6.53E–15 | 1.26E–04 | 7.58E–08 |
| q1 | 7.66 | –247.90 | 5.18E–03 | 0.112 | 1.68E–03 | 1.47E–03 | 1.74E–03 | 3.81E–03 | 8.20E–05 | 3.90E–04 | 3.18E–04 | 3.15E–04 | 2.37E–06 | 3.04E–07 | 3.04E–07 | 6.35E–15 | 1.24E–04 | 7.48E–08 |
| Min | 7.29 | –254.85 | 8.19E–04 | 0.018 | 1.47E–03 | 8.56E–04 | 1.55E–03 | 9.45E–04 | 6.19E–05 | 1.20E–04 | 1.62E–04 | 1.62E–04 | 5.04E–07 | 1.13E–07 | 1.13E–07 | 6.12E–15 | 1.21E–04 | 5.92E–08 |

**Temperate Period 3100 AD**

| | pH | Eh | Cl | TDS | Alkalinidad | Ca | C | Na | K | Mg | S | S(VI) | S(–II) | Fe | Fe(II) | Fe(III) | Si | Al |
|---|---|---|---|---|---|---|---|---|---|---|---|---|---|---|---|---|---|---|
| Mean | 7.96 | –253.55 | 1.84E–03 | 0.040 | 1.76E–03 | 1.00E–03 | 1.79E–03 | 1.62E–03 | 6.66E–05 | 1.83E–04 | 1.99E–04 | 1.98E–04 | 9.41E–07 | 1.68E–07 | 1.68E–07 | 6.17E–15 | 1.22E–04 | 7.69E–08 |
| Max | 8.02 | –222.40 | 5.44E–02 | 1.172 | 1.78E–03 | 8.56E–03 | 1.80E–03 | 3.61E–02 | 3.09E–04 | 3.43E–03 | 2.07E–03 | 2.05E–03 | 2.33E–05 | 3.71E–06 | 3.71E–06 | 8.29E–15 | 1.55E–04 | 7.72E–08 |
| q3 | 8.00 | –254.10 | 1.39E–03 | 0.030 | 1.77E–03 | 9.36E–04 | 1.80E–03 | 1.32E–03 | 6.45E–05 | 1.55E–04 | 1.82E–04 | 1.82E–04 | 7.47E–07 | 1.36E–07 | 1.36E–07 | 6.15E–15 | 1.22E–04 | 7.71E–08 |
| Median | 7.99 | –254.91 | 7.55E–04 | 0.016 | 1.77E–03 | 8.47E–04 | 1.80E–03 | 9.03E–04 | 6.16E–05 | 1.16E–04 | 1.60E–04 | 1.59E–04 | 4.76E–07 | 1.10E–07 | 1.10E–07 | 6.12E–15 | 1.21E–04 | 7.71E–08 |
| q1 | 7.96 | –255.04 | 4.87E–04 | 0.010 | 1.77E–03 | 8.09E–04 | 1.79E–03 | 7.27E–04 | 6.04E–05 | 9.96E–05 | 1.50E–04 | 1.50E–04 | 3.61E–07 | 9.91E–08 | 9.91E–08 | 6.10E–15 | 1.21E–04 | 7.70E–08 |
| Min | 7.40 | –255.07 | 1.81E–04 | 0.004 | 1.55E–03 | 7.66E–04 | 1.63E–03 | 5.26E–04 | 5.90E–05 | 8.07E–05 | 1.39E–04 | 1.39E–04 | 2.30E–07 | 8.61E–08 | 8.61E–08 | 6.09E–15 | 1.21E–04 | 6.80E–08 |

**Temperate Period 6000 AD**

| | pH | Eh | Cl | TDS | Alkalinidad | Ca | C | Na | K | Mg | S | S(VI) | S(–II) | Fe | Fe(II) | Fe(III) | Si | Al |
|---|---|---|---|---|---|---|---|---|---|---|---|---|---|---|---|---|---|---|
| Mean | 8.02 | –254.80 | 1.41E–04 | 0.003 | 1.78E–03 | 7.61E–04 | 1.80E–03 | 5.00E–04 | 5.88E–05 | 7.82E–05 | 1.38E–04 | 1.38E–04 | 2.13E–07 | 8.43E–08 | 8.43E–08 | 6.09E–15 | 1.21E–04 | 2.90E–08 |
| Max | 8.02 | –254.80 | 1.46E–04 | 0.003 | 1.78E–03 | 7.61E–04 | 1.80E–03 | 5.03E–04 | 5.88E–05 | 7.85E–05 | 1.38E–04 | 1.38E–04 | 2.15E–07 | 8.45E–08 | 8.45E–08 | 6.09E–15 | 1.21E–04 | 3.12E–08 |
| q3 | 8.02 | –254.80 | 1.41E–04 | 0.003 | 1.78E–03 | 7.61E–04 | 1.80E–03 | 5.00E–04 | 5.88E–05 | 7.82E–05 | 1.38E–04 | 1.38E–04 | 2.13E–07 | 8.43E–08 | 8.43E–08 | 6.09E–15 | 1.21E–04 | 2.90E–08 |
| Median | 8.02 | –254.80 | 1.41E–04 | 0.003 | 1.78E–03 | 7.61E–04 | 1.80E–03 | 5.00E–04 | 5.88E–05 | 7.82E–05 | 1.38E–04 | 1.38E–04 | 2.13E–07 | 8.43E–08 | 8.43E–08 | 6.09E–15 | 1.21E–04 | 2.90E–08 |
| q1 | 8.02 | –254.80 | 1.41E–04 | 0.003 | 1.78E–03 | 7.61E–04 | 1.80E–03 | 5.00E–04 | 5.88E–05 | 7.82E–05 | 1.38E–04 | 1.38E–04 | 2.13E–07 | 8.43E–08 | 8.43E–08 | 6.09E–15 | 1.21E–04 | 2.90E–08 |
| Min | 8.02 | –254.81 | 1.41E–04 | 0.003 | 1.78E–03 | 7.61E–04 | 1.80E–03 | 5.00E–04 | 5.88E–05 | 7.82E–05 | 1.38E–04 | 1.38E–04 | 2.13E–07 | 8.43E–08 | 8.43E–08 | 6.09E–15 | 1.21E–04 | 2.90E–08 |

**Temperate Period 9000 AD**

| | pH | Eh | Cl | TDS | Alkalinidad | Ca | C | Na | K | Mg | S | S(VI) | S(–II) | Fe | Fe(II) | Fe(III) | Si | Al |
|---|---|---|---|---|---|---|---|---|---|---|---|---|---|---|---|---|---|---|
| Mean | 8.02 | –254.59 | 1.41E–04 | 0.003 | 1.78E–03 | 7.60E–04 | 1.80E–03 | 5.00E–04 | 5.88E–05 | 7.82E–05 | 1.38E–04 | 1.38E–04 | 2.13E–07 | 8.73E–08 | 8.73E–08 | 6.11E–15 | 1.21E–04 | 2.90E–08 |
| Max | 8.02 | –133.37 | 1.41E–04 | 0.003 | 1.78E–03 | 7.61E–04 | 1.80E–03 | 5.00E–04 | 5.88E–05 | 7.82E–05 | 1.38E–04 | 1.38E–04 | 2.13E–07 | 1.79E–06 | 1.79E–06 | 1.55E–14 | 1.21E–04 | 2.90E–08 |
| q3 | 8.02 | –254.80 | 1.41E–04 | 0.003 | 1.78E–03 | 7.61E–04 | 1.80E–03 | 5.00E–04 | 5.88E–05 | 7.82E–05 | 1.38E–04 | 1.38E–04 | 2.13E–07 | 8.43E–08 | 8.43E–08 | 6.09E–15 | 1.21E–04 | 2.90E–08 |
| Median | 8.02 | –254.80 | 1.41E–04 | 0.003 | 1.78E–03 | 7.61E–04 | 1.80E–03 | 5.00E–04 | 5.88E–05 | 7.82E–05 | 1.38E–04 | 1.38E–04 | 2.13E–07 | 8.43E–08 | 8.43E–08 | 6.09E–15 | 1.21E–04 | 2.90E–08 |
| q1 | 8.02 | –254.80 | 1.41E–04 | 0.003 | 1.78E–03 | 7.61E–04 | 1.80E–03 | 5.00E–04 | 5.88E–05 | 7.82E–05 | 1.38E–04 | 1.38E–04 | 2.13E–07 | 8.43E–08 | 8.43E–08 | 6.09E–15 | 1.21E–04 | 2.90E–08 |
| Min | 8.02 | –254.80 | 1.41E–04 | 0.003 | 1.78E–03 | 7.61E–04 | 1.80E–03 | 5.00E–04 | 5.88E–05 | 7.82E–05 | 1.38E–04 | 1.38E–04 | 2.13E–07 | 8.43E–08 | 8.43E–08 | 6.09E–15 | 1.21E–04 | 2.90E–08 |

**Table A3-4. Temperate period: Variant Case of SFR 3. All concentrations and alkalinity are in mol/L, the TDS is in g/L and the Eh is reported in mV.**

| Temperate Period 2500 AD | | | | | | | | | | | | | | | | | |
|---|---|---|---|---|---|---|---|---|---|---|---|---|---|---|---|---|---|
| | pH | Eh | Cl | TDS | Alkalinity | Ca | C | Na | K | Mg | S | S(VI) | S(–II) | Fe | Fe(II) | Fe(III) | Si | Al |
| Mean | 7.29 | –216.71 | 9.87E–02 | 2.126 | 1.48E–03 | 1.50E–02 | 1.55E–03 | 6.52E–02 | 5.13E–04 | 6.17E–03 | 3.66E–03 | 3.61E–03 | 5.53E–05 | 1.23E–05 | 1.23E–05 | 1.36E–14 | 1.83E–04 | 5.88E–08 |
| Max | 7.29 | –216.71 | 9.87E–02 | 2.126 | 1.48E–03 | 1.50E–02 | 1.55E–03 | 6.52E–02 | 5.13E–04 | 6.17E–03 | 3.66E–03 | 3.61E–03 | 5.53E–05 | 1.23E–05 | 1.23E–05 | 1.36E–14 | 1.83E–04 | 5.88E–08 |
| q3 | 7.29 | –216.71 | 9.87E–02 | 2.126 | 1.48E–03 | 1.50E–02 | 1.55E–03 | 6.52E–02 | 5.13E–04 | 6.17E–03 | 3.66E–03 | 3.61E–03 | 5.53E–05 | 1.23E–05 | 1.23E–05 | 1.36E–14 | 1.83E–04 | 5.88E–08 |
| Median | 7.29 | –216.71 | 9.87E–02 | 2.126 | 1.48E–03 | 1.50E–02 | 1.55E–03 | 6.52E–02 | 5.13E–04 | 6.17E–03 | 3.66E–03 | 3.61E–03 | 5.53E–05 | 1.23E–05 | 1.23E–05 | 1.36E–14 | 1.83E–04 | 5.88E–08 |
| q1 | 7.29 | –216.71 | 9.87E–02 | 2.126 | 1.48E–03 | 1.50E–02 | 1.55E–03 | 6.52E–02 | 5.13E–04 | 6.17E–03 | 3.66E–03 | 3.61E–03 | 5.53E–05 | 1.23E–05 | 1.23E–05 | 1.36E–14 | 1.83E–04 | 5.88E–08 |
| Min | 7.29 | –216.71 | 9.87E–02 | 2.126 | 1.48E–03 | 1.50E–02 | 1.55E–03 | 6.52E–02 | 5.13E–04 | 6.17E–03 | 3.66E–03 | 3.61E–03 | 5.53E–05 | 1.23E–05 | 1.23E–05 | 1.36E–14 | 1.83E–04 | 5.88E–08 |

| Temperate Period 2600 AD | | | | | | | | | | | | | | | | | |
|---|---|---|---|---|---|---|---|---|---|---|---|---|---|---|---|---|---|
| | pH | Eh | Cl | TDS | Alkalinidad | Ca | C | Na | K | Mg | S | S(VI) | S(–II) | Fe | Fe(II) | Fe(III) | Si | Al |
| Mean | 7.59 | –235.64 | 2.53E–02 | 0.545 | 1.65E–03 | 4.35E–03 | 1.70E–03 | 1.70E–02 | 1.75E–04 | 1.63E–03 | 1.04E–03 | 1.02E–03 | 2.23E–05 | 1.24E–05 | 1.24E–05 | 6.20E–14 | 1.37E–04 | 7.29E–08 |
| Max | 7.94 | –216.71 | 9.87E–02 | 2.126 | 1.77E–03 | 1.50E–02 | 1.78E–03 | 6.52E–02 | 5.13E–04 | 6.17E–03 | 3.66E–03 | 3.61E–03 | 5.53E–05 | 1.25E–05 | 1.25E–05 | 2.16E–13 | 1.83E–04 | 7.69E–08 |
| q3 | 7.68 | –230.27 | 3.11E–02 | 0.670 | 1.70E–03 | 5.19E–03 | 1.74E–03 | 2.08E–02 | 2.02E–04 | 1.99E–03 | 1.25E–03 | 1.23E–03 | 2.50E–05 | 1.25E–05 | 1.25E–05 | 8.12E–14 | 1.40E–04 | 7.51E–08 |
| Median | 7.60 | –236.24 | 1.95E–02 | 0.420 | 1.66E–03 | 3.52E–03 | 1.71E–03 | 1.32E–02 | 1.48E–04 | 1.28E–03 | 8.39E–04 | 8.20E–04 | 1.98E–05 | 1.24E–05 | 1.24E–05 | 5.78E–14 | 1.33E–04 | 7.39E–08 |
| q1 | 7.51 | –241.60 | 1.27E–02 | 0.274 | 1.62E–03 | 2.54E–03 | 1.68E–03 | 8.75E–03 | 1.17E–04 | 8.55E–04 | 5.97E–04 | 5.80E–04 | 1.66E–05 | 1.23E–05 | 1.23E–05 | 3.88E–14 | 1.29E–04 | 7.19E–08 |
| Min | 7.29 | –258.53 | 1.99E–03 | 0.043 | 1.48E–03 | 1.02E–03 | 1.55E–03 | 1.71E–03 | 6.73E–05 | 1.92E–04 | 2.14E–04 | 2.03E–04 | 1.15E–05 | 1.19E–05 | 1.19E–05 | 1.36E–14 | 1.22E–04 | 5.88E–08 |

| Temperate Period 2800 AD | | | | | | | | | | | | | | | | | |
|---|---|---|---|---|---|---|---|---|---|---|---|---|---|---|---|---|---|
| | pH | Eh | Cl | TDS | Alkalinity | Ca | C | Na | K | Mg | S | S(VI) | S(–II) | Fe | Fe(II) | Fe(III) | Si | Al |
| Mean | 7.73 | –244.96 | 1.30E–02 | 0.280 | 1.71E–03 | 2.59E–03 | 1.74E–03 | 8.93E–03 | 1.18E–04 | 8.72E–04 | 6.07E–04 | 5.90E–04 | 1.70E–05 | 1.19E–05 | 1.19E–05 | 1.04E–13 | 1.29E–04 | 7.50E–08 |
| Max | 7.99 | –216.85 | 9.74E–02 | 2.098 | 1.78E–03 | 1.48E–02 | 1.79E–03 | 6.43E–02 | 5.07E–04 | 6.09E–03 | 3.62E–03 | 3.56E–03 | 5.47E–05 | 1.25E–05 | 1.25E–05 | 2.37E–13 | 1.82E–04 | 7.71E–08 |
| q3 | 7.84 | –240.12 | 1.45E–02 | 0.312 | 1.74E–03 | 2.79E–03 | 1.77E–03 | 9.90E–03 | 1.25E–04 | 9.64E–04 | 6.60E–04 | 6.42E–04 | 1.78E–05 | 1.21E–05 | 1.21E–05 | 1.37E–13 | 1.30E–04 | 7.63E–08 |
| Median | 7.76 | –246.71 | 8.33E–03 | 0.179 | 1.72E–03 | 1.92E–03 | 1.75E–03 | 5.88E–03 | 9.65E–05 | 5.84E–04 | 4.41E–04 | 4.26E–04 | 1.50E–05 | 1.19E–05 | 1.19E–05 | 1.04E–13 | 1.26E–04 | 7.58E–08 |
| q1 | 7.66 | –251.63 | 5.18E–03 | 0.112 | 1.69E–03 | 1.47E–03 | 1.73E–03 | 3.81E–03 | 8.20E–05 | 3.90E–04 | 3.29E–04 | 3.15E–04 | 1.34E–05 | 1.17E–05 | 1.17E–05 | 7.07E–14 | 1.24E–04 | 7.48E–08 |
| Min | 7.29 | –262.27 | 8.19E–04 | 0.018 | 1.48E–03 | 8.51E–04 | 1.55E–03 | 9.45E–04 | 6.19E–05 | 1.20E–04 | 1.73E–04 | 1.62E–04 | 1.13E–05 | 1.14E–05 | 1.14E–05 | 1.38E–14 | 1.21E–04 | 5.92E–08 |

**Temperate Period 3100 AD**

| | pH | Eh | Cl | TDS | Alkalinity | Ca | C | Na | K | Mg | S | S(VI) | S(–II) | Fe | Fe(II) | Fe(III) | Si | Al |
|---|---|---|---|---|---|---|---|---|---|---|---|---|---|---|---|---|---|---|
| Mean | 7.97 | –260.80 | 1.84E–03 | 0.040 | 1.78E–03 | 9.97E–04 | 1.78E–03 | 1.62E–03 | 6.66E–05 | 1.83E–04 | 2.10E–04 | 1.98E–04 | 1.20E–05 | 1.13E–05 | 1.13E–05 | 2.14E–13 | 1.22E–04 | 7.69E–08 |
| Max | 8.02 | –223.43 | 5.44E–02 | 1.172 | 1.79E–03 | 8.55E–03 | 1.79E–03 | 3.61E–02 | 3.09E–04 | 3.43E–03 | 2.08E–03 | 2.05E–03 | 3.59E–05 | 1.24E–05 | 1.24E–05 | 2.51E–13 | 1.55E–04 | 7.72E–08 |
| q3 | 8.01 | –260.60 | 1.39E–03 | 0.030 | 1.79E–03 | 9.31E–04 | 1.79E–03 | 1.32E–03 | 6.45E–05 | 1.55E–04 | 1.94E–04 | 1.82E–04 | 1.18E–05 | 1.13E–05 | 1.13E–05 | 2.39E–13 | 1.22E–04 | 7.71E–08 |
| Median | 7.99 | –262.61 | 7.55E–04 | 0.016 | 1.78E–03 | 8.42E–04 | 1.79E–03 | 9.03E–04 | 6.16E–05 | 1.16E–04 | 1.71E–04 | 1.60E–04 | 1.15E–05 | 1.12E–05 | 1.12E–05 | 2.29E–13 | 1.21E–04 | 7.71E–08 |
| q1 | 7.97 | –263.54 | 4.87E–04 | 0.010 | 1.78E–03 | 8.05E–04 | 1.79E–03 | 7.27E–04 | 6.04E–05 | 9.96E–05 | 1.61E–04 | 1.50E–04 | 1.13E–05 | 1.12E–05 | 1.12E–05 | 2.07E–13 | 1.21E–04 | 7.70E–08 |
| Min | 7.40 | –264.65 | 1.81E–04 | 0.004 | 1.56E–03 | 7.62E–04 | 1.63E–03 | 5.26E–04 | 5.90E–05 | 8.07E–05 | 1.51E–04 | 1.39E–04 | 1.12E–05 | 1.12E–05 | 1.12E–05 | 2.32E–14 | 1.21E–04 | 6.80E–08 |

**Temperate Period 6000 AD**

| | pH | Eh | Cl | TDS | Alkalinity | Ca | C | Na | K | Mg | S | S(VI) | S(–II) | Fe | Fe(II) | Fe(III) | Si | Al |
|---|---|---|---|---|---|---|---|---|---|---|---|---|---|---|---|---|---|---|
| Mean | 8.03 | –264.81 | 1.41E–04 | 0.003 | 1.79E–03 | 7.56E–04 | 1.79E–03 | 5.00E–04 | 5.88E–05 | 7.82E–05 | 1.49E–04 | 1.38E–04 | 1.12E–05 | 1.11E–05 | 1.11E–05 | 2.52E–13 | 1.21E–04 | 3.10E–08 |
| Max | 8.03 | –264.79 | 1.46E–04 | 0.003 | 1.79E–03 | 7.57E–04 | 1.79E–03 | 5.03E–04 | 5.88E–05 | 7.85E–05 | 1.49E–04 | 1.38E–04 | 1.12E–05 | 1.11E–05 | 1.11E–05 | 2.52E–13 | 1.21E–04 | 3.33E–08 |
| q3 | 8.03 | –264.81 | 1.41E–04 | 0.003 | 1.79E–03 | 7.56E–04 | 1.79E–03 | 5.00E–04 | 5.88E–05 | 7.82E–05 | 1.49E–04 | 1.38E–04 | 1.12E–05 | 1.11E–05 | 1.11E–05 | 2.52E–13 | 1.21E–04 | 3.10E–08 |
| Median | 8.03 | –264.81 | 1.41E–04 | 0.003 | 1.79E–03 | 7.56E–04 | 1.79E–03 | 5.00E–04 | 5.88E–05 | 7.82E–05 | 1.49E–04 | 1.38E–04 | 1.12E–05 | 1.11E–05 | 1.11E–05 | 2.52E–13 | 1.21E–04 | 3.10E–08 |
| q1 | 8.03 | –264.81 | 1.41E–04 | 0.003 | 1.79E–03 | 7.56E–04 | 1.79E–03 | 5.00E–04 | 5.88E–05 | 7.82E–05 | 1.49E–04 | 1.38E–04 | 1.12E–05 | 1.11E–05 | 1.11E–05 | 2.52E–13 | 1.21E–04 | 3.10E–08 |
| Min | 8.03 | –264.81 | 1.41E–04 | 0.003 | 1.79E–03 | 7.56E–04 | 1.79E–03 | 5.00E–04 | 5.88E–05 | 7.82E–05 | 1.49E–04 | 1.38E–04 | 1.12E–05 | 1.11E–05 | 1.11E–05 | 2.52E–13 | 1.21E–04 | 3.10E–08 |

**Temperate Period 9000 AD**

| | pH | Eh | Cl | TDS | Alkalinity | Ca | C | Na | K | Mg | S | S(VI) | S(–II) | Fe | Fe(II) | Fe(III) | Si | Al |
|---|---|---|---|---|---|---|---|---|---|---|---|---|---|---|---|---|---|---|
| Mean | 8.02 | –264.68 | 1.41E–04 | 0.003 | 1.79E–03 | 7.55E–04 | 1.79E–03 | 5.00E–04 | 5.88E–05 | 7.82E–05 | 1.49E–04 | 1.38E–04 | 1.12E–05 | 1.12E–05 | 1.12E–05 | 2.52E–13 | 1.21E–04 | 3.10E–08 |
| Max | 8.03 | –191.46 | 1.41E–04 | 0.003 | 1.79E–03 | 7.56E–04 | 1.79E–03 | 5.00E–04 | 5.88E–05 | 7.82E–05 | 1.66E–04 | 1.38E–04 | 2.78E–05 | 2.96E–05 | 2.96E–05 | 2.52E–13 | 1.21E–04 | 3.10E–08 |
| q3 | 8.03 | –264.81 | 1.41E–04 | 0.003 | 1.79E–03 | 7.56E–04 | 1.79E–03 | 5.00E–04 | 5.88E–05 | 7.82E–05 | 1.49E–04 | 1.38E–04 | 1.12E–05 | 1.11E–05 | 1.11E–05 | 2.52E–13 | 1.21E–04 | 3.10E–08 |
| Median | 8.03 | –264.81 | 1.41E–04 | 0.003 | 1.79E–03 | 7.56E–04 | 1.79E–03 | 5.00E–04 | 5.88E–05 | 7.82E–05 | 1.49E–04 | 1.38E–04 | 1.12E–05 | 1.11E–05 | 1.11E–05 | 2.52E–13 | 1.21E–04 | 3.10E–08 |
| q1 | 8.03 | –264.81 | 1.41E–04 | 0.003 | 1.79E–03 | 7.56E–04 | 1.79E–03 | 5.00E–04 | 5.88E–05 | 7.82E–05 | 1.49E–04 | 1.38E–04 | 1.12E–05 | 1.11E–05 | 1.11E–05 | 2.52E–13 | 1.21E–04 | 3.10E–08 |
| Min | 6.85 | –264.81 | 1.41E–04 | 0.003 | 1.09E–03 | 3.85E–04 | 1.42E–03 | 5.00E–04 | 5.88E–05 | 7.82E–05 | 1.49E–04 | 1.38E–04 | 1.12E–05 | 1.11E–05 | 1.11E–05 | 2.48E–14 | 1.21E–04 | 3.10E–08 |

**Table A3-5. Periglacial period (glacial boundary water). Base Case of SFR 1. All concentrations and alkalinity are in mol/L, the TDS is in g/L and the Eh is reported in mV.**

| Periglacial period 0 years | | | | | | | | | | | | | | | | | | |
|---|---|---|---|---|---|---|---|---|---|---|---|---|---|---|---|---|---|---|
| | pH | Eh | Cl | TDS | Alkalinity | Ca | C | Na | K | Mg | S | S(VI) | S(–II) | Fe | Fe(II) | Fe(III) | Si | Al |
| Mean | 8.02 | –242.81 | 1.41E–04 | 0.003 | 0.00178 | 7.61E–04 | 0.0018 | 5.00E–04 | 5.88E–05 | 7.82E–05 | 1.38E–04 | 1.38E–04 | 4.39E–09 | 4.92E–08 | 4.92E–08 | 6.09E–15 | 1.21E–04 | 2.90E–08 |
| Max | 8.02 | –242.81 | 1.41E–04 | 0.003 | 0.00178 | 7.61E–04 | 0.0018 | 5.00E–04 | 5.88E–05 | 7.82E–05 | 1.38E–04 | 1.38E–04 | 4.39E–09 | 4.92E–08 | 4.92E–08 | 6.09E–15 | 1.21E–04 | 2.90E–08 |
| q3 | 8.02 | –242.81 | 1.41E–04 | 0.003 | 0.00178 | 7.61E–04 | 0.0018 | 5.00E–04 | 5.88E–05 | 7.82E–05 | 1.38E–04 | 1.38E–04 | 4.39E–09 | 4.92E–08 | 4.92E–08 | 6.09E–15 | 1.21E–04 | 2.90E–08 |
| Median | 8.02 | –242.81 | 1.41E–04 | 0.003 | 0.00178 | 7.61E–04 | 0.0018 | 5.00E–04 | 5.88E–05 | 7.82E–05 | 1.38E–04 | 1.38E–04 | 4.39E–09 | 4.92E–08 | 4.92E–08 | 6.09E–15 | 1.21E–04 | 2.90E–08 |
| q1 | 8.02 | –242.81 | 1.41E–04 | 0.003 | 0.00178 | 7.61E–04 | 0.0018 | 5.00E–04 | 5.88E–05 | 7.82E–05 | 1.38E–04 | 1.38E–04 | 4.39E–09 | 4.92E–08 | 4.92E–08 | 6.09E–15 | 1.21E–04 | 2.90E–08 |
| Min | 8.02 | –242.81 | 1.41E–04 | 0.003 | 0.00178 | 7.61E–04 | 0.0018 | 5.00E–04 | 5.88E–05 | 7.82E–05 | 1.38E–04 | 1.38E–04 | 4.39E–09 | 4.92E–08 | 4.92E–08 | 6.09E–15 | 1.21E–04 | 2.90E–08 |

| Periglacial period 500 years | | | | | | | | | | | | | | | | | | |
|---|---|---|---|---|---|---|---|---|---|---|---|---|---|---|---|---|---|---|
| | pH | Eh | Cl | TDS | Alkalinity | Ca | C | Na | K | Mg | S | S(VI) | S(–II) | Fe | Fe(II) | Fe(III) | Si | Al |
| Mean | 8.53 | –286.94 | 7.31E–05 | 1.53E–03 | 1.01E–03 | 4.35E–04 | 9.85E–04 | 2.37E–04 | 3.28E–05 | 3.86E–05 | 6.70E–05 | 6.69E–05 | 9.46E–08 | 1.70E–08 | 1.70E–08 | 6.58E–15 | 1.70E–04 | 1.35E–08 |
| Max | 9.15 | –254.45 | 1.41E–04 | 2.95E–03 | 1.78E–03 | 7.61E–04 | 1.80E–03 | 5.00E–04 | 5.88E–05 | 7.82E–05 | 1.38E–04 | 1.38E–04 | 1.90E–07 | 8.26E–08 | 8.26E–08 | 9.64E–15 | 2.05E–04 | 2.90E–08 |
| q3 | 8.71 | –277.01 | 8.66E–05 | 1.81E–03 | 1.16E–03 | 5.00E–04 | 1.15E–03 | 2.89E–04 | 3.80E–05 | 4.64E–05 | 8.10E–05 | 8.09E–05 | 1.16E–07 | 1.98E–08 | 1.98E–08 | 6.89E–15 | 1.85E–04 | 1.66E–08 |
| Median | 8.56 | –289.17 | 6.63E–05 | 1.39E–03 | 9.26E–04 | 4.01E–04 | 9.01E–04 | 2.10E–04 | 3.02E–05 | 3.46E–05 | 5.98E–05 | 5.97E–05 | 8.51E–08 | 9.30E–09 | 9.30E–09 | 6.47E–15 | 1.75E–04 | 1.20E–08 |
| q1 | 8.37 | –298.66 | 5.33E–05 | 1.12E–03 | 7.80E–04 | 3.39E–04 | 7.46E–04 | 1.60E–04 | 2.52E–05 | 2.70E–05 | 4.63E–05 | 4.62E–05 | 6.49E–08 | 5.18E–09 | 5.18E–09 | 6.16E–15 | 1.60E–04 | 9.03E–09 |
| Min | 8.02 | –325.99 | 2.52E–05 | 5.27E–04 | 4.90E–04 | 2.19E–04 | 4.22E–04 | 5.04E–05 | 1.44E–05 | 1.06E–05 | 1.68E–05 | 1.68E–05 | 1.89E–08 | 9.24E–10 | 9.24E–10 | 6.04E–15 | 1.21E–04 | 2.62E–09 |

| Periglacial period 1,000 years | | | | | | | | | | | | | | | | | | |
|---|---|---|---|---|---|---|---|---|---|---|---|---|---|---|---|---|---|---|
| | pH | Eh | Cl | TDS | Alkalinity | Ca | C | Na | K | Mg | S | S(VI) | S(–II) | Fe | Fe(II) | Fe(III) | Si | Al |
| Mean | 8.92 | –311.70 | 4.17E–05 | 8.99E–04 | 6.65E–04 | 2.92E–04 | 6.15E–04 | 1.15E–04 | 2.08E–05 | 2.03E–05 | 3.41E–05 | 3.41E–05 | 4.46E–08 | 6.01E–09 | 6.01E–09 | 8.35E–15 | 1.93E–04 | 6.39E–09 |
| Max | 9.33 | –254.45 | 1.41E–04 | 3.04E–03 | 1.78E–03 | 7.61E–04 | 1.80E–03 | 5.00E–04 | 5.88E–05 | 7.82E–05 | 1.38E–04 | 1.38E–04 | 1.90E–07 | 8.26E–08 | 8.26E–08 | 1.19E–14 | 2.11E–04 | 2.90E–08 |
| q3 | 9.13 | –304.63 | 4.62E–05 | 9.95E–04 | 7.01E–04 | 3.06E–04 | 6.61E–04 | 1.32E–04 | 2.25E–05 | 2.28E–05 | 3.88E–05 | 3.87E–05 | 5.25E–08 | 3.57E–09 | 3.57E–09 | 9.46E–15 | 2.04E–04 | 7.41E–09 |
| Median | 9.01 | –317.65 | 3.27E–05 | 7.04E–04 | 5.61E–04 | 2.48E–04 | 5.06E–04 | 7.97E–05 | 1.73E–05 | 1.50E–05 | 2.47E–05 | 2.47E–05 | 3.09E–08 | 1.59E–09 | 1.59E–09 | 8.47E–15 | 1.99E–04 | 4.34E–09 |
| q1 | 8.81 | –324.83 | 2.62E–05 | 5.64E–04 | 4.99E–04 | 2.23E–04 | 4.33E–04 | 5.42E–05 | 1.48E–05 | 1.11E–05 | 1.78E–05 | 1.78E–05 | 2.01E–08 | 9.93E–10 | 9.93E–10 | 7.26E–15 | 1.90E–04 | 2.84E–09 |
| Min | 8.02 | –334.86 | 1.62E–05 | 3.49E–04 | 4.17E–04 | 1.91E–04 | 3.29E–04 | 1.57E–05 | 1.10E–05 | 5.36E–06 | 7.44E–06 | 7.44E–06 | 3.60E–09 | 4.08E–10 | 4.08E–10 | 6.04E–15 | 1.21E–04 | 5.86E–10 |

**Periglacial period 2,000 years**

| | pH | Eh | Cl | TDS | Alkalinity | Ca | C | Na | K | Mg | S | S(VI) | S(–II) | Fe | Fe(II) | Fe(III) | Si | Al |
|---|---|---|---|---|---|---|---|---|---|---|---|---|---|---|---|---|---|---|
| Mean | 9.32 | –330.23 | 1.76E–05 | 3.79E–04 | 4.34E–04 | 1.98E–04 | 3.47E–04 | 2.10E–05 | 1.15E–05 | 6.16E–06 | 8.88E–06 | 8.87E–06 | 5.56E–09 | 1.03E–09 | 1.03E–09 | 1.20E–14 | 2.11E–04 | 8.98E–10 |
| Max | 9.37 | –256.66 | 1.34E–04 | 2.89E–03 | 1.70E–03 | 7.30E–04 | 1.72E–03 | 4.74E–04 | 5.63E–05 | 7.43E–05 | 1.31E–04 | 1.31E–04 | 1.81E–07 | 7.16E–08 | 7.16E–08 | 1.26E–14 | 2.13E–04 | 2.75E–08 |
| q3 | 9.37 | –330.39 | 1.54E–05 | 3.32E–04 | 4.11E–04 | 1.88E–04 | 3.21E–04 | 1.23E–05 | 1.07E–05 | 4.85E–06 | 6.53E–06 | 6.53E–06 | 2.06E–09 | 3.58E–10 | 3.58E–10 | 1.26E–14 | 2.13E–04 | 3.87E–10 |
| Median | 9.36 | –332.26 | 1.45E–05 | 3.12E–04 | 4.05E–04 | 1.86E–04 | 3.12E–04 | 9.11E–06 | 1.04E–05 | 4.37E–06 | 5.67E–06 | 5.67E–06 | 7.07E–10 | 2.97E–10 | 2.97E–10 | 1.25E–14 | 2.13E–04 | 2.01E–10 |
| q1 | 9.35 | –333.96 | 1.43E–05 | 3.08E–04 | 4.03E–04 | 1.85E–04 | 3.10E–04 | 8.18E–06 | 1.03E–05 | 4.23E–06 | 5.42E–06 | 5.42E–06 | 3.11E–10 | 2.64E–10 | 2.64E–10 | 1.22E–14 | 2.12E–04 | 1.46E–10 |
| Min | 8.06 | –334.85 | 1.41E–05 | 3.04E–04 | 4.02E–04 | 1.85E–04 | 3.08E–04 | 7.44E–06 | 1.02E–05 | 4.12E–06 | 5.22E–06 | 5.22E–06 | 7.56E–12 | 1.64E–10 | 1.64E–10 | 6.04E–15 | 1.26E–04 | 1.03E–10 |

**Periglacial period 5,000 years**

| | pH | Eh | Cl | TDS | Alkalinity | Ca | C | Na | K | Mg | S | S(VI) | S(–II) | Fe | Fe(II) | Fe(III) | Si | Al |
|---|---|---|---|---|---|---|---|---|---|---|---|---|---|---|---|---|---|---|
| Mean | 9.37 | –304.41 | 1.42E–05 | 3.05E–04 | 4.02E–04 | 1.85E–04 | 3.09E–04 | 7.69E–06 | 1.02E–05 | 4.16E–06 | 5.29E–06 | 5.29E–06 | 1.25E–10 | 9.58E–11 | 9.58E–11 | 1.26E–14 | 2.13E–04 | 1.18E–10 |
| Max | 9.37 | –302.12 | 3.34E–05 | 7.19E–04 | 5.68E–04 | 2.51E–04 | 5.14E–04 | 8.24E–05 | 1.76E–05 | 1.54E–05 | 2.54E–05 | 2.54E–05 | 3.10E–08 | 1.65E–09 | 1.65E–09 | 1.26E–14 | 2.13E–04 | 4.50E–09 |
| q3 | 9.37 | –302.54 | 1.41E–05 | 3.04E–04 | 4.02E–04 | 1.85E–04 | 3.08E–04 | 7.39E–06 | 1.02E–05 | 4.11E–06 | 5.21E–06 | 5.21E–06 | 3.70E–14 | 8.41E–11 | 8.41E–11 | 1.26E–14 | 2.13E–04 | 1.00E–10 |
| Median | 9.37 | –302.90 | 1.41E–05 | 3.04E–04 | 4.02E–04 | 1.85E–04 | 3.08E–04 | 7.39E–06 | 1.02E–05 | 4.11E–06 | 5.21E–06 | 5.21E–06 | 3.19E–14 | 8.26E–11 | 8.26E–11 | 1.26E–14 | 2.13E–04 | 1.00E–10 |
| q1 | 9.37 | –303.36 | 1.41E–05 | 3.04E–04 | 4.02E–04 | 1.85E–04 | 3.08E–04 | 7.39E–06 | 1.02E–05 | 4.11E–06 | 5.21E–06 | 5.21E–06 | 2.83E–14 | 8.14E–11 | 8.14E–11 | 1.26E–14 | 2.13E–04 | 1.00E–10 |
| Min | 9.00 | –334.78 | 1.41E–05 | 3.04E–04 | 4.02E–04 | 1.85E–04 | 3.08E–04 | 7.39E–06 | 1.02E–05 | 4.11E–06 | 5.21E–06 | 5.21E–06 | 2.47E–14 | 8.00E–11 | 8.00E–11 | 8.38E–15 | 1.99E–04 | 1.00E–10 |

**Periglacial period 10,000 years**

| | pH | Eh | Cl | TDS | Alkalinity | Ca | C | Na | K | Mg | S | S(VI) | S(–II) | Fe | Fe(II) | Fe(III) | Si | Al |
|---|---|---|---|---|---|---|---|---|---|---|---|---|---|---|---|---|---|---|
| Mean | 9.37 | –303.46 | 1.41E–05 | 3.04E–04 | 4.02E–04 | 1.85E–04 | 3.08E–04 | 7.39E–06 | 1.02E–05 | 4.11E–06 | 5.21E–06 | 5.21E–06 | 4.04E–14 | 8.46E–11 | 8.46E–11 | 1.26E–14 | 2.13E–04 | 1.00E–10 |
| Max | 9.37 | –285.31 | 1.41E–05 | 3.04E–04 | 4.02E–04 | 1.85E–04 | 3.08E–04 | 7.40E–06 | 1.02E–05 | 4.11E–06 | 5.21E–06 | 5.21E–06 | 4.20E–14 | 8.55E–11 | 8.55E–11 | 1.26E–14 | 2.13E–04 | 1.01E–10 |
| q3 | 9.37 | –303.67 | 1.41E–05 | 3.04E–04 | 4.02E–04 | 1.85E–04 | 3.08E–04 | 7.39E–06 | 1.02E–05 | 4.11E–06 | 5.21E–06 | 5.21E–06 | 4.18E–14 | 8.54E–11 | 8.54E–11 | 1.26E–14 | 2.13E–04 | 1.00E–10 |
| Median | 9.37 | –303.70 | 1.41E–05 | 3.04E–04 | 4.02E–04 | 1.85E–04 | 3.08E–04 | 7.39E–06 | 1.02E–05 | 4.11E–06 | 5.21E–06 | 5.21E–06 | 4.12E–14 | 8.53E–11 | 8.53E–11 | 1.26E–14 | 2.13E–04 | 1.00E–10 |
| q1 | 9.37 | –303.74 | 1.41E–05 | 3.04E–04 | 4.02E–04 | 1.85E–04 | 3.08E–04 | 7.39E–06 | 1.02E–05 | 4.11E–06 | 5.21E–06 | 5.21E–06 | 4.08E–14 | 8.52E–11 | 8.52E–11 | 1.26E–14 | 2.13E–04 | 1.00E–10 |
| Min | 9.37 | –303.76 | 1.41E–05 | 3.04E–04 | 4.02E–04 | 1.85E–04 | 3.08E–04 | 7.39E–06 | 1.02E–05 | 4.11E–06 | 5.21E–06 | 5.21E–06 | 1.08E–16 | 4.06E–11 | 4.06E–11 | 1.26E–14 | 2.13E–04 | 1.00E–10 |

**Table A3-6. Periglacial period (glacial boundary water). Variant Case of SFR 1. All concentrations and alkalinity are in mol/L, the TDS is in g/L and the Eh is reported in mV.**

| Periglacial period 0 years | | | | | | | | | | | | | | | | | | |
|---|---|---|---|---|---|---|---|---|---|---|---|---|---|---|---|---|---|---|
| | pH | Eh | Cl | TDS | Alkalinity | Ca | C | Na | K | Mg | S | S(VI) | S(–II) | Fe | Fe(II) | Fe(III) | Si | Al |
| Mean | 7.96784 | –271.32684 | 1.41E–04 | 3.04E–03 | 1.97E–03 | 8.35E–04 | 1.87E–03 | 5.00E–04 | 5.88E–05 | 7.82E–05 | 2.50E–04 | 1.25E–04 | 1.26E–04 | 6.56E–06 | 6.56E–06 | 6.13E–15 | 1.21E–04 | 2.90E–08 |
| Max | 7.96784 | –271.32684 | 1.41E–04 | 3.04E–03 | 1.97E–03 | 8.35E–04 | 1.87E–03 | 5.00E–04 | 5.88E–05 | 7.82E–05 | 2.50E–04 | 1.25E–04 | 1.26E–04 | 6.56E–06 | 6.56E–06 | 6.13E–15 | 1.21E–04 | 2.90E–08 |
| q3 | 7.96784 | –271.32684 | 1.41E–04 | 3.04E–03 | 1.97E–03 | 8.35E–04 | 1.87E–03 | 5.00E–04 | 5.88E–05 | 7.82E–05 | 2.50E–04 | 1.25E–04 | 1.26E–04 | 6.56E–06 | 6.56E–06 | 6.13E–15 | 1.21E–04 | 2.90E–08 |
| Median | 7.96784 | –271.32684 | 1.41E–04 | 3.04E–03 | 1.97E–03 | 8.35E–04 | 1.87E–03 | 5.00E–04 | 5.88E–05 | 7.82E–05 | 2.50E–04 | 1.25E–04 | 1.26E–04 | 6.56E–06 | 6.56E–06 | 6.13E–15 | 1.21E–04 | 2.90E–08 |
| q1 | 7.96784 | –271.32684 | 1.41E–04 | 3.04E–03 | 1.97E–03 | 8.35E–04 | 1.87E–03 | 5.00E–04 | 5.88E–05 | 7.82E–05 | 2.50E–04 | 1.25E–04 | 1.26E–04 | 6.56E–06 | 6.56E–06 | 6.13E–15 | 1.21E–04 | 2.90E–08 |
| Min | 7.96784 | –271.32684 | 1.41E–04 | 3.04E–03 | 1.97E–03 | 8.35E–04 | 1.87E–03 | 5.00E–04 | 5.88E–05 | 7.82E–05 | 2.50E–04 | 1.25E–04 | 1.26E–04 | 6.56E–06 | 6.56E–06 | 6.13E–15 | 1.21E–04 | 2.90E–08 |

| Periglacial period 500 years | | | | | | | | | | | | | | | | | | |
|---|---|---|---|---|---|---|---|---|---|---|---|---|---|---|---|---|---|---|
| | pH | Eh | Cl | TDS | Alkalinity | Ca | C | Na | K | Mg | S | S(VI) | S(–II) | Fe | Fe(II) | Fe(III) | Si | Al |
| Mean | 8.35 | –300.92 | 7.31E–05 | 1.58E–03 | 1.33E–03 | 5.68E–04 | 1.12E–03 | 2.37E–04 | 3.28E–05 | 3.86E–05 | 2.49E–04 | 4.54E–05 | 2.03E–04 | 6.39E–06 | 6.39E–06 | 6.20E–15 | 1.70E–04 | 1.35E–08 |
| Max | 8.76 | –271.33 | 1.41E–04 | 3.04E–03 | 1.97E–03 | 8.35E–04 | 1.87E–03 | 5.00E–04 | 5.88E–05 | 7.82E–05 | 2.58E–04 | 1.25E–04 | 2.57E–04 | 6.56E–06 | 6.56E–06 | 7.07E–15 | 2.05E–04 | 2.90E–08 |
| q3 | 8.47 | –292.37 | 8.66E–05 | 1.87E–03 | 1.44E–03 | 6.16E–04 | 1.26E–03 | 2.89E–04 | 3.80E–05 | 4.64E–05 | 2.54E–04 | 6.19E–05 | 2.33E–04 | 6.41E–06 | 6.41E–06 | 6.29E–15 | 1.85E–04 | 1.66E–08 |
| Median | 8.38 | –302.86 | 6.63E–05 | 1.43E–03 | 1.26E–03 | 5.41E–04 | 1.04E–03 | 2.10E–04 | 3.02E–05 | 3.46E–05 | 2.48E–04 | 3.73E–05 | 2.11E–04 | 6.37E–06 | 6.37E–06 | 6.16E–15 | 1.75E–04 | 1.20E–08 |
| q1 | 8.24 | –311.02 | 5.33E–05 | 1.15E–03 | 1.15E–03 | 4.94E–04 | 9.01E–04 | 1.60E–04 | 2.52E–05 | 2.70E–05 | 2.43E–04 | 2.15E–05 | 1.80E–04 | 6.36E–06 | 6.36E–06 | 6.08E–15 | 1.60E–04 | 9.03E–09 |
| Min | 7.97 | –340.79 | 2.52E–05 | 5.43E–04 | 8.72E–04 | 3.88E–04 | 5.91E–04 | 5.04E–05 | 1.44E–05 | 1.06E–05 | 2.40E–04 | 6.10E–07 | 1.26E–04 | 6.33E–06 | 6.33E–06 | 6.04E–15 | 1.21E–04 | 2.62E–09 |

| Periglacial period 1,000 years | | | | | | | | | | | | | | | | | | |
|---|---|---|---|---|---|---|---|---|---|---|---|---|---|---|---|---|---|---|
| | pH | Eh | Cl | TDS | Alkalinity | Ca | C | Na | K | Mg | S | S(VI) | S(–II) | Fe | Fe(II) | Fe(III) | Si | Al |
| Mean | 8.61 | –325.75 | 4.17E–05 | 8.99E–04 | 1.03E–03 | 4.50E–04 | 7.73E–04 | 1.15E–04 | 2.08E–05 | 2.03E–05 | 2.55E–04 | 1.39E–05 | 2.41E–04 | 6.35E–06 | 6.35E–06 | 6.71E–15 | 1.93E–04 | 6.39E–09 |
| Max | 8.85 | –271.34 | 1.41E–04 | 3.04E–03 | 1.97E–03 | 8.35E–04 | 1.87E–03 | 5.00E–04 | 5.88E–05 | 7.82E–05 | 2.82E–04 | 1.25E–04 | 2.82E–04 | 6.56E–06 | 6.56E–06 | 7.47E–15 | 2.11E–04 | 2.90E–08 |
| q3 | 8.75 | –316.55 | 4.62E–05 | 9.95E–04 | 1.09E–03 | 4.68E–04 | 8.23E–04 | 1.32E–04 | 2.25E–05 | 2.28E–05 | 2.57E–04 | 1.31E–05 | 2.56E–04 | 6.35E–06 | 6.35E–06 | 7.03E–15 | 2.04E–04 | 7.41E–09 |
| Median | 8.67 | –331.75 | 3.27E–05 | 7.04E–04 | 9.48E–04 | 4.12E–04 | 6.70E–04 | 7.97E–05 | 1.73E–05 | 1.50E–05 | 2.55E–04 | 1.86E–06 | 2.51E–04 | 6.34E–06 | 6.34E–06 | 6.77E–15 | 1.99E–04 | 4.34E–09 |
| q1 | 8.53 | –339.73 | 2.62E–05 | 5.64E–04 | 8.81E–04 | 3.90E–04 | 6.01E–04 | 5.42E–05 | 1.48E–05 | 1.11E–05 | 2.52E–04 | 6.84E–07 | 2.44E–04 | 6.33E–06 | 6.33E–06 | 6.40E–15 | 1.90E–04 | 2.84E–09 |
| Min | 7.97 | –349.33 | 1.62E–05 | 3.49E–04 | 8.09E–04 | 3.72E–04 | 5.13E–04 | 1.57E–05 | 1.10E–05 | 5.36E–06 | 2.40E–04 | 2.79E–07 | 1.26E–04 | 6.33E–06 | 6.33E–06 | 6.04E–15 | 1.21E–04 | 5.86E–10 |

**Periglacial period 2,000 years**

| | pH | Eh | Cl | TDS | Alkalinity | Ca | C | Na | K | Mg | S | S(VI) | S(–II) | Fe | Fe(II) | Fe(III) | Si | Al |
|---|---|---|---|---|---|---|---|---|---|---|---|---|---|---|---|---|---|---|
| Mean | 8.85 | –348.49 | 1.76E–05 | 3.79E–04 | 8.21E–04 | 3.78E–04 | 5.27E–04 | 2.10E–05 | 1.15E–05 | 6.16E–06 | 2.80E–04 | 2.01E–06 | 2.78E–04 | 6.33E–06 | 6.33E–06 | 7.50E–15 | 2.11E–04 | 8.98E–10 |
| Max | 8.88 | –273.50 | 1.34E–04 | 2.89E–03 | 1.90E–03 | 8.07E–04 | 1.80E–03 | 4.74E–04 | 5.63E–05 | 7.43E–05 | 2.85E–04 | 1.17E–04 | 2.85E–04 | 6.54E–06 | 6.54E–06 | 7.62E–15 | 2.13E–04 | 2.75E–08 |
| q3 | 8.88 | –350.42 | 1.54E–05 | 3.32E–04 | 8.00E–04 | 3.70E–04 | 5.03E–04 | 1.23E–05 | 1.07E–05 | 4.85E–06 | 2.84E–04 | 2.62E–07 | 2.84E–04 | 6.33E–06 | 6.33E–06 | 7.61E–15 | 2.13E–04 | 3.87E–10 |
| Median | 8.87 | –351.17 | 1.45E–05 | 3.12E–04 | 7.95E–04 | 3.69E–04 | 4.96E–04 | 9.11E–06 | 1.04E–05 | 4.37E–06 | 2.84E–04 | 2.48E–07 | 2.83E–04 | 6.33E–06 | 6.33E–06 | 7.60E–15 | 2.13E–04 | 2.01E–10 |
| q1 | 8.87 | –351.39 | 1.43E–05 | 3.08E–04 | 7.93E–04 | 3.69E–04 | 4.94E–04 | 8.18E–06 | 1.03E–05 | 4.23E–06 | 2.81E–04 | 2.44E–07 | 2.81E–04 | 6.33E–06 | 6.33E–06 | 7.55E–15 | 2.12E–04 | 1.46E–10 |
| Min | 8.00 | –351.57 | 1.41E–05 | 3.04E–04 | 7.92E–04 | 3.69E–04 | 4.92E–04 | 7.44E–06 | 1.02E–05 | 4.12E–06 | 2.40E–04 | 2.41E–07 | 1.31E–04 | 6.33E–06 | 6.33E–06 | 6.04E–15 | 1.26E–04 | 1.03E–10 |

**Periglacial period 5,000 years**

| | pH | Eh | Cl | TDS | Alkalinity | Ca | C | Na | K | Mg | S | S(VI) | S(–II) | Fe | Fe(II) | Fe(III) | Si | Al |
|---|---|---|---|---|---|---|---|---|---|---|---|---|---|---|---|---|---|---|
| Mean | 8.88 | –351.50 | 1.42E–05 | 3.05E–04 | 7.93E–04 | 3.69E–04 | 4.93E–04 | 7.69E–06 | 1.02E–05 | 4.16E–06 | 2.85E–04 | 2.44E–07 | 2.85E–04 | 6.33E–06 | 6.33E–06 | 7.62E–15 | 2.13E–04 | 1.18E–10 |
| Max | 8.88 | –330.83 | 3.34E–05 | 7.19E–04 | 9.56E–04 | 4.15E–04 | 6.78E–04 | 8.24E–05 | 1.76E–05 | 1.54E–05 | 2.85E–04 | 2.12E–06 | 2.85E–04 | 6.34E–06 | 6.34E–06 | 7.62E–15 | 2.13E–04 | 4.50E–09 |
| q3 | 8.88 | –351.58 | 1.41E–05 | 3.04E–04 | 7.92E–04 | 3.69E–04 | 4.92E–04 | 7.39E–06 | 1.02E–05 | 4.11E–06 | 2.85E–04 | 2.41E–07 | 2.85E–04 | 6.33E–06 | 6.33E–06 | 7.62E–15 | 2.13E–04 | 1.00E–10 |
| Median | 8.88 | –351.58 | 1.41E–05 | 3.04E–04 | 7.92E–04 | 3.69E–04 | 4.92E–04 | 7.39E–06 | 1.02E–05 | 4.11E–06 | 2.85E–04 | 2.41E–07 | 2.85E–04 | 6.33E–06 | 6.33E–06 | 7.62E–15 | 2.13E–04 | 1.00E–10 |
| q1 | 8.88 | –351.58 | 1.41E–05 | 3.04E–04 | 7.92E–04 | 3.69E–04 | 4.92E–04 | 7.39E–06 | 1.02E–05 | 4.11E–06 | 2.85E–04 | 2.41E–07 | 2.85E–04 | 6.33E–06 | 6.33E–06 | 7.62E–15 | 2.13E–04 | 1.00E–10 |
| Min | 8.67 | –351.58 | 1.41E–05 | 3.04E–04 | 7.92E–04 | 3.69E–04 | 4.92E–04 | 7.39E–06 | 1.02E–05 | 4.11E–06 | 2.52E–04 | 2.41E–07 | 2.51E–04 | 6.33E–06 | 6.33E–06 | 6.74E–15 | 1.99E–04 | 1.00E–10 |

**Periglacial period 10,000 years**

| | pH | Eh | Cl | TDS | Alkalinity | Ca | C | Na | K | Mg | S | S(VI) | S(–II) | Fe | Fe(II) | Fe(III) | Si | Al |
|---|---|---|---|---|---|---|---|---|---|---|---|---|---|---|---|---|---|---|
| Mean | 8.88 | –351.58 | 1.41E–05 | 3.04E–04 | 7.92E–04 | 3.69E–04 | 4.92E–04 | 7.39E–06 | 1.02E–05 | 4.11E–06 | 2.85E–04 | 2.41E–07 | 2.85E–04 | 6.33E–06 | 6.33E–06 | 7.62E–15 | 2.13E–04 | 1.00E–10 |
| Max | 8.88 | –351.58 | 1.41E–05 | 3.04E–04 | 7.92E–04 | 3.69E–04 | 4.92E–04 | 7.40E–06 | 1.02E–05 | 4.11E–06 | 2.85E–04 | 2.41E–07 | 2.85E–04 | 6.33E–06 | 6.33E–06 | 7.62E–15 | 2.13E–04 | 1.01E–10 |
| q3 | 8.88 | –351.58 | 1.41E–05 | 3.04E–04 | 7.92E–04 | 3.69E–04 | 4.92E–04 | 7.39E–06 | 1.02E–05 | 4.11E–06 | 2.85E–04 | 2.41E–07 | 2.85E–04 | 6.33E–06 | 6.33E–06 | 7.62E–15 | 2.13E–04 | 1.00E–10 |
| Median | 8.88 | –351.58 | 1.41E–05 | 3.04E–04 | 7.92E–04 | 3.69E–04 | 4.92E–04 | 7.39E–06 | 1.02E–05 | 4.11E–06 | 2.85E–04 | 2.41E–07 | 2.85E–04 | 6.33E–06 | 6.33E–06 | 7.62E–15 | 2.13E–04 | 1.00E–10 |
| q1 | 8.88 | –351.58 | 1.41E–05 | 3.04E–04 | 7.92E–04 | 3.69E–04 | 4.92E–04 | 7.39E–06 | 1.02E–05 | 4.11E–06 | 2.85E–04 | 2.41E–07 | 2.85E–04 | 6.33E–06 | 6.33E–06 | 7.62E–15 | 2.13E–04 | 1.00E–10 |
| Min | 8.88 | –351.58 | 1.41E–05 | 3.04E–04 | 7.92E–04 | 3.69E–04 | 4.92E–04 | 7.39E–06 | 1.02E–05 | 4.11E–06 | 2.85E–04 | 2.41E–07 | 2.85E–04 | 6.33E–06 | 6.33E–06 | 7.62E–15 | 2.13E–04 | 1.00E–10 |

**Table A3-7. Periglacial period (glacial boundary water). Base Case of SFR 3. All concentrations and alkalinity are in mol/L, the TDS is in g/L and the Eh is reported in mV.**

| Periglacial period 0 years | | | | | | | | | | | | | | | | | | |
|---|---|---|---|---|---|---|---|---|---|---|---|---|---|---|---|---|---|---|
| | pH | Eh | Cl | TDS | Alkalinity | Ca | C | Na | K | Mg | S | S(VI) | S(–II) | Fe | Fe(II) | Fe(III) | Si | Al |
| Mean | 8.02 | –242.81 | 1.41E–04 | 3.04E–03 | 1.78E–03 | 7.61E–04 | 1.80E–03 | 5.00E–04 | 5.88E–05 | 7.82E–05 | 1.38E–04 | 1.38E–04 | 4.39E–09 | 4.92E–08 | 4.92E–08 | 6.09E–15 | 1.21E–04 | 2.90E–08 |
| Max | 8.02 | –242.81 | 1.41E–04 | 3.04E–03 | 1.78E–03 | 7.61E–04 | 1.80E–03 | 5.00E–04 | 5.88E–05 | 7.82E–05 | 1.38E–04 | 1.38E–04 | 4.39E–09 | 4.92E–08 | 4.92E–08 | 6.09E–15 | 1.21E–04 | 2.90E–08 |
| q3 | 8.02 | –242.81 | 1.41E–04 | 3.04E–03 | 1.78E–03 | 7.61E–04 | 1.80E–03 | 5.00E–04 | 5.88E–05 | 7.82E–05 | 1.38E–04 | 1.38E–04 | 4.39E–09 | 4.92E–08 | 4.92E–08 | 6.09E–15 | 1.21E–04 | 2.90E–08 |
| Median | 8.02 | –242.81 | 1.41E–04 | 3.04E–03 | 1.78E–03 | 7.61E–04 | 1.80E–03 | 5.00E–04 | 5.88E–05 | 7.82E–05 | 1.38E–04 | 1.38E–04 | 4.39E–09 | 4.92E–08 | 4.92E–08 | 6.09E–15 | 1.21E–04 | 2.90E–08 |
| q1 | 8.02 | –242.81 | 1.41E–04 | 3.04E–03 | 1.78E–03 | 7.61E–04 | 1.80E–03 | 5.00E–04 | 5.88E–05 | 7.82E–05 | 1.38E–04 | 1.38E–04 | 4.39E–09 | 4.92E–08 | 4.92E–08 | 6.09E–15 | 1.21E–04 | 2.90E–08 |
| Min | 8.02 | –242.81 | 1.41E–04 | 3.04E–03 | 1.78E–03 | 7.61E–04 | 1.80E–03 | 5.00E–04 | 5.88E–05 | 7.82E–05 | 1.38E–04 | 1.38E–04 | 4.39E–09 | 4.92E–08 | 4.92E–08 | 6.09E–15 | 1.21E–04 | 2.90E–08 |

| Periglacial period 500 years | | | | | | | | | | | | | | | | | | |
|---|---|---|---|---|---|---|---|---|---|---|---|---|---|---|---|---|---|---|
| | pH | Eh | Cl | TDS | Alkalinity | Ca | C | Na | K | Mg | S | S(VI) | S(–II) | Fe | Fe(II) | Fe(III) | Si | Al |
| Mean | 8.56 | –289.04 | 6.98E–05 | 1.50E–03 | 9.69E–04 | 4.19E–04 | 9.45E–04 | 2.24E–04 | 3.15E–05 | 3.66E–05 | 6.35E–05 | 6.34E–05 | 8.95E–08 | 1.51E–08 | 1.51E–08 | 6.65E–15 | 1.73E–04 | 1.28E–08 |
| Max | 9.09 | –254.45 | 1.41E–04 | 3.04E–03 | 1.78E–03 | 7.61E–04 | 1.80E–03 | 5.00E–04 | 5.88E–05 | 7.82E–05 | 1.38E–04 | 1.38E–04 | 1.90E–07 | 8.26E–08 | 8.26E–08 | 9.07E–15 | 2.03E–04 | 2.90E–08 |
| q3 | 8.73 | –280.11 | 8.09E–05 | 1.74E–03 | 1.09E–03 | 4.72E–04 | 1.08E–03 | 2.67E–04 | 3.58E–05 | 4.31E–05 | 7.51E–05 | 7.50E–05 | 1.08E–07 | 1.63E–08 | 1.63E–08 | 6.95E–15 | 1.85E–04 | 1.53E–08 |
| Median | 8.60 | –291.82 | 6.24E–05 | 1.34E–03 | 8.82E–04 | 3.82E–04 | 8.55E–04 | 1.95E–04 | 2.87E–05 | 3.23E–05 | 5.58E–05 | 5.57E–05 | 7.92E–08 | 7.89E–09 | 7.89E–09 | 6.57E–15 | 1.78E–04 | 1.11E–08 |
| q1 | 8.42 | –299.72 | 5.20E–05 | 1.12E–03 | 7.66E–04 | 3.33E–04 | 7.30E–04 | 1.55E–04 | 2.47E–05 | 2.63E–05 | 4.49E–05 | 4.48E–05 | 6.28E–08 | 4.86E–09 | 4.86E–09 | 6.21E–15 | 1.65E–04 | 8.74E–09 |
| Min | 8.02 | –322.34 | 2.84E–05 | 6.12E–04 | 5.20E–04 | 2.31E–04 | 4.58E–04 | 6.31E–05 | 1.57E–05 | 1.25E–05 | 2.02E–05 | 2.02E–05 | 2.44E–08 | 1.18E–09 | 1.18E–09 | 6.04E–15 | 1.21E–04 | 3.37E–09 |

| Periglacial period 1,000 years | | | | | | | | | | | | | | | | | | |
|---|---|---|---|---|---|---|---|---|---|---|---|---|---|---|---|---|---|---|
| | pH | Eh | Cl | TDS | Alkalinity | Ca | C | Na | K | Mg | S | S(VI) | S(–II) | Fe | Fe(II) | Fe(III) | Si | Al |
| Mean | 8.96 | –313.82 | 3.92E–05 | 8.45E–04 | 6.39E–04 | 2.81E–04 | 5.86E–04 | 1.05E–04 | 1.98E–05 | 1.88E–05 | 3.15E–05 | 3.15E–05 | 4.07E–08 | 5.20E–09 | 5.20E–09 | 8.55E–15 | 1.95E–04 | 5.82E–09 |
| Max | 9.31 | –254.45 | 1.41E–04 | 3.04E–03 | 1.78E–03 | 7.61E–04 | 1.80E–03 | 5.00E–04 | 5.88E–05 | 7.82E–05 | 1.38E–04 | 1.38E–04 | 1.90E–07 | 8.26E–08 | 8.26E–08 | 1.16E–14 | 2.11E–04 | 2.90E–08 |
| q3 | 9.14 | –308.43 | 4.20E–05 | 9.05E–04 | 6.56E–04 | 2.88E–04 | 6.12E–04 | 1.16E–04 | 2.09E–05 | 2.04E–05 | 3.44E–05 | 3.44E–05 | 4.59E–08 | 2.82E–09 | 2.82E–09 | 9.57E–15 | 2.05E–04 | 6.45E–09 |
| Median | 9.05 | –319.89 | 3.06E–05 | 6.59E–04 | 5.41E–04 | 2.40E–04 | 4.82E–04 | 7.16E–05 | 1.65E–05 | 1.38E–05 | 2.25E–05 | 2.25E–05 | 2.75E–08 | 1.37E–09 | 1.37E–09 | 8.74E–15 | 2.01E–04 | 3.86E–09 |
| q1 | 8.87 | –325.49 | 2.56E–05 | 5.51E–04 | 4.94E–04 | 2.21E–04 | 4.27E–04 | 5.19E–05 | 1.46E–05 | 1.08E–05 | 1.72E–05 | 1.72E–05 | 1.92E–08 | 9.49E–10 | 9.49E–10 | 7.55E–15 | 1.93E–04 | 2.71E–09 |
| Min | 8.02 | –334.41 | 1.71E–05 | 3.68E–04 | 4.23E–04 | 1.93E–04 | 3.38E–04 | 1.90E–05 | 1.13E–05 | 5.85E–06 | 8.33E–06 | 8.32E–06 | 5.03E–09 | 4.51E–10 | 4.51E–10 | 6.04E–15 | 1.21E–04 | 7.78E–10 |

**Periglacial period 2,000 years**

| | pH | Eh | Cl | TDS | Alkalinity | Ca | C | Na | K | Mg | S | S(VI) | S(–II) | Fe | Fe(II) | Fe(III) | Si | Al |
|---|---|---|---|---|---|---|---|---|---|---|---|---|---|---|---|---|---|---|
| Mean | 9.33 | –330.28 | 1.70E–05 | 3.67E–04 | 4.29E–04 | 1.96E–04 | 3.40E–04 | 1.88E–05 | 1.13E–05 | 5.83E–06 | 8.28E–06 | 8.28E–06 | 4.66E–09 | 8.79E–10 | 8.79E–10 | 1.21E–14 | 2.11E–04 | 7.69E–10 |
| Max | 9.37 | –256.58 | 1.35E–04 | 2.91E–03 | 1.71E–03 | 7.31E–04 | 1.72E–03 | 4.75E–04 | 5.63E–05 | 7.45E–05 | 1.31E–04 | 1.31E–04 | 1.82E–07 | 7.20E–08 | 7.20E–08 | 1.26E–14 | 2.13E–04 | 2.75E–08 |
| q3 | 9.37 | –329.82 | 1.51E–05 | 3.25E–04 | 4.08E–04 | 1.87E–04 | 3.18E–04 | 1.11E–05 | 1.06E–05 | 4.67E–06 | 6.21E–06 | 6.21E–06 | 1.55E–09 | 3.39E–10 | 3.39E–10 | 1.26E–14 | 2.13E–04 | 3.17E–10 |
| Median | 9.37 | –332.06 | 1.45E–05 | 3.12E–04 | 4.04E–04 | 1.86E–04 | 3.12E–04 | 8.78E–06 | 1.03E–05 | 4.32E–06 | 5.58E–06 | 5.58E–06 | 5.63E–10 | 2.87E–10 | 2.87E–10 | 1.25E–14 | 2.13E–04 | 1.81E–10 |
| q1 | 9.35 | –333.72 | 1.43E–05 | 3.08E–04 | 4.03E–04 | 1.85E–04 | 3.10E–04 | 8.12E–06 | 1.03E–05 | 4.22E–06 | 5.41E–06 | 5.41E–06 | 2.83E–10 | 2.60E–10 | 2.60E–10 | 1.23E–14 | 2.12E–04 | 1.43E–10 |
| Min | 8.05 | –334.85 | 1.41E–05 | 3.04E–04 | 4.02E–04 | 1.85E–04 | 3.08E–04 | 7.47E–06 | 1.02E–05 | 4.12E–06 | 5.23E–06 | 5.23E–06 | 1.81E–11 | 1.83E–10 | 1.83E–10 | 6.04E–15 | 1.26E–04 | 1.05E–10 |

**Periglacial period 5,000 years**

| | pH | Eh | Cl | TDS | Alkalinity | Ca | C | Na | K | Mg | S | S(VI) | S(–II) | Fe | Fe(II) | Fe(III) | Si | Al |
|---|---|---|---|---|---|---|---|---|---|---|---|---|---|---|---|---|---|---|
| Mean | 9.37 | –304.21 | 1.42E–05 | 3.05E–04 | 4.02E–04 | 1.85E–04 | 3.09E–04 | 7.63E–06 | 1.02E–05 | 4.15E–06 | 5.27E–06 | 5.27E–06 | 9.77E–11 | 9.35E–11 | 9.35E–11 | 1.26E–14 | 2.13E–04 | 1.14E–10 |
| Max | 9.37 | –302.12 | 3.39E–05 | 7.30E–04 | 5.73E–04 | 2.53E–04 | 5.19E–04 | 8.43E–05 | 1.78E–05 | 1.57E–05 | 2.59E–05 | 2.59E–05 | 3.18E–08 | 1.70E–09 | 1.70E–09 | 1.26E–14 | 2.13E–04 | 4.61E–09 |
| q3 | 9.37 | –302.60 | 1.41E–05 | 3.04E–04 | 4.02E–04 | 1.85E–04 | 3.08E–04 | 7.39E–06 | 1.02E–05 | 4.11E–06 | 5.21E–06 | 5.21E–06 | 3.72E–14 | 8.42E–11 | 8.42E–11 | 1.26E–14 | 2.13E–04 | 1.00E–10 |
| Median | 9.37 | –302.97 | 1.41E–05 | 3.04E–04 | 4.02E–04 | 1.85E–04 | 3.08E–04 | 7.39E–06 | 1.02E–05 | 4.11E–06 | 5.21E–06 | 5.21E–06 | 3.25E–14 | 8.28E–11 | 8.28E–11 | 1.26E–14 | 2.13E–04 | 1.00E–10 |
| q1 | 9.37 | –303.38 | 1.41E–05 | 3.04E–04 | 4.02E–04 | 1.85E–04 | 3.08E–04 | 7.39E–06 | 1.02E–05 | 4.11E–06 | 5.21E–06 | 5.21E–06 | 2.89E–14 | 8.16E–11 | 8.16E–11 | 1.26E–14 | 2.13E–04 | 1.00E–10 |
| Min | 8.99 | –334.78 | 1.41E–05 | 3.04E–04 | 4.02E–04 | 1.85E–04 | 3.08E–04 | 7.39E–06 | 1.02E–05 | 4.11E–06 | 5.21E–06 | 5.21E–06 | 2.47E–14 | 8.00E–11 | 8.00E–11 | 8.32E–15 | 1.99E–04 | 1.00E–10 |

**Periglacial period 10,000 years**

| | pH | Eh | Cl | TDS | Alkalinity | Ca | C | Na | K | Mg | S | S(VI) | S(–II) | Fe | Fe(II) | Fe(III) | Si | Al |
|---|---|---|---|---|---|---|---|---|---|---|---|---|---|---|---|---|---|---|
| Mean | 9.37 | –303.50 | 1.41E–05 | 3.04E–04 | 4.02E–04 | 1.85E–04 | 3.08E–04 | 7.39E–06 | 1.02E–05 | 4.11E–06 | 5.21E–06 | 5.21E–06 | 4.06E–14 | 8.48E–11 | 8.47E–11 | 1.26E–14 | 2.13E–04 | 1.00E–10 |
| Max | 9.37 | –285.31 | 1.41E–05 | 3.04E–04 | 4.02E–04 | 1.85E–04 | 3.08E–04 | 7.41E–06 | 1.02E–05 | 4.11E–06 | 5.21E–06 | 5.21E–06 | 4.20E–14 | 8.55E–11 | 8.55E–11 | 1.26E–14 | 2.13E–04 | 1.01E–10 |
| q3 | 9.37 | –303.67 | 1.41E–05 | 3.04E–04 | 4.02E–04 | 1.85E–04 | 3.08E–04 | 7.39E–06 | 1.02E–05 | 4.11E–06 | 5.21E–06 | 5.21E–06 | 4.18E–14 | 8.54E–11 | 8.54E–11 | 1.26E–14 | 2.13E–04 | 1.00E–10 |
| Median | 9.37 | –303.69 | 1.41E–05 | 3.04E–04 | 4.02E–04 | 1.85E–04 | 3.08E–04 | 7.39E–06 | 1.02E–05 | 4.11E–06 | 5.21E–06 | 5.21E–06 | 4.11E–14 | 8.53E–11 | 8.52E–11 | 1.26E–14 | 2.13E–04 | 1.00E–10 |
| q1 | 9.37 | –303.74 | 1.41E–05 | 3.04E–04 | 4.02E–04 | 1.85E–04 | 3.08E–04 | 7.39E–06 | 1.02E–05 | 4.11E–06 | 5.21E–06 | 5.21E–06 | 4.08E–14 | 8.52E–11 | 8.52E–11 | 1.26E–14 | 2.13E–04 | 1.00E–10 |
| Min | 9.37 | –303.76 | 1.41E–05 | 3.04E–04 | 4.02E–04 | 1.85E–04 | 3.08E–04 | 7.39E–06 | 1.02E–05 | 4.11E–06 | 5.21E–06 | 5.21E–06 | 1.08E–16 | 4.06E–11 | 4.06E–11 | 1.26E–14 | 2.13E–04 | 1.00E–10 |

**Table A3-8. Periglacial period (glacial boundary water). Variant Case of SFR 3. All concentrations and alkalinity are in mol/L, the TDS is in g/L and the Eh is reported in mV.**

| Periglacial period 0 years | | | | | | | | | | | | | | | | | | |
|---|---|---|---|---|---|---|---|---|---|---|---|---|---|---|---|---|---|---|
| | pH | Eh | Cl | TDS | Alkalinity | Ca | C | Na | K | Mg | S | S(VI) | S(–II) | Fe | Fe(II) | Fe(III) | Si | Al |
| Mean | 7.97 | –271.33 | 1.41E–04 | 3.04E–03 | 1.97E–03 | 8.35E–04 | 1.87E–03 | 5.00E–04 | 5.88E–05 | 7.82E–05 | 2.50E–04 | 1.25E–04 | 1.26E–04 | 6.56E–06 | 6.56E–06 | 6.13E–15 | 1.21E–04 | 2.90E–08 |
| Max | 7.97 | –271.33 | 1.41E–04 | 3.04E–03 | 1.97E–03 | 8.35E–04 | 1.87E–03 | 5.00E–04 | 5.88E–05 | 7.82E–05 | 2.50E–04 | 1.25E–04 | 1.26E–04 | 6.56E–06 | 6.56E–06 | 6.13E–15 | 1.21E–04 | 2.90E–08 |
| q3 | 7.97 | –271.33 | 1.41E–04 | 3.04E–03 | 1.97E–03 | 8.35E–04 | 1.87E–03 | 5.00E–04 | 5.88E–05 | 7.82E–05 | 2.50E–04 | 1.25E–04 | 1.26E–04 | 6.56E–06 | 6.56E–06 | 6.13E–15 | 1.21E–04 | 2.90E–08 |
| Median | 7.97 | –271.33 | 1.41E–04 | 3.04E–03 | 1.97E–03 | 8.35E–04 | 1.87E–03 | 5.00E–04 | 5.88E–05 | 7.82E–05 | 2.50E–04 | 1.25E–04 | 1.26E–04 | 6.56E–06 | 6.56E–06 | 6.13E–15 | 1.21E–04 | 2.90E–08 |
| q1 | 7.97 | –271.33 | 1.41E–04 | 3.04E–03 | 1.97E–03 | 8.35E–04 | 1.87E–03 | 5.00E–04 | 5.88E–05 | 7.82E–05 | 2.50E–04 | 1.25E–04 | 1.26E–04 | 6.56E–06 | 6.56E–06 | 6.13E–15 | 1.21E–04 | 2.90E–08 |
| Min | 7.97 | –271.33 | 1.41E–04 | 3.04E–03 | 1.97E–03 | 8.35E–04 | 1.87E–03 | 5.00E–04 | 5.88E–05 | 7.82E–05 | 2.50E–04 | 1.25E–04 | 1.26E–04 | 6.56E–06 | 6.56E–06 | 6.13E–15 | 1.21E–04 | 2.90E–08 |

| Periglacial period 500 years | | | | | | | | | | | | | | | | | | |
|---|---|---|---|---|---|---|---|---|---|---|---|---|---|---|---|---|---|---|
| | pH | Eh | Cl | TDS | Alkalinity | Ca | C | Na | K | Mg | S | S(VI) | S(–II) | Fe | Fe(II) | Fe(III) | Si | Al |
| Mean | 8.37 | –302.81 | 6.98E–05 | 1.50E–03 | 1.30E–03 | 5.56E–04 | 1.08E–03 | 2.24E–04 | 3.15E–05 | 3.66E–05 | 2.49E–04 | 4.15E–05 | 2.08E–04 | 6.39E–06 | 6.39E–06 | 6.22E–15 | 1.73E–04 | 1.28E–08 |
| Max | 8.72 | –271.33 | 1.41E–04 | 3.04E–03 | 1.97E–03 | 8.35E–04 | 1.87E–03 | 5.00E–04 | 5.88E–05 | 7.82E–05 | 2.57E–04 | 1.25E–04 | 2.53E–04 | 6.56E–06 | 6.56E–06 | 6.94E–15 | 2.03E–04 | 2.90E–08 |
| q3 | 8.48 | –295.10 | 8.09E–05 | 1.74E–03 | 1.39E–03 | 5.95E–04 | 1.20E–03 | 2.67E–04 | 3.58E–05 | 4.31E–05 | 2.55E–04 | 5.51E–05 | 2.35E–04 | 6.39E–06 | 6.39E–06 | 6.31E–15 | 1.85E–04 | 1.53E–08 |
| Median | 8.40 | –305.12 | 6.24E–05 | 1.34E–03 | 1.23E–03 | 5.27E–04 | 9.99E–04 | 1.95E–04 | 2.87E–05 | 3.23E–05 | 2.50E–04 | 3.26E–05 | 2.17E–04 | 6.37E–06 | 6.37E–06 | 6.19E–15 | 1.78E–04 | 1.11E–08 |
| q1 | 8.28 | –311.96 | 5.20E–05 | 1.12E–03 | 1.14E–03 | 4.89E–04 | 8.87E–04 | 1.55E–04 | 2.47E–05 | 2.63E–05 | 2.44E–04 | 2.00E–05 | 1.88E–04 | 6.36E–06 | 6.36E–06 | 6.09E–15 | 1.65E–04 | 8.74E–09 |
| Min | 7.97 | –337.13 | 2.84E–05 | 6.12E–04 | 9.03E–04 | 3.97E–04 | 6.24E–04 | 6.31E–05 | 1.57E–05 | 1.25E–05 | 2.40E–04 | 9.23E–07 | 1.26E–04 | 6.34E–06 | 6.34E–06 | 6.04E–15 | 1.21E–04 | 3.37E–09 |

| Periglacial period 1,000 years | | | | | | | | | | | | | | | | | | |
|---|---|---|---|---|---|---|---|---|---|---|---|---|---|---|---|---|---|---|
| | pH | Eh | Cl | TDS | Alkalinity | Ca | C | Na | K | Mg | S | S(VI) | S(–II) | Fe | Fe(II) | Fe(III) | Si | Al |
| Mean | 8.63 | –327.93 | 3.92E–05 | 8.45E–04 | 1.01E–03 | 4.41E–04 | 7.45E–04 | 1.05E–04 | 1.98E–05 | 1.88E–05 | 2.55E–04 | 1.19E–05 | 2.44E–04 | 6.35E–06 | 6.35E–06 | 6.76E–15 | 1.95E–04 | 5.82E–09 |
| Max | 8.85 | –271.34 | 1.41E–04 | 3.04E–03 | 1.97E–03 | 8.35E–04 | 1.87E–03 | 5.00E–04 | 5.88E–05 | 7.82E–05 | 2.76E–04 | 1.25E–04 | 2.76E–04 | 6.56E–06 | 6.56E–06 | 7.46E–15 | 2.11E–04 | 2.90E–08 |
| q3 | 8.76 | –320.44 | 4.20E–05 | 9.05E–04 | 1.05E–03 | 4.52E–04 | 7.76E–04 | 1.16E–04 | 2.09E–05 | 2.04E–05 | 2.57E–04 | 8.55E–06 | 2.56E–04 | 6.35E–06 | 6.35E–06 | 7.06E–15 | 2.05E–04 | 6.45E–09 |
| Median | 8.70 | –334.46 | 3.06E–05 | 6.59E–04 | 9.25E–04 | 4.04E–04 | 6.47E–04 | 7.16E–05 | 1.65E–05 | 1.38E–05 | 2.55E–04 | 1.29E–06 | 2.51E–04 | 6.34E–06 | 6.34E–06 | 6.85E–15 | 2.01E–04 | 3.86E–09 |
| q1 | 8.57 | –340.37 | 2.56E–05 | 5.51E–04 | 8.76E–04 | 3.89E–04 | 5.95E–04 | 5.19E–05 | 1.46E–05 | 1.08E–05 | 2.53E–04 | 6.38E–07 | 2.49E–04 | 6.33E–06 | 6.33E–06 | 6.49E–15 | 1.93E–04 | 2.71E–09 |
| Min | 7.97 | –348.82 | 1.71E–05 | 3.68E–04 | 8.11E–04 | 3.73E–04 | 5.17E–04 | 1.90E–05 | 1.13E–05 | 5.85E–06 | 2.40E–04 | 2.96E–07 | 1.26E–04 | 6.33E–06 | 6.33E–06 | 6.04E–15 | 1.21E–04 | 7.78E–10 |

**Periglacial period 2,000 years**

| | pH | Eh | Cl | TDS | Alkalinity | Ca | C | Na | K | Mg | S | S(VI) | S(–II) | Fe | Fe(II) | Fe(III) | Si | Al |
|---|---|---|---|---|---|---|---|---|---|---|---|---|---|---|---|---|---|---|
| Mean | 8.85 | –348.98 | 1.70E–05 | 3.67E–04 | 8.16E–04 | 3.77E–04 | 5.21E–04 | 1.88E–05 | 1.13E–05 | 5.83E–06 | 2.81E–04 | 1.67E–06 | 2.79E–04 | 6.33E–06 | 6.33E–06 | 7.52E–15 | 2.11E–04 | 7.69E–10 |
| Max | 8.88 | –273.42 | 1.35E–04 | 2.91E–03 | 1.90E–03 | 8.08E–04 | 1.80E–03 | 4.75E–04 | 5.63E–05 | 7.45E–05 | 2.85E–04 | 1.17E–04 | 2.85E–04 | 6.54E–06 | 6.54E–06 | 7.62E–15 | 2.13E–04 | 2.75E–08 |
| q3 | 8.88 | –350.70 | 1.51E–05 | 3.25E–04 | 7.98E–04 | 3.70E–04 | 5.00E–04 | 1.11E–05 | 1.06E–05 | 4.67E–06 | 2.84E–04 | 2.57E–07 | 2.84E–04 | 6.33E–06 | 6.33E–06 | 7.61E–15 | 2.13E–04 | 3.17E–10 |
| Median | 8.87 | –351.25 | 1.45E–05 | 3.12E–04 | 7.94E–04 | 3.69E–04 | 4.95E–04 | 8.78E–06 | 1.03E–05 | 4.32E–06 | 2.84E–04 | 2.47E–07 | 2.84E–04 | 6.33E–06 | 6.33E–06 | 7.60E–15 | 2.13E–04 | 1.81E–10 |
| q1 | 8.87 | –351.41 | 1.43E–05 | 3.08E–04 | 7.93E–04 | 3.69E–04 | 4.94E–04 | 8.12E–06 | 1.03E–05 | 4.22E–06 | 2.82E–04 | 2.44E–07 | 2.82E–04 | 6.33E–06 | 6.33E–06 | 7.57E–15 | 2.12E–04 | 1.43E–10 |
| Min | 8.00 | –351.56 | 1.41E–05 | 3.04E–04 | 7.92E–04 | 3.69E–04 | 4.92E–04 | 7.47E–06 | 1.02E–05 | 4.12E–06 | 2.40E–04 | 2.42E–07 | 1.30E–04 | 6.33E–06 | 6.33E–06 | 6.04E–15 | 1.26E–04 | 1.05E–10 |

**Periglacial period 5,000 years**

| | pH | Eh | Cl | TDS | Alkalinity | Ca | C | Na | K | Mg | S | S(VI) | S(–II) | Fe | Fe(II) | Fe(III) | Si | Al |
|---|---|---|---|---|---|---|---|---|---|---|---|---|---|---|---|---|---|---|
| Mean | 8.88 | –351.52 | 1.42E–05 | 3.05E–04 | 7.93E–04 | 3.69E–04 | 4.93E–04 | 7.63E–06 | 1.02E–05 | 4.15E–06 | 2.85E–04 | 2.43E–07 | 2.85E–04 | 6.33E–06 | 6.33E–06 | 7.62E–15 | 2.13E–04 | 1.14E–10 |
| Max | 8.88 | –330.18 | 3.39E–05 | 7.30E–04 | 9.61E–04 | 4.17E–04 | 6.83E–04 | 8.43E–05 | 1.78E–05 | 1.57E–05 | 2.85E–04 | 2.32E–06 | 2.85E–04 | 6.34E–06 | 6.34E–06 | 7.62E–15 | 2.13E–04 | 4.61E–09 |
| q3 | 8.88 | –351.58 | 1.41E–05 | 3.04E–04 | 7.92E–04 | 3.69E–04 | 4.92E–04 | 7.39E–06 | 1.02E–05 | 4.11E–06 | 2.85E–04 | 2.41E–07 | 2.85E–04 | 6.33E–06 | 6.33E–06 | 7.62E–15 | 2.13E–04 | 1.00E–10 |
| Median | 8.88 | –351.58 | 1.41E–05 | 3.04E–04 | 7.92E–04 | 3.69E–04 | 4.92E–04 | 7.39E–06 | 1.02E–05 | 4.11E–06 | 2.85E–04 | 2.41E–07 | 2.85E–04 | 6.33E–06 | 6.33E–06 | 7.62E–15 | 2.13E–04 | 1.00E–10 |
| q1 | 8.88 | –351.58 | 1.41E–05 | 3.04E–04 | 7.92E–04 | 3.69E–04 | 4.92E–04 | 7.39E–06 | 1.02E–05 | 4.11E–06 | 2.85E–04 | 2.41E–07 | 2.85E–04 | 6.33E–06 | 6.33E–06 | 7.62E–15 | 2.13E–04 | 1.00E–10 |
| Min | 8.66 | –351.58 | 1.41E–05 | 3.04E–04 | 7.92E–04 | 3.69E–04 | 4.92E–04 | 7.39E–06 | 1.02E–05 | 4.11E–06 | 2.52E–04 | 2.41E–07 | 2.51E–04 | 6.33E–06 | 6.33E–06 | 6.73E–15 | 1.99E–04 | 1.00E–10 |

**Periglacial period 10,000 years**

| | pH | Eh | Cl | TDS | Alkalinity | Ca | C | Na | K | Mg | S | S(VI) | S(–II) | Fe | Fe(II) | Fe(III) | Si | Al |
|---|---|---|---|---|---|---|---|---|---|---|---|---|---|---|---|---|---|---|
| Mean | 8.88 | –351.58 | 1.41E–05 | 3.04E–04 | 7.92E–04 | 3.69E–04 | 4.92E–04 | 7.39E–06 | 1.02E–05 | 4.11E–06 | 2.85E–04 | 2.41E–07 | 2.85E–04 | 6.33E–06 | 6.33E–06 | 7.62E–15 | 2.13E–04 | 1.00E–10 |
| Max | 8.88 | –351.58 | 1.41E–05 | 3.04E–04 | 7.92E–04 | 3.69E–04 | 4.92E–04 | 7.41E–06 | 1.02E–05 | 4.11E–06 | 2.85E–04 | 2.41E–07 | 2.85E–04 | 6.33E–06 | 6.33E–06 | 7.62E–15 | 2.13E–04 | 1.01E–10 |
| q3 | 8.88 | –351.58 | 1.41E–05 | 3.04E–04 | 7.92E–04 | 3.69E–04 | 4.92E–04 | 7.39E–06 | 1.02E–05 | 4.11E–06 | 2.85E–04 | 2.41E–07 | 2.85E–04 | 6.33E–06 | 6.33E–06 | 7.62E–15 | 2.13E–04 | 1.00E–10 |
| Median | 8.88 | –351.58 | 1.41E–05 | 3.04E–04 | 7.92E–04 | 3.69E–04 | 4.92E–04 | 7.39E–06 | 1.02E–05 | 4.11E–06 | 2.85E–04 | 2.41E–07 | 2.85E–04 | 6.33E–06 | 6.33E–06 | 7.62E–15 | 2.13E–04 | 1.00E–10 |
| q1 | 8.88 | –351.58 | 1.41E–05 | 3.04E–04 | 7.92E–04 | 3.69E–04 | 4.92E–04 | 7.39E–06 | 1.02E–05 | 4.11E–06 | 2.85E–04 | 2.41E–07 | 2.85E–04 | 6.33E–06 | 6.33E–06 | 7.62E–15 | 2.13E–04 | 1.00E–10 |
| Min | 8.88 | –351.58 | 1.41E–05 | 3.04E–04 | 7.92E–04 | 3.69E–04 | 4.92E–04 | 7.39E–06 | 1.02E–05 | 4.11E–06 | 2.85E–04 | 2.41E–07 | 2.85E–04 | 6.33E–06 | 6.33E–06 | 7.62E–15 | 2.13E–04 | 1.00E–10 |